

Observer Design and Identification
Methods for Hybrid Systems
Theory and Experiments

PROEFSCHRIFT

ter verkrijging van de graad van doctor aan de
Technische Universiteit Eindhoven,
op gezag van de Rector Magnificus, prof.dr. R.A. van Santen,
voor een commissie aangewezen door het College voor
Promoties in het openbaar te verdedigen op
dinsdag 9 november 2004 om 16.00 uur

door

Aleksandar Ljiljana Juloski

geboren te Belgrado, Servië en Montenegro

Dit proefschrift is goedgekeurd door de promotoren:

prof.dr.ir. P.P.J. van den Bosch

en

prof.dr. H. Nijmeijer

Copromotor:

dr.ir. W.P.M.H. Heemels

CIP-DATA LIBRARY TECHNISCHE UNIVERSITEIT EINDHOVEN

Juloski, Aleksandar Lj.

Observer design and identification methods for hybrid systems : theory and experiments / by Aleksandar Ljiljana Juloski. – Eindhoven : Technische Universiteit Eindhoven, 2004.

Proefschrift. – ISBN 90-386-1623-6

NUR 959

Trefw.: nietlineaire dynamische systemen / schattingstheorie /
systeemidentificatie / parameterschatting.

Subject headings: nonlinear dynamical systems / observers / identification
/ piecewise linear techniques.

mojoj majci
to my mother

Eerste promotor: prof.dr.ir. P.P.J. van den Bosch

Tweede promotor: prof.dr. H. Nijmeijer

Copromotor: dr.ir. W.P.M.H. Heemels

Kerncommissie:

prof.dr. A.J. van der Schaft

dr. G. Ferrari-Trecate

The Ph.D. work is supported by the Technology Foundation
STW/PROGRESS grant EES.5173.

The Ph.D. work forms a part of the research program of the Dutch
Institute of Systems and Control (DISC).

Contents

Summary	3
1 Introduction	5
1.1 Hybrid systems	5
1.2 Piecewise affine systems	8
1.3 Observer design for hybrid systems	10
1.4 Identification of hybrid systems	15
1.5 Experiments	20
1.6 Overview	21
2 Observer Design for Lur'e Systems with Multivalued Mappings	23
2.1 Introduction	23
2.2 Preliminaries	26
2.3 Problem statement	29
2.4 Main results	30
2.5 Experimental example	35
2.6 Conclusions	38
3 Observer Design for a Class of Bimodal PWL Systems	41
3.1 Introduction	41
3.2 Preliminaries and notation	43
3.3 Problem statement	44
3.4 Main results for the continuous time case	46
3.4.1 Continuous dynamics	47
3.4.2 Discontinuous dynamics	50
3.5 Sliding mode analysis	53
3.6 Examples	55
3.7 Main results for the discrete time case	62
3.7.1 Continuous dynamics	63
3.7.2 Discontinuous dynamics	65
3.8 Examples	65
3.9 Conclusions	69

4	Identification of an Experimental Hybrid System	71
4.1	Introduction	71
4.2	Experimental setup	74
4.3	Identification algorithm	79
4.4	Identification with free and impact modes	82
4.5	Identification with saturations	86
4.6	Conclusion	93
5	A Bayesian Approach to Identification of Hybrid Systems	95
5.1	Introduction	95
5.2	Preliminaries	98
5.3	Model class	99
5.4	Problem statement	100
5.5	Suboptimal identification algorithm	103
5.6	Particle filtering approximation	105
5.7	Partition estimation	107
5.8	Example	109
5.9	Initialization	111
5.9.1	Initialization using mode knowledge	112
5.9.2	Initialization via clustering procedure	113
5.9.3	Brute force initialization	114
5.10	Experimental example	115
5.10.1	Bi-modal identification	117
5.10.2	Identification with lower saturation	119
5.11	Conclusions	123
6	Conclusions and recommendations	125
6.1	Summary of contributions	125
6.2	Observer design for hybrid systems	126
6.2.1	Detailed overview of contributions	126
6.2.2	Discussion and recommendations	127
6.3	Identification of hybrid systems	129
6.3.1	Detailed overview of contributions	129
6.3.2	Discussion and recommendations	130
6.4	Outlook	131
	References	132
	Acknowledgement	142
	Samenvatting	145

Summary

In this thesis we consider observer design and identification techniques for certain classes of hybrid systems. Hybrid systems are a broad class of dynamical systems that arise when the discrete behavior (usually described by a finite state machine) and continuous behavior (usually described by differential or difference equations) interact. These systems are typically nonlinear, non-smooth and multi-modal. Examples of hybrid dynamics can be found in many fields and disciplines, such as embedded systems, process control, automated traffic-management systems, electrical circuits, mechanical and bio-mechanical systems, biological and bio-medical systems and economics.

We will present a novel constructive observer design procedure for a class of nonsmooth dynamical systems, namely systems of Lur'e type with a monotone multivalued mapping in the feedback path. Examples of such systems include various classes of hybrid systems, such as relay systems, linear complementarity systems, electrical circuits with switching elements and certain piece-wise affine systems. Under the assumptions that the observed system is well behaved and certain LMI conditions are satisfied, we will prove that the proposed observers are well-posed (i.e. that there exists a unique solution to the observer dynamics), and that the observer asymptotically recovers the state of the observed system. The results are illustrated on an experimental case study of a drill-string setup.

We also present a novel observer design procedure for a class of bi-modal piece-wise affine systems, in both continuous and discrete time. We propose Luenberger-type observers, and derive sufficient conditions for the observation error dynamics to be globally asymptotically stable. The derived conditions imply that the system dynamics is continuous over the switching plane. When the dynamics is discontinuous, we derive conditions that guarantee that the relative estimation error will be asymptotically bounded with respect to the state of the observed system. The presented theory is illustrated with several academic examples and an experimental example of a piecewise linear beam with a one-sided spring.

The second part of the thesis focuses on on identification methods for hybrids systems and starts with an experimental case study in the identification of the electronic component placement process in pick-and-place machines. Unilateral contact and saturation phenomena characterize the discrete dynamics of the system. Furthermore, the mode switch cannot be measured

and identification algorithms for hybrid systems, that are capable to reconstruct both the modes and the switching law, must be applied. Piece-Wise AutoRegressive eXogenous (PWARX) models, which consist of a number of ARX modes together with the partition of the regressor space into regions where each model is valid are identified using a clustering-based procedure. The reconstructed models are able to capture the relevant dynamics of the experimental setup. This case study yields many practical insights into hybrid system identification, and highlights the need for incorporating the available a priori knowledge into the identification procedure.

Motivated by the need for incorporating a priori knowledge, a novel procedure for the identification of hybrid systems in the class of PWARX systems is developed. The presented method facilitates the use of available a priori knowledge on the system to be identified, but can also be used as a black-box method. We treat the unknown parameters as random variables, described by their probability density functions. The identification problem is posed as the problem of maximizing the total probability that the observed data is generated by the identified model. A particle filtering method is used for the numerical implementation of the proposed procedure. A modified version of the multi-category robust linear programming (MRLP) classification procedure, which uses the information derived in the previous steps of the identification algorithm, is used for estimating the partition of the PWARX map. The proposed procedure is applied for the identification of a component placement process in pick-and-place machines.

Introduction

1.1 Hybrid systems	1.4 Identification of hybrid
1.2 Piecewise affine systems	systems
1.3 Observer design for	1.5 Experiments
hybrid systems	1.6 Overview

In this thesis we will present methods for observer design and identification for certain classes of hybrid systems. In this chapter we will discuss the relevance of the problems treated in this thesis, and discuss connections with the existing literature.

1.1 Hybrid systems

Hybrid systems are a broad class of dynamical systems that arise when the discrete behavior (usually described by a finite state machine) and continuous behavior (usually described by differential or difference equations) interact. This means that in the operation of a hybrid system several discrete states (modes) can be distinguished, while different laws govern the evolution of the continuous state in each of the discrete modes (cf. figure 1.1). Examples of hybrid dynamics can be found in many fields and disciplines, such as embedded systems, process control, automated traffic-management systems, electrical circuits, mechanical and bio-mechanical systems, biological and bio-medical systems and economics.

Almost all modern consumer products (cars, home appliances, entertainment products) are controlled by embedded software. Software control makes it possible for manufacturers to design and produce flexible and economical products with a multitude of functions. The controlled process (the car engine, the temperature in the refrigerator, the motor in the DVD drive) is time continuous, while the control algorithm, implemented in software, takes the form of a finite state machine, rendering the overall dynamics hybrid.

Examples of hybrid dynamics can also be found in mechanical systems that display multi-modal behavior. For example, in mechanical systems

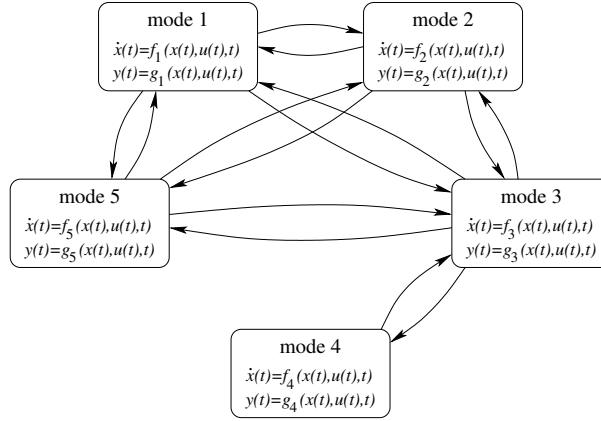


Figure 1.1: A hybrid system

with friction it is possible to make a clear distinction between stick and slip phases. Other examples include mechanical systems with contacts, where the evolution of the system depends on whether a contact is active or not.

Example 1.1.1 As an example of a hybrid mechanical system take the simplified scheme of the mounting head of the pick-and-place machine, depicted in figure 1.2 (Juloski et al. (2003b, 2004b)). This example originates from an industrial case study, done for the pick-and-place machines manufactured by Assembleon, Eindhoven.

The pick-and-place machine works as follows: the printed circuit board (PCB) is placed in the working area of the mounting head. The mounting head, carrying an electronic component (using, for instance, a vacuum pipette), is navigated to the position where the component should be placed on the PCB. Next, the component is placed, released, and the process is repeated for the next component.

Figure 1.2 depicts the mounting head carrying the electronic component, powered by the electric motor (force \vec{F}), together with supporting elements (spring c_1), and frictions (damper d_1 , dry friction f_1). The total moving mass is denoted by M . The lower part of the figure depicts the printed circuit board (PCB), where the elasticity and damping of the PCB are represented by the spring c_2 and friction blocks d_2 and f_2 .

Assume now that the head is in the proper position above the place on the PCB, where the component should be placed. The component should be pressed against the PCB, with sufficient, but not excessive force, and

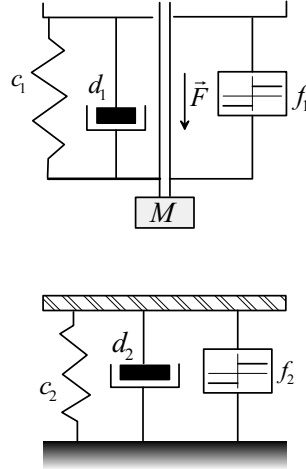


Figure 1.2: Schematic representation of the mounting head of the pick-and-place machine

subsequently released. Several modes can be distinguished:

- free mode - when the mounting head is not in contact with the PCB
- impact mode - the mounting head is in contact with the PCB
- upper saturation - the mounting head can not move upwards, due to physical constraints
- lower saturation - the mounting head can not move downwards, due to physical constraints

During normal operation of the pick-and-place machine only switching between free and impact modes occurs. In the case of an error (for example, if there is no PCB present under the head) saturations may occur.

Hybrid models can also be used to describe many complex nonlinear processes, by combining several simple models together with laws that govern the switching between these models. Any nonlinear dynamical system can be approximated, up to an arbitrary accuracy, with a piecewise affine system, that consists of several affine dynamics, and a state-dependant switching law (Sontag (1981)). As an example, in Del Vecchio et al. (2003) it is demonstrated that the complex human motions can be decomposed into a sequence of elementary building blocks, each being a linear dynamical systems.

Due to their ubiquity and many potential applications, hybrid systems attracted a lot of attention in the control community recently (Morse et al. (1999); Antsaklis and Nerode (1998); Antsaklis (2000)). Numerous results on modelling, analysis, verification and control appeared in the literature. Several studies on fundamental system theoretic properties such as well-posedness, stability, controllability and observability also appeared recently for some classes of hybrid systems.

Most of these developments start with an assumption that the accurate quantitative model of the hybrid system is readily available, and that all states, continuous and discrete, can be measured. Relatively less attention has been paid to the following problems:

- *The observer design problem:* given a hybrid system together with input/output measurements construct an estimator/observer such that the current state is estimated as accurately as possible
- *The identification problem:* given input-output data generated by a hybrid system, construct a model within a pre-defined class of hybrid models, that explains the data as accurately as possible.

Such observer design and identification problems show up in a wide variety of situations in the practice of control, robotics, computer vision, and machine learning, when accurate models of a complex physical process are often impossible to obtain from first principles and/or only a limited number of variables are measured. Recently, finding effective solutions to state estimation and identification problems of hybrid systems has become an ever pressing issue in numerous emerging applications such as recognition of human gaits from video, segmentation of dynamic textures, piecewise approximation of nonlinear dynamics, fault detection, mode detection in autonomous navigation and multi-agent localization and mapping.

Therefore, in this thesis we will discuss methods to solve observer design and identification problems for certain classes of hybrid systems.

1.2 Piecewise affine systems

A vast majority of results literature on hybrid systems deals with hybrid systems where continuous dynamics in each of the modes is linear or affine. Classes of switched linear systems and piecewise affine (PWA) systems receive special attention.

Piecewise affine systems comprise several affine dynamics, and a state dependent mode switching law. Continuous time piecewise affine systems

have the following form:

$$\begin{aligned} \dot{x}(t) &= A_i x(t) + B_i u(t) + a_i \\ y(t) &= C_i x(t) + D_i u(t) + c_i, \quad \text{for } \begin{bmatrix} x(t) \\ u(t) \end{bmatrix} \in \mathcal{X}_i \end{aligned} \quad (1.1)$$

where $t \in \mathbb{R}^+$ and $x(t) \in \mathbb{R}^n$ is the state vector, $u(t) \in \mathbb{R}^p$ is the input vector and $y(t) \in \mathbb{R}^m$ is the measurement vector. Matrices A_i, B_i, C_i and vectors a_i, c_i are assumed to be of appropriate dimensions, and the index set of modes is denoted with I . $\{\mathcal{X}_i\}_{i \in I} \subseteq \mathbb{R}^{n+p}$ is a partition of \mathbb{R}^{n+p} space into a finite number of closed polyhedral cells with pairwise disjoint interiors.

The literature on piecewise affine systems is broad, and here we list only a few references. A number of techniques are developed for:

- well posedness analysis (Çamlıbel and Schumacher (2002), Imura and van der Schaft (2000)),
- stability analysis (Johansson and Rantzer (1998a), Decarlo et al. (2000)),
- controllability and observability analysis (Bemporad et al. (2000a); Vidal et al. (2003b); Babaali and Egerstedt (2004); Collins and van Schuppen (2004)),
- control (Rantzer and Johansson (2000); Rodrigues et al. (2000); Rodrigues and How (2001); Hedlund and Rantzer (2002)),
- verification (Bemporad et al. (2000c)) and
- approximation of nonlinear systems with PWA systems (van Bokhoven (1981); Angelis (2001)).

In addition, under mild assumptions discrete-time PWA systems are equivalent to several other hybrid modelling formalisms (Heemels et al. (2001)), such as mixed logic dynamical systems (Bemporad and Morari (1999)), linear complementarity systems (van der Schaft and Schumacher (1996); Heemels (1999); Heemels et al. (2000)), and min-max-plus-scaling systems (De Schutter and van den Boom (2001)), which makes the transfer of techniques and tools from one class to another possible.

We will study observer design and identification techniques mainly for subclasses of PWA systems.

1.3 Observer design for hybrid systems

The first topic that will be considered in this thesis is the observer design for hybrid systems. Loosely speaking, the goal of an observer is to obtain an estimate of the current state of the hybrid system, given the model and the input-output data.

The state estimation problem for hybrid systems has been considered before. Observer designs for switched linear systems when the currently active mode is known were presented in Alessandri and Coletta (2001a,b, 2003); Iulia Bara et al. (2000); Schinkel et al. (2003). We will briefly present one such design below.

A more difficult case, when the discrete mode is not known is presented in Balluchi et al. (2002). In that work the proposed observers use discrete inputs and outputs of the discrete-time hybrid plant, augmented with discrete signals derived from the continuous measurements when necessary, to obtain an estimate of the mode. Subsequently, the estimate of the continuous state can be obtained, for example, using the techniques of Alessandri and Coletta (2001a,b, 2003); Iulia Bara et al. (2000). The designed observers correctly identify the mode of the plant after a finite number of time steps, and the continuous observation error exponentially converges to a bounded set.

Another approach, based on moving horizon estimation was presented in Ferrari-Trecate et al. (2002). This approach is applicable to the general class of discrete-time piecewise affine systems, but it is computationally demanding, which may be an obstacle for implementing it in applications with limited computational resources.

For the observer to function properly, the underlying system has to be *observable*. Observability is the property of the observed system that ensures that the state of the system can be uniquely recovered from the measurements of the system's outputs, for any input signal. Precise definitions of observability and results for some classes of piecewise affine and switched systems can be found in Bemporad et al. (2000a), Collins and van Schuppen (2004), Babaali and Egerstedt (2004), Vidal et al. (2003a).

In this thesis we will present observer designs for two classes of hybrid systems. We will first consider systems of Lur'e type with a set-valued nonlinearity in the feedback path. Mechanical systems with dry friction are an important practical example that belongs to this class. The second considered class is a class of bimodal piecewise affine systems. The dynamics of several practical systems, such as suspension bridges and building cranes belongs to this class. We will consider the case when the discrete mode is not known. The considered class of systems has a more restricted structu-

re than the classes of hybrid systems studied in Balluchi et al. (2002) and Ferrari-Trecate et al. (2002). However, we propose more direct and less computationally demanding approach to state estimation.

When the discrete mode of the hybrid system is known, the observer design simplifies considerably. Consider the continuous-time switched linear system:

$$\begin{aligned}\dot{x}(t) &= A_{\sigma(t)}x(t) + B_{\sigma(t)}u(t) \\ y(t) &= C_{\sigma(t)}x(t)\end{aligned}\tag{1.2}$$

for $t \geq 0$ where $x(t) \in \mathbb{R}^n$ is the state vector, $u(t) \in \mathbb{R}^p$ is the input vector, $y(t) \in \mathbb{R}^m$ is the measurement vector, and $\sigma : [0, \infty) \mapsto \{1, 2, \dots, N\}$ is a switching function that maps time into an index set $\{1, 2, \dots, N\}$, where $N > 1$ is the number of modes. The switching sequence is arbitrary, but *known*, i.e. the value $\sigma(t)$ is available at each time t .

A switching observer for the system (1.2) can be taken in the following form:

$$\begin{aligned}\dot{\hat{x}}(t) &= A_{\sigma(t)}\hat{x}(t) + B_{\sigma(t)}u(t) + L_{\sigma(t)}(\hat{y}(t) - y(t)), \quad t \geq 0 \\ \hat{y}(t) &= C_{\sigma(t)}\hat{x}(t)\end{aligned}\tag{1.3}$$

The observer design consists in determining observer gains L_i for indices $i \in \{1, 2, \dots, N\}$.

The design of the observer (1.3) is straightforward. The dynamics of the estimation error $e := x - \hat{x}$ is given by:

$$\dot{e}(t) = (A_{\sigma(t)} - L_{\sigma(t)}C_{\sigma(t)})e(t).\tag{1.4}$$

The estimation error is governed by a switched system. To ensure stability of the error dynamics it is not sufficient to stabilize each of the modes separately, as the switching among several stable systems may still yield unstable behavior (Branicky (1998)).

To ensure stability under arbitrary switching we search for a common quadratic Lyapunov function (for details see Liberzon et al. (1999); Johansson and Rantzer (1998a)) of the form

$$V(e) = e^\top P e,$$

where $P = P^\top > 0$, such that

$$\dot{V}(e(t)) < 0,$$

along the trajectories of (1.4), when $e \neq 0$. This yields the following proposition:

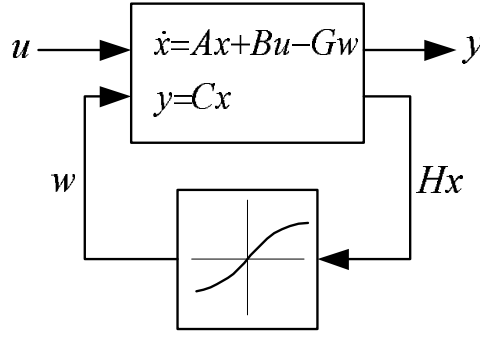


Figure 1.3: Lur'e system

Proposition 1.3.1 (Alessandri and Coletta (2001a)) Consider the system (1.2) and the observer (1.3). If there exist a symmetric positive definite matrix P and observer gains L_1, \dots, L_N such that:

$$(A_i - L_i C_i)^\top P + P(A_i - L_i C_i) < 0, \quad i = 1, 2, \dots, N, \quad (1.5)$$

then the estimation error (1.4) is globally asymptotically stable¹.

Proposition 1.3.1 gives an answer to the question how to design the observer when the current mode of the hybrid system is known. But, how to design the observer when the current mode of the observed system is not known?

To gain some insight into this problem we will consider a linear system interconnected in a feedback configuration with a static nonlinearity (see figure 1.3). This class of systems is known as Lur'e systems (Vidyasagar (1993)).

We start by considering the case studied in Arcak and Kokotović (2001). Consider the *locally Lipschitz* nonlinear system:

$$\begin{aligned} \dot{x}(t) &= Ax(t) + Bu(t) + G\gamma(Hx(t)) \\ y(t) &= Cx(t) \end{aligned} \quad (1.6)$$

where $x(t) \in \mathbb{R}^n, y(t) \in \mathbb{R}^m, u(t) \in \mathbb{R}^p, H \in \mathbb{R}^{1 \times n}$ and the static nonlinear function $\gamma : \mathbb{R} \mapsto \mathbb{R}$ satisfies a *slope bound* condition:

$$0 \leq \frac{\gamma(v) - \gamma(w)}{v - w} \leq b, \quad \forall v, w \in \mathbb{R}, v \neq w. \quad (1.7)$$

¹for a definition of global asymptotic stability see e.g. Vidyasagar (1993)

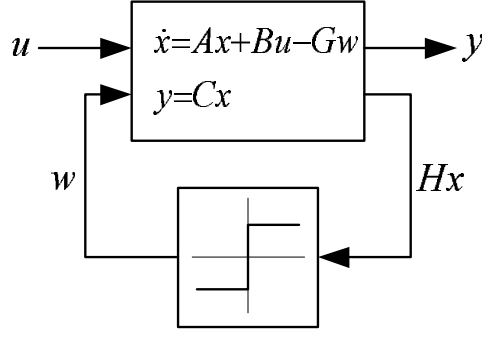


Figure 1.4: Relay system

For this system a Luenberger-type observer (1.6) of the form:

$$\begin{aligned}\dot{\hat{x}}(t) &= A\hat{x}(t) + Bu(t) + L(\hat{y}(t) - y(t)) + G\gamma(H\hat{x}(t) + K(\hat{y}(t) - y(t))) \\ \hat{y}(t) &= C\hat{x}(t)\end{aligned}\quad (1.8)$$

was chosen.

The design of an observer (1.8) consists of finding gains L and K , such that the estimation error dynamics $e = x - \hat{x}$ is stable. The solution is given by the following proposition.

Proposition 1.3.2 (Arcak and Kokotović (2001)) *If a matrix $P = P^\top > 0$, a constant $\nu > 0$ and observer gains L and K can be found such that:*

$$\begin{bmatrix} (A + LC)^\top P + P(A + LC) + \nu I & PG + (H + KC)^\top \\ G^\top P + (H + KC) & -2/b \end{bmatrix} \leq 0 \quad (1.9)$$

then the estimation error is globally exponentially stable.

Several classes of hybrid systems, such as relay systems (figure 1.4), linear complementarity systems and electrical circuits with switching elements can be described as Lur'e-type systems, but the nonlinearities in the feedback path are neither smooth, nor locally Lipschitz. This poses serious problems, as even the existence and uniqueness of solutions is not guaranteed any more, and the proposition 1.3.2 does not apply.

How to design the observer for these classes of systems? Intuitively, one might set $b = \infty$ in (1.9), and try to design the observer by solving the resulting matrix inequality. Will this approach yield an useable observer?

The answer to the previous question is “Yes”. However, to establish an observer design procedure and formally prove that it is correct we have to resort to the framework of convex analysis (Tyrell Rockafellar (1970); Tyrell Rockafellar and Wets (1998)) and differential inclusions (Aubin and Cellina (1984); Brezis (1973)). We will consider absolutely continuous solutions, as this is the standard solution concept used in the literature on differential inclusions. The main problems are to characterize the set of admissible nonlinearities, to prove that the designed observers have solutions and that solutions are unique, and finally, that the observers indeed provide an estimate of the state of the observed system. These problems will be studied further in chapter 2.

To see how the result of proposition 1.3.2 can be applied for another class of hybrid systems, consider the case of system (1.6) with:

$$\gamma(Hx) = \max(0, Hx).$$

This nonlinearity satisfies (1.7) with $b = 1$. Then the system (1.6) is equivalent to:

$$\begin{aligned} \dot{x}(t) &= \begin{cases} A_1 x(t) + Bu(t), & \text{if } Hx(t) \leq 0 \\ A_2 x(t) + Bu(t), & \text{if } Hx(t) > 0 \end{cases} \\ y(t) &= Cx(t), \end{aligned} \quad (1.10)$$

where $A_2 = A_1 + GH$, and the observer (1.8) becomes

$$\begin{aligned} \dot{\hat{x}}(t) &= \begin{cases} A_1 \hat{x}(t) + Bu(t) + L(\hat{y}(t) - y(t)), & \text{if } H\hat{x}(t) + K(\hat{y}(t) - y(t)) \leq 0 \\ A_2 \hat{x}(t) + Bu(t) + L(\hat{y}(t) - y(t)), & \text{if } H\hat{x}(t) + K(\hat{y}(t) - y(t)) > 0 \end{cases} \\ \hat{y}(t) &= C\hat{x}(t) \end{aligned} \quad (1.11)$$

The system (1.10) is a bimodal piecewise linear system, where the vector field that governs the evolution of the system is continuous over the switching plane $Hx = 0$. The observer (1.11) is a bimodal piecewise linear system, with a continuous vector field. Moreover, the observer (1.11) does not require the information about the currently active linear dynamics of the system (1.10), yet it is still able to recover the state of the observed system.

How to treat the more general case, when the observed system and the designed observer are discontinuous? Proposition 1.3.2 does not provide an answer to this question. We will address this question in chapter 3.

1.4 Identification of hybrid systems

As discussed in section 1.1 the second main problem considered in this thesis is the identification of hybrid systems. The goal of identification is to construct a model of the system within a given model class, based on the input-output data. Research on the identification of hybrid systems has been mainly concerned with the construction of PieceWise AutoRegressive eXogenous (PWARX) models, which form a subclass of piecewise affine (PWA) systems. In this thesis we will also be concerned with the identification of PWARX models.

As will be discussed in the sequel, the PWARX identification problem can be cast as a problem of piecewise affine regression. The problem of PWA regression has been considered before, mainly in the neural networks community, and to date several approaches exist (see Roll et al. (2004) for an overview). As pointed out in Roll et al. (2004) most of the existing approaches can construct only continuous maps, while the approaches that allow for discontinuities started appearing only recently (Ferrari-Trecate et al. (2001, 2003); Bemporad et al. (2003); Vidal et al. (2003b)). We are mainly interested in methods that can construct discontinuous maps.

PWARX models are a hybrid generalization of classical ARX models, obtained when the regressor space is partitioned into a finite number of convex polyhedral regions, and an ARX model is defined over each of the regions. A PWARX model has the form:

$$y(k) = f(x(k)) + e(k), \quad (1.12)$$

where $e(k)$ is an unmeasured disturbance term, and

$$f(x) = \begin{cases} \theta_1^\top \begin{bmatrix} x \\ 1 \end{bmatrix} & \text{if } x \in \mathcal{X}_1 \\ \vdots \\ \theta_s^\top \begin{bmatrix} x \\ 1 \end{bmatrix} & \text{if } x \in \mathcal{X}_s \end{cases} \quad (1.13)$$

is a piece-wise affine map, and $x(k)$ is a vector of regressors, defined as

$$x(k) = \begin{bmatrix} y(k-1) & \dots & y(k-n_a), & u(k-1)^\top & \dots & u(k-n_b)^\top \end{bmatrix}^\top. \quad (1.14)$$

In (1.14) $y(k) \in \mathbb{R}$ and $u(k) \in \mathbb{R}^p$ represent the measured output and the input of the system, respectively. We will assume that the model orders n_a

and n_b are given. The sets \mathcal{X}_i are assumed to be convex polyhedrons, with mutually non-intersecting interiors.

The identification task consists of determining the unknown parameters of the piecewise affine map f (i.e. $\theta_1, \dots, \theta_s, \mathcal{X}_1, \dots, \mathcal{X}_s$), given the data set $\{(x(k), y(k))\}_{k=1}^T$. Thus, the PWARX identification problem coincides with the PWA regression problem (Ferrari-Trecate et al. (2003)).

Example 1.4.1 As an illustration consider the following PWA map:

$$f(x) = \begin{cases} \begin{bmatrix} 0.5 & 0.5 \end{bmatrix} \begin{bmatrix} x \\ 1 \end{bmatrix}, & \text{if } x \leq 0 \\ \begin{bmatrix} -1 & 2 \end{bmatrix} \begin{bmatrix} x \\ 1 \end{bmatrix}, & \text{if } x > 0. \end{cases} \quad (1.15)$$

The map (1.15) is depicted in figure 1.5. The data set for identification, consisting of pairs $(x(k), y(k))$ for $k = 1, 2, \dots, 100$, is depicted in figure 1.6. If we assume that the number of modes $s = 2$ is given, the identification task is to determine parameters θ_1, θ_2 and to estimate the regions of the regressor space $\mathcal{X}_1, \mathcal{X}_2$, where each of the submodels is valid. Note that in this case the region estimation amounts to finding a point $x_0 \in \mathbb{R}$ that separates \mathcal{X}_1 from \mathcal{X}_2 . In the original map (1.15) $x_0 = 0$.

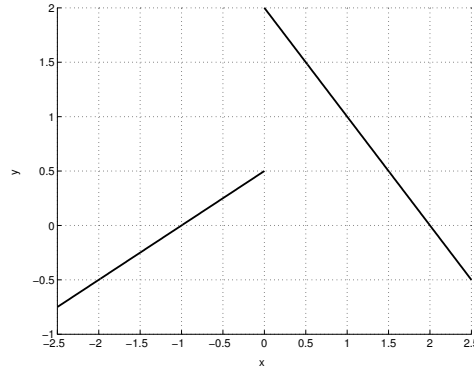


Figure 1.5: Piecewise affine map

If the regions \mathcal{X}_1 and \mathcal{X}_2 were known, the identification problem would boil down to two linear regression problems. In our example it is possible to do a direct search for x_0 , so as to get a good model, but this becomes

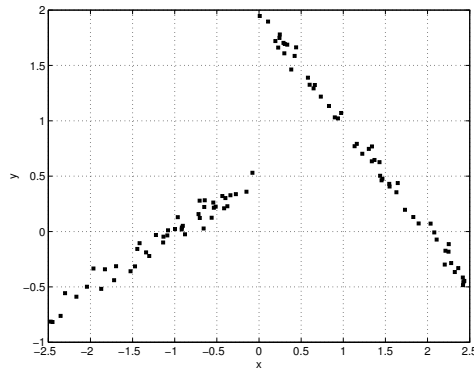


Figure 1.6: Collected data set

infeasible for higher dimensional maps and/or maps with higher number of submodels.

Another possible approach is to try to *classify* the data first, i.e. to assign each data pair $(x(k), y(k))$ to one of the submodels, and to determine the parameters θ_1 and θ_2 subsequently. When the classification problem is solved, the problem of region estimation is to find polyhedral surfaces in the regressor space that mutually separate different groups of data points. The latter problem has been studied extensively in the pattern recognition community, and can be solved using techniques such as support vector machines (SVM) (Vapnik (1998)) or multi-category robust linear programming (MRLP) (Bennet and Mangasarian (1994)).

In our example, we have $s = 2$ modes, $T = 100$ data points and the total number of possible data classifications is $2^{100} = 1.26 \cdot 10^{30}$. Finding the optimal classification is in most cases computationally infeasible, and therefore suboptimal techniques have to be considered. Here, we will briefly present three existing procedures: the clustering-based procedure (Ferrari-Trecate et al. (2003)), the greedy procedure (Bemporad et al. (2003)) and the algebraic procedure (Vidal et al. (2003b)).

The rationale behind the *clustering-based procedure* is that regressors that lie close to each other in the regressor space are likely to belong to the same region, and consequently to the same ARX model. For each data pair $(x(k), y(k))$ a local data set \mathcal{C}_k is built, containing $c > n_a + n_b + 1$ nearest data points. For each local data set \mathcal{C}_k a parameter estimate θ^k can be obtained, using e.g. least squares criterion. Parameter estimates obtained from local data sets that belong to the same ARX submodel will be similar, i.e. they

will form a cluster in the parameter space. Suboptimal clustering techniques are subsequently used to recover s clusters in the parameter space. The mapping of the data points onto the parameter space is bijective. The data points that belong to the same cluster are classified to the same mode. The clustering procedure will be treated in more detail in section 4.3.

In the *greedy procedure* a bound $\delta > 0$ on the prediction error is selected. Each data pair $(x(k), y(k))$ should satisfy

$$\|y(k) - \theta_i^\top [x(k)^\top \ 1]^\top\| \leq \delta, \quad \forall k = 1, \dots, T, \quad (1.16)$$

for some θ_i . The system of linear inequalities (1.16) is in general infeasible for a single parameter vector θ , hence, it should be partitioned in the minimal number of feasible subsystems \bar{s} , and the corresponding parameter vectors $\{\theta_i\}_{i=1}^{\bar{s}}$ should be determined. Unfortunately, the problem of partitioning (1.16) into a minimal number of feasible systems of inequalities is NP-hard, and only a suboptimal algorithm based on thermal relaxations is proposed to solve it. The outcome is the set of parameter vectors $\{\theta_i\}_{i=1}^s$. Data point $(x(k), y(k))$ is classified to the mode i if it satisfies (1.16) for θ_i .

Example 1.4.2 Assume that we identified the PWA map from example 1.4.1 using the greedy procedure on the given data set, and that the parameter vectors θ_1 and θ_2 were estimated perfectly. In the figure 1.7 we plotted the data set for the PWA map (1.15), together with the chosen bound on the prediction error $\delta = 0.2$. Most of the data points satisfy (1.16) for only one parameter vector. However there are a few points (around (1, 1)) that satisfy (1.16) for both parameter vectors. How to classify those points? If incorrectly classified, those data points can foil the region estimation.

In Bemporad et al. (2003) data points satisfying (1.16) for more than one θ_i are called *undecidable*. Undecidable points are discarded during the region estimation. While discarding undecidable points is arguably better than wrongly classifying them, we still loose the information that those points may carry.

The *algebraic procedure* (Vidal et al. (2003b)) approaches the problem of identifying a PWARX model as an algebraic geometric problem. In the *noiseless case* ($e = 0$) the data pair $(x(k), y(k))$ satisfies the equality

$$y(k) - [x(k)^\top \ 1]^\top \theta_i = 0 \quad (1.17)$$

for one of the parameter vectors θ_i . Hence, the equality

$$\prod_{i=1}^s (y(k) - \theta_i^\top [x(k)^\top \ 1]^\top) = 0, \quad (1.18)$$

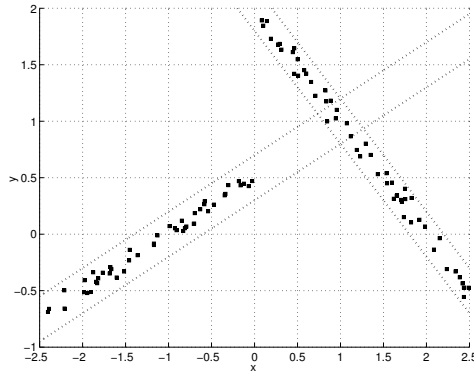


Figure 1.7: Data set with error bounds

always holds. In Vidal et al. (2003b) it is shown that parameters θ_i can be recovered as a solution of a system of polynomial equations resulting from (1.18). Data pair $(x(k), y(k))$ is classified to the submodel μ satisfying the rule:

$$\mu(k) = \arg \min_{1 \leq i \leq s} (y(k) - [x(k)^\top \ 1]^\top \theta_i)^2. \quad (1.19)$$

Example 1.4.3 Consider again the example 1.4.2 and assume that parameters θ_1 and θ_2 are identified perfectly using the algebraic procedure. Then, it is probable that the classification rule (1.19) will wrongly classify some of the “undecidable” data points. (see Niessen et al. (2004) for details)

If noise is present in the identification data set, then solving the set of polynomial equations (1.18) frequently gives complex numbers as parameter values, and the procedure fails. As a consequence, the applicability of the algebraic procedure seems to be limited in practical situations.

We will start our study in hybrid identification with an experimental case study in chapter 4. We will use the clustering-based procedure to identify the model of the electronic component placement process in pick-and place machines (cf. figure 1.2). This experimental work will demonstrate that identification is indeed a viable way of obtaining hybrid models in practice, and will also show the need for incorporating the a priori knowledge into the identification procedures.

Example 1.4.4 Consider again figure 1.2. Although the mode switch does not always occur at a fixed height of the head (because of the dynamics of

the PCB), with a degree of certainty data points below² a certain height may be attributed to the free mode, and, analogously data points above a certain height may be attributed to the impact mode. Data points that belong to saturations can also be distinguished. We would like to use this information on the modes of the physical system and to force the identification procedure to identify the model where modes can be interpreted in terms of free, impact and saturation modes of the physical system.

None of the three procedures presented above is equipped to include such requirements. In chapter 5 we will develop a novel identification procedure, that is able to handle the provided a priori knowledge. In our procedure the unknown parameters are treated as random variables, and described with probability density functions. The available a priori knowledge may be formulated by choosing the a priori probability density function of the parameter. We will classify the data one point at a time, and refine the a priori information using Bayes' rule. We will also provide a way to use the "undecidable" data points, without discarding them (cf. examples 1.4.2 and 1.4.3).

1.5 Experiments

To bridge the gap that exists between the theory and practice we include three experimental case studies to complement the theoretical results of the thesis. This will demonstrate the applicability of the presented theoretical results.

In chapter 2 we will present a case study on a drill-string setup. This experimental setup is realized at the Dynamics and Control Technology laboratory at the Mechanical Engineering Department of the Eindhoven University of Technology. A number of friction induced and vibration phenomena can be observed in the setup. An accurate model of the setup was obtained by Mihajlović et al. (2004). For our purposes we will use a simplified model in the form of Lur'e system with a non-smooth set-valued friction law. Our model can describe some of the friction induced phenomena, most notably friction induced slip-stick oscillations. Slip-stick oscillations have a hybrid character, as slip and stick modes can be clearly distinguished. We will design and implement an observer and demonstrate that the designed observer is able to accurately reconstruct the unmeasured states of the setup, under the conditions captured by the model. Practical systems with similar dy-

²Position axis is pointing downwards. See chapter 4 for details.

namics, for example, are deep-sea oil-drilling equipment with a drill-string, and rotor mechanical systems with dry friction.

In chapter 3 we will design an observer for a piecewise linear beam with a one-sided spring. This experimental setup is also realized at the Dynamics and Control Technology laboratory at the Mechanical Engineering Department of Eindhoven University of Technology. Starting from a finite element model and using model reduction techniques the model of the setup was obtained in the form of a bimodal piecewise linear system with continuous dynamics. We will demonstrate that the designed observer is able to reconstruct the state of the system with the accuracy that is commensurate to the accuracy of the model. Practical systems with similar dynamics are, for example, suspension bridges and building cranes.

In chapters 4 and 5 we will identify the process of the electronic component placement in pick-and-place machines. This experimental setup was realized at the Electrical Engineering Department of the Eindhoven University of Technology, in collaboration with the company Assembleon from Eindhoven. Unilateral constraints and saturation phenomena characterize the hybrid dynamics of the process. We will obtain models of the process in the PWARX form, first with the clustering-based procedure and subsequently with our newly developed identification procedure. We will demonstrate that PWARX models are able to capture the dynamics of the setup. We will also demonstrate how to use physical insights and a priori knowledge in order to improve the results of the identification.

1.6 Overview

The main results of this thesis are presented in four chapters, which are based on published or submitted papers. In chapter 2 we will design observers of Luenberger type for the class of Lur'e systems with set valued maps in the feedback path. We will present novel theoretical analysis which proves that the designed observers are well-posed (i.e. that there exists exactly one solution to the observer dynamics) and that they asymptotically reconstruct the state of the observed system. Our results will be illustrated on the experimental case study with a drill-string setup.

In chapter 3 we will consider a class of bimodal piecewise affine systems, and propose a novel constructive procedure for the design of Luenberger type observers. When the dynamics of the observed system is continuous, the proposed observers are able to asymptotically reconstruct the state, i.e. the estimation error dynamics is globally asymptotically stable. In the case

of discontinuous dynamics the obtained observers have bounded estimation error with respect to the state of the observed system. We will illustrate our results by several academic examples, and an experimental example of a piecewise linear beam with a one sided spring.

In chapter 4 we present an experimental study in the identification of an electronic component placement process in pick-and-place machines. We will identify hybrid models of the process, using the clustering-based procedure. We will show that the identified models are able to capture the relevant dynamics of the experimental setup. This case study yields many practical insights into hybrid system identification, and highlights the need for incorporating the available a priori knowledge into the identification procedure.

In chapter 5 we will develop a new identification procedure that is able to include the provided a priori knowledge. We will treat the unknown model parameters as random variables, and describe them with their probability density functions. The available a priori knowledge may be formulated by choosing the a priori probability density function of the parameter. Subsequently, the identification algorithm will process the provided data set and recursively compute the a posteriori probability density functions of the parameters using Bayes' rule. We will present a modification of the multicategory robust linear programming procedure, which uses information from the classification phase of the algorithm. We will also demonstrate how to identify the model of the electronic component placement process using the newly derived procedure.

In chapter 6 we summarize the main results and conclusions of the thesis. We also offer some ideas and directions for future research.

Observer Design for Lur'e Systems with Multivalued Mappings

2.1 Introduction 2.2 Preliminaries 2.3 Problem statement	2.4 Main results 2.5 Experimental example 2.6 Conclusions
--	---

In this paper we present a constructive observer design procedure for a class of nonsmooth dynamical systems, namely systems of Lur'e type with a monotone multivalued mapping in the feedback path. Examples of such systems include various classes of hybrid systems, such as relay systems, linear complementarity systems, electrical circuits with switching elements and certain piece-wise affine systems. Under the assumption that the observed system is well behaved, we prove that the proposed observers are well-posed (i.e. that there exists a unique solution to the observer dynamics), and that the observer asymptotically recovers the state of the observed system. The results are illustrated on an experimental case study with a drill-string setup.

This chapter is based on Juloski et al. (2004a). The experimental work presented in section (2.5) was preformed together with N. Mihajlović, and is also a part of his PhD work.

2.1 Introduction

In this paper an observer design procedure for systems of Lur'e type with maximal monotone multivalued mapping in the feedback path (see figure 2.1) is developed. A multivalued or set-valued mapping is a mapping that assigns a set of possible values to its input argument, and the output of the mapping can be any value in this set. The requirements that the mapping is maximal and monotone generalize the usually considered concept of continuous, sector bounded nonlinearity (Vidyasagar (1993)). Systems of the

considered type may arise as a natural consequence of modelling (e.g. models of friction phenomena, ideal diodes), or the used solution concept (e.g. Filippov solutions (Filippov (1988))).

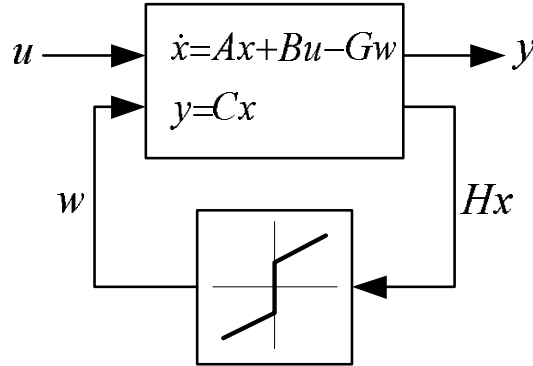


Figure 2.1: Lur'e type system with maximal monotone multivalued mapping

Examples of systems obtained by interconnecting linear dynamics in a feedback configuration with maximal monotone mapping, as in figure 2.1, include various classes of hybrid systems: certain piece-wise linear systems (Sontag (1981); Johansson and Rantzer (1998b)) (fig. 2.2a), linear relay systems Johansson et al. (1999) (figure 2.2b), linear complementarity systems (Heemels et al. (2000); van der Schaft and Schumacher (1998, 1996)) (figure 2.2c), and electric circuits with switching elements (e.g. ideal diodes, fig. 2.2c, MOS transistors, characteristic in fig. 2.2d).

Two observer structures are proposed in the paper, which are based on rendering the linear part of the error dynamics strictly positive real (SPR). As the considered class of systems and the proposed observers are non-smooth, tools of nonsmooth analysis are needed to formally analyze and prove their properties. Since the considered systems can be non-Lipschitz, existence and uniqueness of solutions (i.e. well-posedness) of the system and observer is not guaranteed. Under the natural assumption that there exists a solution of the observed system, it is proven that there exists a solution of the proposed observer, and that this solution is unique. Well-posedness of the system is an important theoretical question, and, from a practical standpoint, if an observer is to be numerically implemented, well-posedness is necessary to ensure the proper behavior of the implementation.

From the existence of solutions to both the observed system and the observer, the existence of solutions to the error dynamics follows. It is further

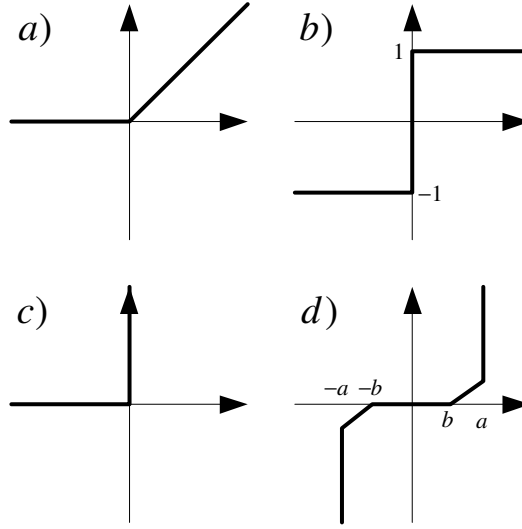


Figure 2.2: Examples of maximal monotone mappings

shown that the observer recovers asymptotically the state of the observed system (i.e. that the error dynamics is globally asymptotically stable). These results are illustrated on the experimental drill-string setup, with the set-valued dry friction with Stribeck effect (Mihajlović et al. (2004)).

Stability of Lur'e type systems with SPR linear part and the discontinuous nonlinearity has been studied in Yakubovich (1964,1965), but the problem of existence and uniqueness of solutions for this systems was not considered. Existence and uniqueness of solutions, as well as stability of autonomous Lur'e type systems with maximal monotone nonlinear mappings have been studied in Brogliato (2004). The main results in this paper generalize results from Brogliato (2004) to the case of systems with external inputs.

An observer design methodology for Lur'e type systems with *locally Lipschitz* slope restricted nonlinearities was studied before in Arcak and Kokotović (2001). However, since nonsmooth and non-Lipschitz nonlinearities are allowed in the system studied here, the results of Arcak and Kokotović (2001) are not applicable, and we have to resort to a framework of convex analysis, to establish an observer design procedure for the considered class of systems.

The paper is structured as follows. In section 2.2 some basic concepts of convex analysis and differential inclusions are given. The material in this

section is taken from Tyrell Rockafellar (1970); Aubin and Cellina (1984); Brezis (1973). In section 2.3 the observer design problem is formally stated. Section 2.4 contains the main results of the paper. The experimental example of the drill-string system is presented in section 2.5, and conclusions are presented in section 2.6.

2.2 Preliminaries

With $\mathcal{L}_{loc}^1[0, \infty)$ and $\mathcal{L}_{loc}^2[0, \infty)$ we denote the Lebesgue spaces of locally integrable and square integrable functions defined on $[0, \infty)$.

A mapping $\rho : \mathbb{X} \rightarrow \mathbb{Y}$, where $\mathbb{X}, \mathbb{Y} \subseteq \mathbb{R}^l$, is said to be *multivalued* if it assigns to each element $x \in \mathbb{X}$ a subset $\rho(x) \subset \mathbb{Y}$ (which may be empty). The domain of the mapping $\rho(\cdot)$, $\text{dom } \rho$ is defined as $\text{dom } \rho = \{x | x \in \mathbb{X}, \rho(x) \neq \emptyset\}$. We define the graph of the mapping ρ as:

$$\text{Graph } \rho = \{(x, x^*) \mid x^* \in \rho(x)\}. \quad (2.1)$$

A multivalued mapping ρ is said to be *monotone*, if

$$\forall x_1, x_2 \in \text{dom } \rho, \quad \forall x_1^* \in \rho(x_1) \forall x_2^* \in \rho(x_2) \quad \langle x_1^* - x_2^*, x_1 - x_2 \rangle \geq 0, \quad (2.2)$$

where $\langle \cdot, \cdot \rangle$ denotes the inner product. For example, the set-valued mapping depicted in figure 2.3 is monotone. It is easy to see that the condition (2.2) is satisfied for every $x_1, x_2 \in \mathbb{R}$.

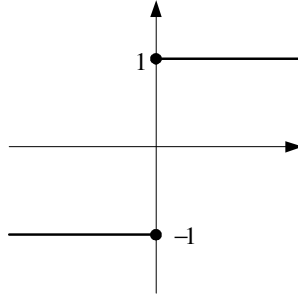


Figure 2.3: Monotone mapping

A multivalued mapping ρ is said to be *maximally monotone* if its graph is not strictly contained in the graph of any other monotone mapping. In other words, maximality means that new elements can not be added to the $\text{Graph } \rho$ without violating the monotonicity of the mapping. All the

examples in figure 2.2 are maximal monotone mappings. The monotone mapping depicted in the figure 2.3 is not maximal. Namely, by adding any pair of the form $(0, a)$ where $-1 < a < 1$ to the graph of this mapping, we can obtain a monotone mapping whose graph strictly contains a graph of the mapping depicted in the figure 2.3. Maximally monotone “completion” of the mapping from figure 2.3 is depicted in the figure 2.2b.

A *differential inclusion* (DI) is given by an expression of the form

$$\dot{x} \in F(t, x) \quad (2.3)$$

where F is a set-valued mapping, that associates to the state x of the system and time t the set of admissible velocities. An *absolutely continuous* (AC) function $x : \mathbb{R}^+ \mapsto \mathbb{R}^n$ is considered to be a *strong solution* of the DI (2.3) if (2.3) is satisfied almost everywhere. A point x_0 is a *fixed point* (*equilibrium*) of the DI (2.3) if:

$$0 \in F(t, x_0), \quad \forall t \quad (2.4)$$

For an exposition on differential inclusions see e.g. Aubin and Cellina (1984).

An important result concerning differential inclusions of the form

$$\dot{x}(t) \in -A(x(t)), \quad x(0) \in \text{dom } A \quad (2.5)$$

where A is a maximal monotone mapping is that there exists a unique strong solution x , defined on $[0, \infty)$ (Brezis, 1973, section 3.1), (Aubin and Cellina, 1984, chapter 3).

To generalize the previous result to nonautonomous DIs we consider the system of the form:

$$\dot{x}(t) \in -A(x(t)) + u(t), \quad x(0) \in \text{dom } A \quad (2.6)$$

where A is a multivalued mapping and the external input signal $u \in \mathcal{L}_{loc}^1[0, \infty)$. Following (Brezis, 1973, section 3.2) we define a continuous function x to be a *weak solution* to (2.6) if there exist sequences $u_n \in \mathcal{L}_{loc}^1[0, \infty)$ and $x_n \in \mathcal{C}[0, \infty)$ such that x_n is a strong solution to

$$\dot{x}_n \in -A(x_n(t)) + u_n,$$

$u_n \rightarrow u$ in $\mathcal{L}_{loc}^1[0, \infty)$ sense and $x_n \rightarrow x$ uniformly on $[0, \infty)$.

Proposition 2.2.1 (Brezis, 1973, theorem 3.4) *For the case when the mapping A in (2.6) is maximal monotone mapping there exists a unique weak solution x to (2.6) for every $u \in \mathcal{L}_{loc}^1[0, \infty)$.*

The proof of the proposition 2.2.1 is based on *Yoshida* approximations (Aubin and Cellina (1984); Brezis (1973)). Given $\lambda > 0$ and the maximal monotone multivalued mapping A , Yoshida approximation A_λ is globally Lipschitz¹ maximal monotone single-valued map, with the property that $A_\lambda \rightarrow A$ in a certain sense, as $\lambda \rightarrow 0$. It is further shown that solutions x_λ of the *differential equation*²

$$\dot{x}_\lambda = -A_\lambda(x_\lambda) + u$$

uniformly converge to the unique weak solution of the differential inclusion (2.6), as $\lambda \rightarrow 0$.

A difference between weak and strong solutions is that the weak solution, while continuous, is not necessarily absolutely continuous. However, the following holds:

Proposition 2.2.2 (*Brezis, 1973, proposition 3.2*): *For the case when the mapping A in (2.6) is a maximal monotone mapping we have the following properties:*

- *If a strong solution to (2.6) exists, it is unique*
- *Any AC function x which is a weak solution to (2.6) is also a strong solution to (2.6).*

Following (Wen, 1988, theorem 1), we call a linear system

$$\begin{aligned} \dot{x} &= Ax + Bu \\ y &= Cx, \end{aligned}$$

where B has full column rank (i.e. $\text{Ker}\{B\} = \emptyset$), strictly positive real (SPR) if there exist a $P = P^\top > 0$ and a $Q = Q^\top > 0$ such that:

$$PA + A^\top P = -Q \tag{2.7a}$$

$$B^\top P = C \tag{2.7b}$$

¹with Lipschitz constant $1/\lambda$

²as the mapping A_λ is globally Lipschitz these solutions exist and are unique

2.3 Problem statement

Consider the system whose state space equations are given by the following differential inclusion (see figure 2.1):

$$\dot{x} = Ax - Gw + Bu \quad (2.8a)$$

$$w \in \varrho(Hx) \quad (2.8b)$$

$$y = Cx \quad (2.8c)$$

where $Hx(0) \in \text{dom } \varrho$ and $A \in \mathbb{R}^{n \times n}$, $B \in \mathbb{R}^{n \times m}$, $G \in \mathbb{R}^{n \times l}$ is full column rank, $H \in \mathbb{R}^{l \times n}$ and $C \in \mathbb{R}^{p \times n}$. The mapping $\varrho : \mathbb{R}^l \rightarrow \mathbb{R}^l$ is assumed to be maximally monotone.

Remark 2.3.1 Certain multivalued mappings $\varrho(\cdot)$ that are not monotone, can be transformed into monotone mappings by using loop transformation technique (see for instance (Vidyasagar, 1993, section 5.6.2)). An example of such a mapping is given in figure 2.5, section 2.5. With loop transformation, a new mapping is defined, as $\tilde{\varrho}(z) = \varrho(z) - Mz$, where M is a matrix of appropriate dimensions, chosen so that the mapping $\tilde{\varrho}(z)$ is maximal monotone. If we then replace the system matrix A in (2.8) by $\tilde{A} = A - GMH$, we obtain a system (2.8) that satisfies the above mentioned assumptions.

We assume that for the system (2.8) the following holds.

Assumption 2.3.2 For all initial states $x(0)$ such that $Hx(0) \in \text{dom } \varrho$ and inputs $u \in \mathcal{L}_{loc}^1[0, \infty)$ of interest, we assume that the system (2.8) has a strong solution.

For a given system (2.8) one can check the existence of solutions using some of the general results that are available in the literature (Aubin and Cellina (1984); Brezis (1973)). Results on existence and uniqueness of solutions to particular instances of (2.8) (e.g. complementarity systems, relay systems, piecewise linear systems) can also be found in the literature (Heemels et al. (2000); Pogromsky et al. (2003); Filippov (1988); van der Schaft and Schumacher (1998, 1996); Çamlibel and Schumacher (2002); Çamlibel et al. (2003)).

The first proposed observer (“basic” observer scheme) for the system (2.8) has the following form:

$$\dot{\hat{x}} = (A - LC)\hat{x} - G\hat{w} + Ly + Bu \quad (2.9a)$$

$$\hat{w} \in \varrho(H\hat{x}) \quad (2.9b)$$

$$\hat{y} = C\hat{x} \quad (2.9c)$$

where $L \in \mathbb{R}^{n \times p}$ and $\hat{H}\hat{x}(0) \in \text{dom } \varrho(\cdot)$.

The second proposed observer (“extended” observer scheme) has the following form:

$$\dot{\hat{x}} = (A - LC)\hat{x} - G\hat{w} + Ly + Bu \quad (2.10a)$$

$$\hat{w} \in \varrho((H - KC)\hat{x} + Ky) \quad (2.10b)$$

$$\hat{y} = C\hat{x} \quad (2.10c)$$

where $K \in \mathbb{R}^{l \times p}$ and $\hat{x}(0)$ are such that $(H - KC)\hat{x}(0) + Ky(0) \in \text{dom } \varrho(\cdot)$.

The basic observer is a special case of the extended observer with $K = 0$. The reason for treating these two cases separately is that the well-posedness conditions for the two proposed observers (i.e. conditions for the existence and uniqueness of solutions) are somewhat different. Also, the well-posedness proofs are more readable if the cases are treated separately. Stability of the error dynamics will be treated only for the case of the extended observer, as the result for the basic observer follows then immediately.

2.4 Main results

The problem of observer design consists in finding the gain L (L , K , respectively) which will guarantee that there exists a unique solution \hat{x} for the observer dynamics on $[0, \infty)$, and that $\hat{x}(t) \rightarrow x(t)$ as $t \rightarrow \infty$. In this section we will prove that if L and K are chosen such that the triple $(A - LC, G, H)$ (respectively $(A - LC, G, H - KC)$) is SPR the obtained observer (2.9) ((2.10), respectively) will satisfy the mentioned requirements.

Before we prove this we will first show how the gains L and K can be computed such that $(A - LC, G, H - KC)$ is SPR. This can be achieved by solving the matrix inequality:

$$(A - LC)^\top P + P(A - LC) < 0 \quad (2.11a)$$

$$G^\top P = H - KC. \quad (2.11b)$$

Inequality (2.11) is a linear matrix inequality in variables $P, K, L^\top P$. For necessary and sufficient conditions for the existence of solutions for (2.11), see for instance, Arcak and Kokotović (2001) and references therein.

To prove that the SPR property of $(A - LC, G, H - KC)$ guarantees the well-posedness of the observer, we start of with two lemmas on well-posedness. Note that well posedness of the observers (2.9) and (2.10) is also essential in ensuring the proper behavior of a numerical implementation.

Lemma 2.4.1 *Consider the system (2.8) under assumption 2.3.2, and the observer (2.9). If the triple $(A - LC, G, H)$ is SPR, then the observer dynamics (2.9) has a unique weak solution on $[0, \infty)$.*

Proof: Since the triple $(A - LC, G, H)$ is SPR and G has full column rank there exist P, Q that satisfy (2.7). Introduce the change of variables in (2.9):

$$z = R\hat{x} \quad (2.12)$$

where $RR = P$. Then, (2.9) transforms into:

$$\dot{z} = R(A - LC)R^{-1}z - RG\hat{w} + RBu + RLy \quad (2.13a)$$

$$\hat{w} \in \varrho(HR^{-1}z) \quad (2.13b)$$

$$\hat{y} = CR^{-1}z \quad (2.13c)$$

Since $H\hat{x}(0) \in \text{dom } \varrho(\cdot)$, we have $HR^{-1}z(0) \in \text{dom } \varrho(\cdot)$. Define the mapping $f : \mathbb{R}^n \rightarrow \mathbb{R}^n$ as $f(z) = R^{-1}H^\top \varrho(HR^{-1}z)$. Note that using the SPR condition (2.7b), (2.13) can now be written as:

$$\dot{z} \in R(A - LC)R^{-1}z - f(z) + RBu + RLy \quad (2.14)$$

where $z \in \text{dom } f(\cdot)$. From the SPR condition (2.7b) it follows that H and HR^{-1} have full row rank, and together with the fact that ϱ is maximal monotone we have that f is maximal monotone as well (Tyrell Rockafellar and Wets, 1998, theorem 12.43).

From the SPR condition (2.7a) it follows that $R(A - LC)R^{-1} + R(A - LC^\top)R^{-1}$ is negative definite. Hence the mapping $z \rightarrow -R(A - LC)R^{-1}z + f(z)$ is maximal monotone (Tyrell Rockafellar and Wets, 1998, corollary 12.44). Since the control signal u lies in $\mathcal{L}_{loc}^1[0, \infty)$, by assumption 2.3.2, and y is AC, and hence $y \in \mathcal{L}_{loc}^1[0, \infty)$, existence and uniqueness of weak solutions to (2.14) and (2.9) follow from proposition 2.2.1. \blacksquare

Remark 2.4.2 The proof of lemma 2.4.1 extends the proof of lemma 1 in Brogliato (2004) to the non-autonomous case.

In the following lemma we address the questions of well-posedness of the extended observer scheme.

Lemma 2.4.3 *Consider the system (2.8), under assumption 2.3.2, and the observer (2.10). If the triple $(A - LC, G, H - KC)$ is SPR, the observer dynamics (2.10) has a unique weak solution on $[0, \infty)$.*

Proof: Since the triple $(A - LC, G, H - KC)$ is SPR and G has full column rank there exist P, Q that satisfy (2.7). Introduce the change of variables:

$$z = R(\hat{x} + g), \quad (2.15)$$

in (2.10), where, as before, $RR = P$ and define

$$g = (H - KC)^\top ((H - KC)(H - KC)^\top)^{-1} Ky. \quad (2.16)$$

From the SPR condition it follows that $H - KC$ has full row rank (as $H - KC = G^\top P$), and hence the inverse in (2.16) exists. Note that the part of the expression on the right hand side of (2.16) is a pseudo-inverse of $H - KC$. In the same way as in the proof of lemma (2.4.1), (2.10) transforms into:

$$\dot{z} \in R(A - LC)R^{-1}z - f(z) + RBu + RLy + R\dot{g} \quad (2.17)$$

where $z(0) \in \text{dom } f(\cdot)$. The multivalued mapping $-R(A - LC)R^{-1}z + f(z)$ is maximal monotone by similar arguments as in the proof of lemma 2.4.1. By assumption we have $u \in \mathcal{L}_{loc}^1[0, \infty)$, $y \in \mathcal{L}_{loc}^1[0, \infty)$. Moreover, y is AC and thus it follows that $\dot{g} \in \mathcal{L}_{loc}^1[0, \infty)$. By virtue of proposition 2.2.1, (2.17) and hence (2.10) posses a unique weak solution. ■

From lemmas 2.4.1 and 2.4.3 it follows that both proposed observers have, at least, weak solutions. To ensure the existence of strong solutions more stringent assumptions have to be imposed on the original system and proposed observers. If we consider again the inclusion (2.17), conservative sufficient conditions for existence of strong solutions are given for instance in (Brezis, 1973, theorem 3.6), which state that:

- $u \in \mathcal{L}_2^{loc}[0, \infty)$, $\dot{y} \in \mathcal{L}_2^{loc}[0, \infty)$
- there exists a proper convex lower semicontinuous function ξ with $\xi(z) \geq \delta$, for all z and some δ , such that:

$$-R(A - LC)R^{-1}z + f(z) = \partial\xi(z) \quad (2.18)$$

where $\partial\xi$ denotes the subdifferential of ξ (for details see Brezis (1973); Tyrell Rockafellar (1970); Tyrell Rockafellar and Wets (1998)). For (2.18) to hold, it is required that the mapping $z \rightarrow -R(A - LC)R^{-1}z + f(z)$ satisfies a property called maximal cyclic monotonicity. In our case this would mean that $R(A - LC)R^{-1}$ is symmetric positive semi-definite as shown in (Tyrell Rockafellar, 1970, chapter 24), and that ϱ can be written as $\varrho = \partial\varphi$ for some proper lower semicontinuous function φ (Tyrell Rockafellar, 1970, theorems 24.8, 24.9).

It is of interest to further explore the relation between weak and strong solutions of observers (2.9) and (2.10). However, we see the issue of weak versus strong solutions as largely technical, as the only additional requirement that needs to be imposed on weak solutions to get strong solutions is absolute continuity, which is needed to ensure that the solution is differentiable almost everywhere. Therefore, we make the following assumption.

Assumption 2.4.4 Weak solutions for observers (2.9) and (2.10) are AC (and thus, weak solutions are strong solutions by proposition 2.2.2).

For the extended observer (2.10) the observation error $e := x - \hat{x}$ dynamics can be formed as:

$$\dot{e} = (A - LC)e - G(w - \hat{w}) \quad (2.19a)$$

$$w \in \varrho(Hx) \quad (2.19b)$$

$$\hat{w} \in \varrho(H\hat{x} + K(y - \hat{y})) \quad (2.19c)$$

Note that the point e_0 is a fixed point (equilibrium) of system (2.19) for a given x -trajectory if it satisfies the following inclusion for all $t > 0$:

$$0 \in (A - LC)e_0 - G[\varrho(Hx(t)) - \varrho(H\hat{x}(t) + KCe_0)] \quad (2.20)$$

where $\hat{x}(t) = x(t) - e_0$. The following theorem states the main result of the paper.

Theorem 2.4.5 Consider the observed system (2.8) under assumption 2.3.2, the extended observer (2.10), where the triple $(A - LC, G, H - KC)$ is SPR, under assumption 2.4.4, and the observation error dynamics (2.19). The point $e = 0$ is the unique fixed point of the observation error dynamics (2.19) and is globally exponentially stable.

Proof: Note that $e_0 = 0$ is indeed a fixed point of (2.19). For $e_0 = 0$, $x = \hat{x}$, and since the arguments of the $\varrho(\cdot)$ mappings in (2.19b), (2.19c) are the same it follows that $0 \in \varrho(Hx(t)) - \varrho(H\hat{x}(t) + KCe_0)$ for all $t \geq 0$, and hence $e_0 = 0$ satisfies the inclusion (2.20).

Next, we show that $e_0 = 0$ is the only fixed point. From $(A - LC)e_0 \in G(\varrho(Hx) - \varrho(H\hat{x} + KCe_0))$ for all $t \geq 0$ it follows that $P(A - LC)e_0 \in PG(\varrho(Hx(t)) - \varrho(H\hat{x}(t) + KCe_0))$ for some t . Using the SPR condition (2.7b) we get the following condition for the fixed point e_0 :

$$e_0^\top P(A - LC)e_0 = ((H - KC)e_0)^\top (w - \hat{w})$$

where $w \in \varrho(Hx(t))$ and $\hat{w} \in \varrho(H\hat{x}(t) + KCe_0)$. From the SPR condition (2.7a) it follows that $e_0^\top P(A - LC)e_0 \leq 0$. From the monotonicity condition (2.2) for $\varrho(\cdot)$ it follows that $e_0^\top P(A - LC)e_0 = ((H - KC)e_0)^\top (w - \hat{w}) \geq 0$. Hence, $e_0 = 0$ is the only solution of the inclusion (2.20).

To show that the unique fixed point $e_0 = 0$ is globally exponentially stable consider the Lyapunov function $V = \frac{1}{2}e^\top Pe$. Since by assumption 2.3.2 x is AC, and by assumption 2.4.4 \hat{x} is AC it follows that e is also AC, and \dot{e} exists almost everywhere. Hence, V is also AC, and the derivative \dot{V} exists almost everywhere. \dot{V} satisfies:

$$\begin{aligned}\dot{V} &= e^\top P\dot{e} \\ &= e^\top P((A - LC)e - G(w - \hat{w})) \\ &= -\frac{1}{2}e^\top Qe - e^\top (H - KC)^\top (w - \hat{w}) \leq -\frac{1}{2}e^\top Qe\end{aligned}$$

for some w, \hat{w} satisfying (2.19b), (2.19c). From

$$V(t) \leq V(0) - \frac{1}{2} \int_0^t e^\top(\tau) Qe(\tau) d\tau$$

it follows that the AC function of time V is nonincreasing, and

$$\frac{1}{2} \lambda_{\min}(P) e^\top(t) e(t) \leq V(0) - \frac{1}{2} \int_0^t \lambda_{\min}(Q) e^\top(\tau) e(\tau) d\tau$$

where $\lambda_{\min}(\cdot)$ denotes the minimal eigenvalue. From Gronwall's lemma (Vidyasagar (1993)):

$$\frac{1}{2} \lambda_{\min}(P) e^\top(t) e(t) \leq V(0) \exp\left(-\frac{\lambda_{\min}(Q)}{\lambda_{\min}(P)} t\right). \quad (2.22)$$

This proves the exponential convergence of the observation error. ■

Remark 2.4.6 Solutions $\hat{x}(\cdot)$ of the observers (2.9) and (2.10) can be obtained using some of the numerical methods for solving differential inclusions. See e.g. the survey article Dontchev and Lempio (1992). To give one numerical method, we aim to approximate the solution $\hat{x}(\cdot)$ of the DIs (2.9) and (2.10) with a piecewise constant function $\eta(\cdot)$, where $\eta(t) = \eta(t_k)$ for $t \in [t_k, t_{k+1})$, $t_{k+1} - t_k = h$, for a given step size h . From the proofs of lemmas 2.4.1 and 2.4.3 it follows that both observers are of the form:

$$\dot{\hat{x}} \in -A(t, \hat{x}) \quad (2.23)$$

where $A(\cdot, \cdot)$ is a maximal monotone mapping. In particular, for this class of DIs the approximations of the (unique) solution with good numerical properties (e.g. no chattering) can be computed using implicit Runge-Kutta methods (Kastner-Maresch (1991)). For instance, the *implicit midpoint rule* takes the following form:

$$\eta(t_{k+1}) \in \eta(t_k) - hA(t_k + \frac{1}{2}h, \frac{1}{2}(\eta(t_k) + \eta(t_{k+1}))), \quad (2.24)$$

which has first order of convergence as a function of h , on time intervals where the solution \hat{x} is 2 times continuously differentiable. See Dontchev and Lempio (1992); Kastner-Maresch (1991) for more details and numerical methods with higher order of convergence.

2.5 Experimental example

In this section we will present an experimental case study on a drill-string setup. Practical systems with similar dynamics are, for example, deep-sea oil-drilling equipment with a string, and rotor mechanical systems with dry friction.

The experimental setup with a drill-string was realized by Mihajlović et al. (2004). A simplified scheme of the setup with is depicted in figure 2.4. The setup consists of a power amplifier, a DC motor, two rotational discs (upper and lower), a low stiffness string, and an additional rubber break, applied to the lower disc. The input voltage u is fed to the DC motor, via the power amplifier. The DC-motor is connected, via the gear box, to the upper disc. The upper and lower discs are connected via a low stiffness steel string. The angular positions of the upper and lower discs are measured using incremental encoders. The angular velocities of both discs are obtained by differentiation of the angular positions and filtering the resulting signals using the low-pass filter with a cut-off frequency of 200Hz.

In Mihajlović et al. (2004) it was shown that the dynamics of the experimental setup can be accurately described by the following model:

$$\dot{x}_1 = x_2 - x_3 \quad (2.25a)$$

$$\dot{x}_2 = \frac{k_m}{J_u}u - \frac{k_\theta}{J_u}x_1 - \frac{1}{J_u}T_{fru}(x_2) \quad (2.25b)$$

$$\dot{x}_3 \in \frac{k_\theta}{J_l}x_1 - \frac{1}{J_l}T_{frl}(x_3), \quad (2.25c)$$

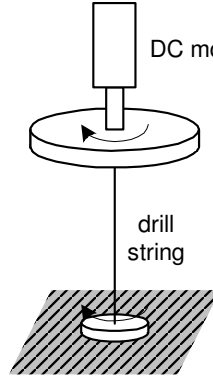


Figure 2.4: Schematic representation of the drill-string setup

where x_1 is the difference in angular positions of the discs, x_2 is the angular velocity of the upper disc and x_3 is the angular velocity of the lower disc. The measured variable is taken to be $y = x_1$.

$T_{fru}(\cdot)$ and $T_{frl}(\cdot)$ denote the friction moments at the upper and the lower disc, respectively. $T_{fru}(\cdot)$ is dominated by the viscous friction, and for simplicity, is here taken to be equal to $b_{up}x_2$. The friction moment at the lower disc $T_{frl}(\cdot)$ is a dry friction with the Stribeck effect, i.e. negative damping appears at a certain range of angular velocities. To describe this friction torque a set-valued characteristic based on neural networks is used in Mihajlović et al. (2004):

$$T_{frl}(x_3) = \begin{cases} (T_{stickl} + T_1(1 - \frac{2}{1+e^{w_1|x_3|}}) + T_2(1 - \frac{2}{1+e^{w_2|x_3|}})) \text{sign}(x_3) + b_l x_3 & \text{for } x_3 \neq 0 \\ [-T_{stickl}, T_{stickl}] & \text{for } x_3 = 0 \end{cases} \quad (2.26)$$

Numerical values of the parameters in (2.25) and (2.26) are given in table 2.1. The set valued friction law (2.26), with parameter values from table 2.1 is depicted in figure 2.5.

For the purpose of simulation the input signal u in (2.25) is chosen to be a constant signal, $u = 2V$. It is easy to check that for the chosen input signal the system (2.25) satisfies the conditions of (Filippov, 1988, theorem 2.7.1), and hence has a solution on an arbitrarily long time interval for every initial condition x_0 , i.e. the system (2.25) satisfies assumption 2.3.2.

The friction mapping depicted in figure 2.5 is not monotone, but by using

J_u	$0.4765 \frac{\text{kgm}^2}{\text{rad}}$	T_{stickl}	0.1642Nm
J_l	$0.0326 \frac{\text{kgm}^2}{\text{rad}}$	T_1	0.0603Nm
k_m	$3.9950 \frac{\text{Nm}}{\text{V}}$	T_2	-0.2267Nm
k_θ	$0.0727 \frac{\text{rad}}{\text{V}}$	w_1	5.7468
b_{up}	$2.2247 \frac{\text{kgm}}{\text{rads}}$	w_2	0.2941
b_l	$0.0109 \frac{\text{kgm}}{\text{rads}}$		

Tabel 2.1: Parameter values of the model (2.25), (2.26)

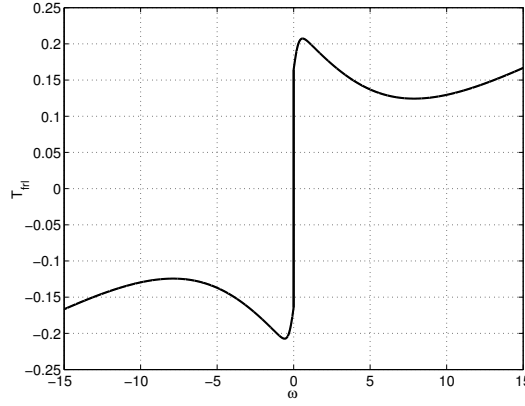


Figure 2.5: Dry friction characteristic

the technique described in remark 2.3.1, can be transformed to a monotone one. The new friction mapping is defined as $\tilde{T}_{frl}(\omega) = T_{frl}(\omega) - \eta\omega$, where $\eta = -0.02$ is the maximal negative slope of the graph in figure 2.5. The system matrix A is replaced by $\tilde{A} = A - \eta GH$.

We will design the observer (2.10). Observer design of the form (2.10) for system (2.25) entails finding gains L and K such that the triple $(\tilde{A} - LC, G, H - KC)$ is SPR. The following values for P , Q , L and K are found:

$$P = \begin{bmatrix} 0.8044 & 0.0299 & 0.0660 \\ 0.0299 & 0.1104 & -0.0000 \\ 0.0660 & -0.0000 & 0.0326 \end{bmatrix},$$

$$Q = \begin{bmatrix} 0.5483 & -0.0000 & -0.0000 \\ -0.0000 & 0.9706 & -0.0361 \\ -0.0000 & -0.0361 & 0.0921 \end{bmatrix},$$

$$L = \begin{bmatrix} 2.4768 & 5.1993 & -26.2200 \end{bmatrix}^\top, K = -2.0254.$$

We will show simulations for the initial state for the system taken as $x(0) = [0 \ 0 \ 0]^\top$ and for the observer as $\hat{x}(0) = [3 \ 3 \ 3]^\top$. The solution of the system (2.25) is constructed using the dedicated technique for simulating friction based on the switched friction models presented in Leine et al. (1998). The solution of the observer (2.10) is computed using the implicit midpoint rule (2.24).

The simulation results are depicted in the figure 2.6 and the estimation error is depicted in figure 2.7. When a constant input voltage is applied (i.e. a constant torque is applied to the upper disc) slip-stick oscillations in the angular velocity of the second disc x_3 occur due to the negative damping in the friction law (2.26). During this oscillations the velocity of the third disc alternates between 0 (stick phase), and a positive value (slip phase). As guaranteed by the theory, the designed observer is able to provide the correct estimate of the state. Moreover, based on (2.22) we can provide a bound on the decrease of the squared estimation error. This is indicated by the dashed line in figure 2.7. The estimation error does not converge to zero, but oscillates around a small residual value ($\approx 10^{-3}$). This residual error can be attributed to the numerical errors of the schemes that are used to simulate the system and the observer.

The responses of the experimental setup were measured as well, under the same conditions as for simulations, and the designed observer is applied for the state estimation. The results are depicted in figure 2.8. The experimental estimation error is depicted in figure 2.9, together with the theoretical bound (2.22).

Experimental results show that the designed observer is able to provide accurate estimate of the states of the experimental setup. The estimation error does not converge to zero, but oscillates around the value of $\approx 10^{-1}$. This residual error can be attributed to model errors.

2.6 Conclusions

In this paper we consider an observer design for Lur'e type systems with maximal monotone multivalued mappings in the feedback path. In contrast with the previous work on nonlinear observer design, the considered class of systems is nonsmooth and the standard theory does not apply. Even the existence and uniqueness of solutions is not a priori guaranteed.

We proposed two observer structures, together with a constructive design method. The approach taken in the paper is based on rendering the

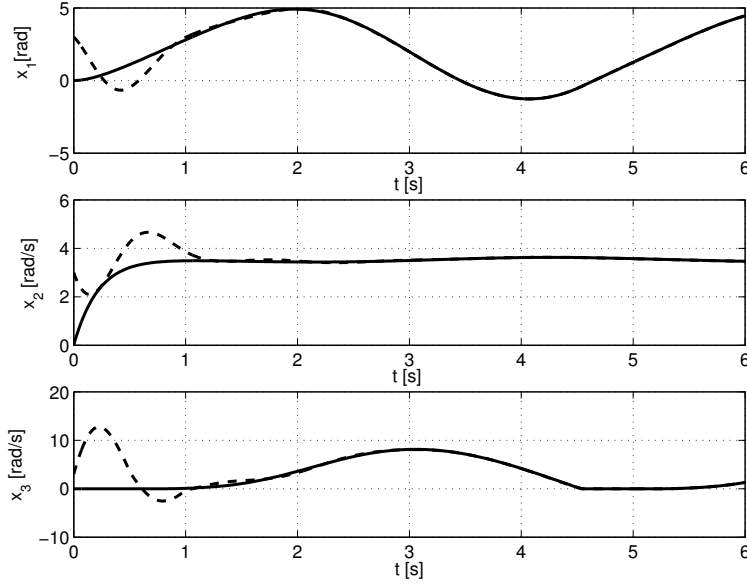


Figure 2.6: Responses of the system (solid) and the observer (dashed): x_1 (upper), x_2 (in the middle), x_3 (lower) under the constant input voltage

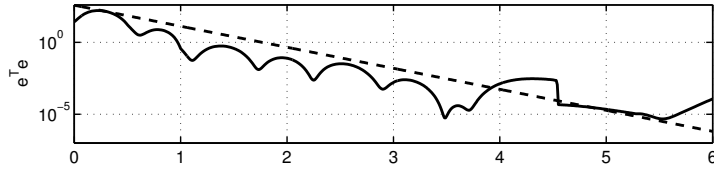


Figure 2.7: The norm of the estimation error (solid) and the envelope of the error norm (2.22) (dashed)

linear part of the observation error dynamics SPR, by choosing appropriate observer gains. Under the natural assumption that the observed system has a solution, and that the control input belongs to a certain admissible class, it is shown that there exists a unique solution for the estimated state, and that the observer recovers the state of the original system asymptotically. The relevance and applicability of the presented results is demonstrated on the experimental case study with a drill string setup.

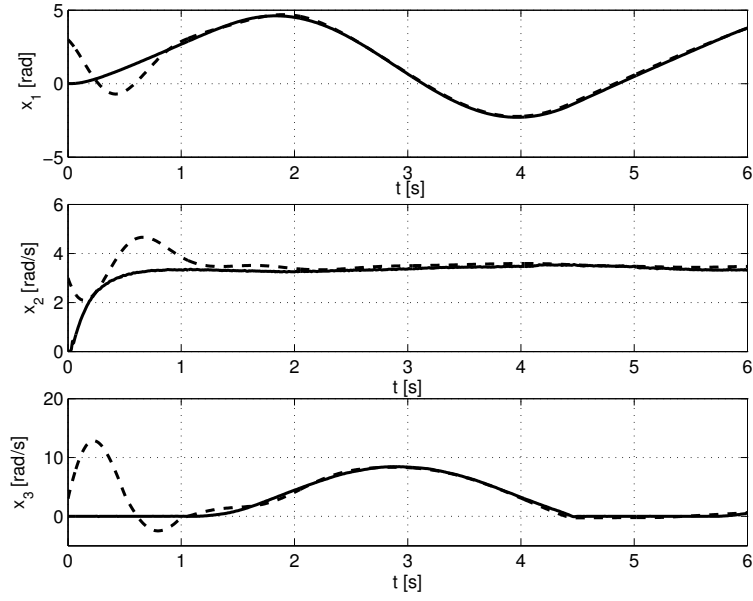


Figure 2.8: Measured response (solid) and the estimation (dashed): x_1 (upper), x_2 (in the middle), x_3 (lower) under the constant input voltage

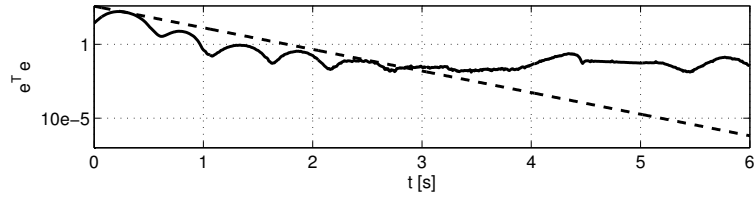


Figure 2.9: The norm of the experimental estimation error (solid) and the theoretical bound of the error norm (2.22) (dashed), in logarithmic scale

Future work will investigate the observer design for more general solution concepts (e.g. solution concepts that allow for state jumps), and the applicability of the proposed observers for state feedback controller design. Also, further investigation of numerical methods and the development of software tools for computing solutions for differential inclusions is of great practical interest.

Observer Design for a Class of Bimodal Piecewise Linear Systems

3.1 Introduction 3.2 Preliminaries and notation 3.3 Problem statement 3.4 Main results for the continuous time case 3.5 Sliding mode analysis	3.6 Examples 3.7 Main results for the discrete time case 3.8 Examples 3.9 Conclusions
--	---

In this chapter we present observer design procedures for a class of bimodal piece-wise affine systems, in both continuous and discrete time. We propose Luenberger-type observers, and derive sufficient conditions for the observation error dynamics to be globally asymptotically stable, in the case when the system dynamics is continuous over the switching plane. When the dynamics is discontinuous, we derive conditions that guarantee that the relative estimation error with respect to the state of the observed system will be asymptotically small. The presented theory is illustrated with several academic examples and experimental example of a piecewise linear beam with a one sided spring.

This chapter is based on Juloski et al. (2002) and Juloski et al. (2003a). The experimental work presented in the example 3.6.1 was performed together with A. Doris, and is also a part of his PhD work.

3.1 Introduction

In this chapter we present observer design procedures for a class of bimodal piecewise linear systems, in both continuous and discrete time. The systems of the considered class comprise two linear dynamics with the same input distribution matrix. The characteristic feature of our approach is that the state reconstruction is performed on the basis of input and measured output signals only, while the information on the active linear dynamics (or mode) is not required.

Observer designs for the case when the mode of the hybrid system is known, in continuous and discrete time, are presented in Alessandri and Coletta (2001a,b); Iulia Bara et al. (2000). The proposed observers are of Luenberger type, and achieve global asymptotic stability of the observation error.

A more difficult case, set in discrete time, when the discrete mode is not known, was considered in Balluchi et al. (2002). The proposed observers use discrete inputs and outputs of the hybrid plant, augmented with discrete signals derived from the continuous measurements when necessary, to obtain the estimate of the mode. Subsequently, the estimate of the continuous state can be obtained, for example, using the techniques of Alessandri and Coletta (2001a,b); Iulia Bara et al. (2000). The designed observers correctly identify the mode of the plant after a finite number of time steps, and the continuous observation error exponentially converges to a bounded set. The class of systems considered in this chapter does not have discrete inputs and outputs and therefore we propose a more direct approach for state estimation.

Another approach to state estimation for discrete time hybrid systems, based on moving horizon estimation, was considered in Ferrari-Trecate et al. (2002). This approach is applicable to the general class of piecewise affine systems, but it is computationally demanding (mixed integer quadratic programming problems), which may be an obstacle for implementing it in applications with limited computational resources. Observers presented here exploit the structure of the considered class of piecewise affine systems, and can be implemented in a numerically efficient way.

For the observer to function properly, the underlying system has to be *observable*. Loosely speaking, the observability is the property that ensures that the state of the observed system can be recovered from the measurements of the system output, for any input signal. Precise definitions of observability and results for some classes of piecewise affine and switched systems can be found in Bemporad et al. (2000a), Collins and van Schuppen (2004), Babaali and Egerstedt (2004), Vidal et al. (2003a).

In this chapter we will be interested in Luenberger-type observers. In this case the state estimation error dynamics, defined by interconnecting the bimodal system with the bimodal observer has four modes. Contrary to the classical Luenberger observer for linear systems and to the case when the mode is known, the error dynamics is not autonomous, but depends on the state of the observed system, and hence, indirectly, on the control input. Global asymptotic stability of the estimation error may still be achieved, in particular when the bi-modal system is continuous over the switching plane. In the case of a discontinuous system, our approach guarantees that the norm

of the error will asymptotically not exceed a certain bound, relative to the bound on the state of the observed system.

In the case when the system has continuous dynamics over the switching plane, it may be represented as a Lur'e type system with a $\max(0, \cdot)$ nonlinearity in the feedback path (see, for instance Vidyasagar (1993)). Observer design for Lur'e type systems, when the signal that enters the nonlinearity in the feedback path is not measured, is presented in Arcak and Kokotović (2001). A link to this result will be established.

The observers which we consider here are designed for situations where the state of the system (continuous state or discrete mode) is of independent interest (e.g. for diagnostics or discrete mode change detection). Output feedback controller design (which implicitly consists of an observer part and a state feedback part) was presented in Rodrigues et al. (2000) and Rodrigues and How (2001). It is not straightforward to extract the observer design from the proposed control methodology.

The chapter is organized as follows. In section 3.3 we introduce the considered class of bi-modal piecewise affine systems. In section 3.4 we present the observer design procedures, for continuous and discontinuous dynamics. Sliding modes, for the continuous time case, are analyzed in section 3.5. In section 3.6 we will present an experimental example with the piecewise linear beam. The discrete time case is analyzed in section 3.7 and examples are given in section 3.8. Conclusions are presented in section 3.9.

3.2 Preliminaries and notation

Definition 3.2.1 A function $x : \mathbb{R}^+ \rightarrow \mathbb{R}^n$ is said to be *bounded* by a constant $x_{max} > 0$, if

$$\|x(t)\| \leq x_{max}$$

for all $t > 0$, i.e. $\sup_{t \in \mathbb{R}^+} \|x(t)\| \leq x_{max}$. A function x is said to be *eventually bounded* by x_{max} , if for all $\delta > 0$ there exists a $T_0 > 0$ such that

$$\|x(t)\| \leq x_{max} + \delta,$$

for all $t > T_0$, i.e. $\limsup_{t \rightarrow \infty} \|x(t)\| \leq x_{max}$.

Definition 3.2.2 The sequence $(x(0), x(1), x(2), \dots)$ is said to be *bounded* by x_{max} if

$$\forall k \geq 0 \quad \|x(k)\| \leq x_{max}.$$

The sequence $(x(0), x(1), x(2), \dots)$ is said to be *eventually bounded* by x_{\max} , if

$$\forall \delta > 0 \quad \exists k_0 > 0 \quad \forall k \geq k_0 \quad \|x(k)\| \leq x_{\max} + \delta.$$

i.e. $\limsup_{k \rightarrow \infty} \|x(k)\| \leq x_{\max}$.

M^\top denotes the transpose of the matrix M . For a square matrix M , $M > 0$ means that M is symmetric i.e. $M = M^\top$ and positive definite. The operators $\ker M$ and $\text{im } M$ denote the kernel and the image of the matrix M , respectively.

The operator $\text{col}(\cdot, \cdot)$ stacks its operands into a column vector, i.e. for $v_1 \in \mathbb{R}^n, v_2 \in \mathbb{R}^m$

$$\text{col}(v_1, v_2) = \begin{bmatrix} v_1 \\ v_2 \end{bmatrix} \in \mathbb{R}^{n+m}.$$

In matrices we denote by $(*)$ at position (i, j) the transposed matrix element at position (j, i) , e.g.

$$\begin{bmatrix} A & B \\ (*) & C \end{bmatrix} \quad \text{means} \quad \begin{bmatrix} A & B \\ B^\top & C \end{bmatrix}.$$

3.3 Problem statement

We consider the following system:

$$\dot{x}(t) = \begin{cases} A_1 x(t) + Bu(t), & \text{if } H^\top x(t) < 0 \\ A_2 x(t) + Bu(t), & \text{if } H^\top x(t) > 0 \end{cases} \quad (3.1a)$$

$$y(t) = Cx(t), \quad (3.1b)$$

where $x(t) \in \mathbb{R}^n$, $y(t) \in \mathbb{R}^p$ and $u(t) \in \mathbb{R}^m$ are the state, output and the input of the system, respectively in time $t \in \mathbb{R}^+$. The input $u : \mathbb{R}^+ \rightarrow \mathbb{R}^m$ is assumed to be an integrable function. We will consider Filippov solutions of the system (3.1) (Filippov (1988)). The matrices $A_1, A_2 \in \mathbb{R}^{n \times n}$, $B \in \mathbb{R}^{n \times m}$, $C \in \mathbb{R}^{p \times n}$ and $H \in \mathbb{R}^n$. The hyperplane defined by $\ker H^\top$ separates the state space \mathbb{R}^n into the two half-spaces. The considered class of bimodal piecewise linear systems has identical input distribution matrix B and output distribution matrix C for both modes.

Analogously, in the discrete time case we will consider the following system:

$$x(k+1) = \begin{cases} A_1 x(k) + Bu(k), & \text{if } H^\top x(k) < 0 \\ A_2 x(k) + Bu(k), & \text{if } H^\top x(k) > 0 \end{cases} \quad (3.2a)$$

$$y(k) = Cx(k), \quad (3.2b)$$

where all matrices have the same dimensions as before, and $k \in \mathbb{N}$ denotes the time index.

Remark 3.3.1 It is possible to consider a somewhat more general class of bimodal piecewise linear systems, where the output distribution matrices would be different for each of the modes, and to derive observer design procedure following the procedure presented here. Stability properties of the designed observers remain the same as for the class studied here. For reasons of ease of exposition, here we treat the classes (3.1) and (3.2).

Depending on the values of A_1 and A_2 we distinguish two situations:

1. the vector field of the system is continuous over the switching plane, i.e. $A_1x = A_2x$, when $H^\top x = 0$. It is straightforward to show that in this case:

$$A_2 = A_1 + GH^\top \quad (3.3)$$

for some vector G of appropriate dimensions. In this case equation (3.1a) can be rewritten as:

$$\dot{x} = A_1x + G \max(0, H^\top x) + Bu,$$

or, in the discrete time case (3.2a)

$$x(k+1) = A_1x(k) + G \max(0, H^\top x(k)) + Bu(k).$$

Moreover, from (3.3) it follows that $\text{rank}(\Delta A) = 1$, where ΔA is defined as

$$\Delta A := A_1 - A_2.$$

2. the vector field of the system is not continuous over the switching plane, i.e. a parametrization as in (3.3) does not exist.

The problem at hand is to design a state estimation procedure, which, on the basis of the known system model, input u , and measured output y provides a state estimate \hat{x} , without directly measuring the mode of the system.

Remark 3.3.2 Information on the currently active linear dynamics may be available to the observer if $H^\top x$ can be reconstructed from the measured output, i.e. $H \in \text{im } C^\top$. In this case the results from Alessandri and Coletta (2001a,b); Iulia Bara et al. (2000) apply.

3.4 Main results for the continuous time case

As an observer for the system (3.1), we propose a continuous time bimodal system with the following structure:

$$\dot{\hat{x}} = \begin{cases} A_1\hat{x} + Bu + L_1(y - \hat{y}), & \text{if } H^\top \hat{x} + K^\top(y - \hat{y}) < 0 \\ A_2\hat{x} + Bu + L_2(y - \hat{y}), & \text{if } H^\top \hat{x} + K^\top(y - \hat{y}) > 0 \end{cases} \quad (3.4a)$$

$$\hat{y} = C\hat{x}, \quad (3.4b)$$

where $\hat{x}(t) \in \mathbb{R}^n$ is the estimated state at time t and $L_1, L_2 \in \mathbb{R}^{n \times p}$ and $K \in \mathbb{R}^p$.

The dynamics of the state estimation error, $e := x - \hat{x}$, is then described by

$$\dot{e} = \begin{cases} (A_1 - L_1C)e, & H^\top x < 0, \quad H^\top \hat{x} + K^\top(y - \hat{y}) < 0 \\ (A_2 - L_2C)e + \Delta Ax, & H^\top x < 0, \quad H^\top \hat{x} + K^\top(y - \hat{y}) > 0 \\ (A_1 - L_1C)e - \Delta Ax, & H^\top x > 0, \quad H^\top \hat{x} + K^\top(y - \hat{y}) < 0 \\ (A_2 - L_2C)e, & H^\top x > 0, \quad H^\top \hat{x} + K^\top(y - \hat{y}) > 0, \end{cases} \quad (3.5)$$

where x satisfies (3.1a) and \hat{x} satisfies (3.4a). By substituting $\hat{x} = x - e$ in (3.5), we see that the right-hand side of the state estimation error dynamics is piecewise linear in the variable $\text{col}(e, x)$.

Note that the error dynamics in the first and the fourth mode of (3.5) is described by an n -dimensional autonomous state equation, while in the two other modes the external signal x is present, which, by (3.1a), depends on the input u . For given (open loop) input signals $u : \mathbb{R}^+ \rightarrow \mathbb{R}^m$ it is possible to consider the evolution of the error e in (3.5) as a time varying switched equation of the form

$$\frac{de}{dt}(t) = f_i(t, e(t)), \quad i = 1, 2, 3, 4. \quad (3.6)$$

Hence, concepts and results of Lyapunov stability theory for hybrid systems (see for instance Branicky (1998); Johansson and Rantzer (1998a); Vidyasagar (1993)) can now be applied to equation (3.6).

The problems of observer design can now be formally stated as:

Problem 3.4.1 Determine the observer gains L_1, L_2 and K in (3.4) such that global asymptotic stability of the estimation error dynamics (3.5) is achieved, for all functions $x : \mathbb{R}^+ \rightarrow \mathbb{R}^n$, satisfying (3.1) for some given locally integrable $u : \mathbb{R}^+ \rightarrow \mathbb{R}^m$.

Problem 3.4.2 Determine $\eta > 0$, and L_1, L_2 and K in (3.4) such that for all bounded trajectories $x : \mathbb{R}^+ \rightarrow \mathbb{R}^n$ it holds that

$$\limsup_{t \rightarrow \infty} \|e(t)\| \leq \eta \limsup_{t \rightarrow \infty} \|x(t)\|, \quad (3.7)$$

which means that if $x(t)$ is (eventually) bounded by x_{max} , then $e(t)$ should be eventually bounded by ηx_{max} .

The constant η can be seen as an asymptotic upper bound of the estimation error relative to the state, and it is desirable to design the observer so that η is as small as possible.

3.4.1 Continuous dynamics

Consider system (3.1), observer (3.4), and the error dynamics (3.5).

Theorem 3.4.3 *The state estimation error dynamics (3.5) is globally asymptotically stable for all $x : \mathbb{R}^+ \rightarrow \mathbb{R}^n$ (in the sense of Lyapunov), if there exist matrices $P > 0$, L_1, L_2, K and constants $\lambda_1, \lambda_2 \geq 0$, $\mu > 0$ such that the following set of matrix inequalities is satisfied:*

$$\begin{bmatrix} (A_2 - L_2 C)^\top P + P(A_2 - L_2 C) + \mu I & P\Delta A + \lambda_1 \frac{1}{2}(H - C^\top K)H^\top \\ \Delta A^\top P + \lambda_1 \frac{1}{2}H(H^\top - K^\top C) & -\lambda_1 H H^\top \end{bmatrix} \leq 0 \quad (3.8a)$$

$$\begin{bmatrix} (A_1 - L_1 C)^\top P + P(A_1 - L_1 C) + \mu I & -P\Delta A + \lambda_2 \frac{1}{2}(H - C^\top K)H^\top \\ -\Delta A^\top P + \lambda_2 \frac{1}{2}H(H^\top - K^\top C) & -\lambda_2 H H^\top \end{bmatrix} \leq 0 \quad (3.8b)$$

Remark 3.4.4 The inequalities (3.8a)-(3.8b) are nonlinear matrix inequalities in $\{P, L_1, L_2, \lambda_1, \lambda_2, \mu\}$, but are linear in $\{P, L_1^\top P, L_2^\top P, \lambda_1, \lambda_2, \mu\}$, and thus can be efficiently solved using available software packages (such as the free software LMItool).

Proof: In order to guarantee that the system (3.5) is globally asymptotically stable it suffices to have a Lyapunov function $V(e)$ of the form

$$V(e) = e^\top P e, \quad (3.9)$$

where $P > 0$ is such that

$$\dot{V} \leq -\mu e^\top e \quad (3.10)$$

for some $\mu > 0$.

Requirement (3.10) yields the following set of inequalities:

$$e^\top \{(A_1 - L_1 C)^\top P + P(A_1 - L_1 C) + \mu I\} e \leq 0, \quad (3.11a)$$

for $H^\top x \leq 0, H^\top(x - e) \leq 0$,

$$\begin{bmatrix} e \\ x \end{bmatrix}^\top \begin{bmatrix} (A_2 - L_2 C)^\top P + P(A_2 - L_2 C) + \mu I & P\Delta A \\ \Delta A^\top P & 0 \end{bmatrix} \begin{bmatrix} e \\ x \end{bmatrix} \leq 0, \quad (3.11b)$$

for $H^\top x \leq 0, H^\top(x - e) > 0$,

$$\begin{bmatrix} e \\ x \end{bmatrix}^\top \begin{bmatrix} (A_1 - L_1 C)^\top P + P(A_1 - L_1 C) + \mu I & -P\Delta A \\ -\Delta A^\top P & 0 \end{bmatrix} \begin{bmatrix} e \\ x \end{bmatrix} \leq 0, \quad (3.11c)$$

for $H^\top x > 0, H^\top(x - e) \leq 0$,

$$e^\top \{(A_2 - L_2 C)^\top P + P(A_2 - L_2 C) - \mu I\} e \leq 0, \quad (3.11d)$$

for $H^\top x > 0, H^\top(x - e) > 0$.

Note that requirements (3.11a)-(3.11d) can not be satisfied in the complete (e, x) space unless $\Delta A = 0$.

Regions of the (e, x) space where the second and the third linear dynamics of the error (3.5) is active can be covered with the quadratic constraint in the following way:

$$\begin{bmatrix} e \\ x \end{bmatrix}^\top \begin{bmatrix} 0 & -\frac{1}{2}(H - C^\top K)H^\top \\ -\frac{1}{2}H(H^\top - K^\top C) & HH^\top \end{bmatrix} \begin{bmatrix} e \\ x \end{bmatrix} \leq 0 \quad (3.12)$$

Inequality (3.12) is derived by multiplying the mode constraints:

$$x^\top H(H^\top(x - e) + K^\top C e) \leq 0.$$

The quadratic constraint (3.12) is by construction negative in the region of interest, 0 at the boundaries, and nonnegative elsewhere. Combining (3.10) with (3.12), using the S -procedure (Boyd et al. (1994); Johansson and Rantzer (1998a)), yields the inequalities (3.8a)-(3.8b). Note that inequalities (3.11a) and (3.11d) are implied by (3.8a) and (3.8b) respectively, and therefore can be omitted.

Note that the relaxed inequalities (3.8a),(3.8b) can be only negative semidefinite by construction (because $-\lambda_i HH^\top$ is negative semidefinite), but that derivatives (3.11b),(3.11c) are guaranteed to be negative whenever the appropriate dynamics is active and $e \neq 0$. Hence, the computed derivative of the candidate Lyapunov function (3.9) is negative definite in e , and the global asymptotic stability of the error dynamics (3.5) is guaranteed. ■

Suppose that a feasible solution to (3.8a)-(3.8b) exists. Assume that $M > 0$ is a matrix. Since $M \leq 0$ and $z^\top M z = 0$ imply that $z \in \ker(M)$, it follows that

$$\text{col}(0, h) \in \ker$$

$$\begin{bmatrix} (A_2 - L_2 C)^\top P + P(A_2 - L_2 C) + \mu I & P\Delta A + \lambda_1 \frac{1}{2}(H - C^\top K)H^\top \\ \Delta A^\top P + \lambda_1 \frac{1}{2}H(H^\top - K^\top C) & -\lambda_1 H H^\top \end{bmatrix}$$

(and analogously for the inequality (3.8b)), where $h \in \ker(HH^\top) = \ker(H^\top)$. Hence, we have that

$$\ker(H^\top) \subseteq \ker(P\Delta A) = \ker \Delta A,$$

since $P > 0$. From this inclusion it follows that the state evolution matrices of the two modes are not independent, but are related via:

$$A_2 = A_1 + GH^\top$$

for some vector G of appropriate dimensions. This relation implies the continuity of the vector fields over the switching plane, as detailed in the section 3.3. Hence an equivalent representation of the continuous bi-modal system (3.1) is:

$$\dot{x} = A_1 x + G \max(0, z) + Bu \quad (3.13a)$$

$$z = H^\top x \quad (3.13b)$$

$$y = Cx, \quad (3.13c)$$

which is a Lur'e system (Vidyasagar (1993)), with $\max(0, \cdot) \in [0, 1]$ nonlinearity in the feedback path.

Observer design for this type of systems with slope restricted nonlinearities was presented in Arcak and Kokotović (2001) (see also proposition 1.3.2). Here we show that the observer design from Arcak and Kokotović (2001) is a special case of our observer design. We will simplify our observer structure by assuming the same gain $L_1 = L_2 = L$ for both modes and the same multiplicative constant $\lambda_1 = \lambda_2 = \lambda$. Equation (3.8a) can then be transformed into equation (3.8b), by pre-multiplying it with Q^\top and post-multiplying it with Q , where

$$Q = \begin{bmatrix} I & 0 \\ I & -I \end{bmatrix}.$$

Equation (3.8b) can be represented as:

$$T^\top \begin{bmatrix} (A_1 - LC)^\top P + P(A_1 - LC) + \mu I & PG + \lambda(H - C^\top K) \\ G^\top P + \lambda(H^\top - K^\top C) & -2\lambda I \end{bmatrix} T \leq 0 \quad (3.14)$$

where

$$T = \begin{bmatrix} I & 0 \\ 0 & H^\top \end{bmatrix}.$$

Pre- and post-multiplication with a matrix T introduces a kernel in the matrix inequality (3.14), but does not change feasibility conditions. The condition (3.14) is therefore equivalent to the LMI condition obtained in Arcak and Kokotović (2001) (up to the scaling constant λ).

3.4.2 Discontinuous dynamics

Theorem 3.4.3 gives sufficient conditions for the solution of problem 3.4.1. A drawback of the obtained result is that a necessary condition for the feasibility of (3.8a)-(3.8b) is the continuity of the bi-modal piece-wise affine system.

In order to give an approach for discontinuous systems as well we need to consider the relaxed problem 3.4.2. The following theorem provides an answer to this problem .

Theorem 3.4.5 *The state estimation error dynamics (3.5) is eventually bounded by a constant e_{max} (in the sense of definition 3.2.1), under the assumption that x is eventually bounded by x_{max} , if there exist matrices $P = P^\top > 0$, L_1, L_2 and constants $\lambda_1, \lambda_2, \varepsilon \geq 0$ and $\mu, \alpha > 0$ such that the following set of matrix inequalities is satisfied:*

$$\begin{bmatrix} (A_2 - L_2 C)^\top P & P \Delta A + \frac{\lambda_1}{2} (H - C^\top K) H^\top \\ +P(A_2 - L_2 C) + (\mu + \alpha)I & \\ \Delta A^\top P + \lambda_1 \frac{\lambda_2}{2} H(H^\top - K^\top C) & -\lambda_1 H H^\top - \alpha \varepsilon^2 I \end{bmatrix} < 0 \quad (3.15a)$$

$$\begin{bmatrix} (A_1 - L_1 C)^\top P & -P \Delta A + \frac{\lambda_2}{2} (H - C^\top K) H^\top \\ +P(A_1 - L_1 C) + (\mu + \alpha)I & \\ -\Delta A^\top P + \frac{\lambda_2}{2} H(H^\top - K^\top C) & -\lambda_2 H H^\top - \alpha \varepsilon^2 I \end{bmatrix} < 0 \quad (3.15b)$$

Moreover, if

$$\gamma_1 I \leq P \leq \gamma_2 I, \quad (3.16)$$

then

$$e_{max} \leq \sqrt{\frac{\gamma_2}{\gamma_1}} \varepsilon x_{max}. \quad (3.17)$$

Proof: Note that the matrix inequalities (3.15) are relaxations of (3.8) by using the S -procedure with the quadratic constraint

$$\|e\|^2 \geq \varepsilon^2 \|x\|^2, \quad (3.18)$$

and the multiplication constant α (see Boyd et al. (1994); Johansson and Rantzer (1998a)). Hence, they imply that the function $V(e) = e^\top P e$ satisfies:

$$\dot{V}(e) \leq \mu e^\top e \text{ when } \|e\|^2 \geq \varepsilon^2 \|x\|^2$$

.

For an arbitrary $\delta > 0$, denote

$$V_{max}^\delta := \sup_{\|e\| \leq \varepsilon x_{max} + \delta} V(e).$$

Define the bounded set S_δ by:

$$S_\delta = \{e \in \mathbb{R}^n \mid V(e) < V_{max}^\delta\}.$$

Since $\dot{V}(e) < 0$ for $e \notin S_\delta$, it follows that S_δ is positively invariant i.e. if for $T_0 > 0$

$$V(e(T_0)) < V_{max}^\delta \implies V(e(t)) < V_{max}^\delta \quad \forall t > T_0.$$

Moreover, S_δ satisfies a strong variant of attractivity in the sense that

$$\exists T_0 > 0 \quad V(T_0) < V_{max}^\delta.$$

From (3.16) it follows that:

$$V_{max}^\delta \leq \gamma_2 [\varepsilon x_{max} + \delta]^2$$

and consequently,

$$\forall \delta > 0 \exists T_0 > 0 \forall t > T_0 \quad \|e(t)\| \leq \sqrt{\frac{\gamma_2}{\gamma_1}} [\varepsilon x_{max} + \delta].$$

This means that

$$e_{max} := \limsup_{t \rightarrow \infty} \|e(t)\| \leq \sqrt{\frac{\gamma_2}{\gamma_1}} \varepsilon x_{max}.$$

■

Remark 3.4.6 If there exists a feasible solution for the system of inequalities

$$P > 0 \quad (3.19a)$$

$$(A_1 - L_1 C)^\top P + P(A_1 - L_1 C) + \mu I < 0 \quad (3.19b)$$

$$(A_2 - L_2 C)^\top P + P(A_2 - L_2 C) + \mu I < 0 \quad (3.19c)$$

(which implies that the pairs (A_1, C) and (A_2, C) are detectable) an ε can always be found such that (3.15a) and (3.15b) are feasible. Conditions (3.19) are exactly the conditions required for the observer design in the case when the current mode is known (Alessandri and Coletta (2001a,b)).

Remark 3.4.7 The equation

$$P \geq I \quad (3.20)$$

can be added to (3.15a), (3.15b) without changing feasibility. Namely, if $\{P, L_1, L_2, \lambda_1, \lambda_2, \mu_1, \mu_2, \varepsilon\}$ is the feasible solution of (3.15a), (3.15b), so is the scaled set $\{\frac{1}{\gamma_1}P, L_1, L_2, \frac{1}{\gamma_1}\lambda_1, \frac{1}{\gamma_1}\lambda_2, \frac{1}{\gamma_1}\mu_1, \frac{1}{\gamma_1}\mu_2, \varepsilon\}$, and $P^* = \frac{1}{\gamma_1}P \geq I$. The second part of the double inequality (3.16) follows from:

$$P - \gamma_2 I < 0. \quad (3.21)$$

Remark 3.4.8 Condition (3.18) can be stated in a more general form, when $\|\cdot\|$ is replaced by $\|\cdot\|_Q$. An interesting case is when $\|e\|$ is replaced by $\|e\|_P$. Then, given a certain $\eta_{spec} > 0$, existence of an observer that achieves bound $e_{max} \leq \eta_{spec} x_{max}$ follows from the feasibility of bilinear matrix inequalities (BMI) similar in form to (3.15) and (3.20) with $\varepsilon = \eta_{spec}$. The drawback is that BMIs can not be solved in an efficient way.

Remark 3.4.9 Equations (3.15) are bi-linear in the variables $\{P, L_1, L_2, \varepsilon, \lambda_1, \lambda_2, \mu, \alpha\}$. When ε is fixed, with the same change of variables as in remark 3.4.4 we get a set of linear matrix inequalities.

Any feasible solution of the equations (3.15), (3.20) and (3.21) is a solution for the problem 2a, with $\eta = \sqrt{\gamma_2} \varepsilon$. An sub-optimal algorithm that aims to minimize the value of η follows from theorem 3.4.5, and remarks 3.4.7 and 3.4.9. Under the conditions of remark 3.4.6 a minimal ε can be found when (3.15a), (3.15b) cease to be feasible. For a feasible value of ε close to the infeasible value an optimization problem:

$$\min \gamma_2$$

under (3.15a),(3.15b),(3.20),(3.21) is solved. Then $e_{max} < \sqrt{\gamma_2} \varepsilon x_{max}$.

Another problem that occurs is that the above minimization problem frequently gives observer gains L_1, L_2 of an unacceptably high magnitude. The “size” of the gains can be indirectly included in the optimization problem, by adding the matrix inequalities like:

$$\begin{aligned} L_1^\top P L_1 &< \xi_1 I \\ L_2^\top P L_2 &< \xi_2 I. \end{aligned}$$

Here, ξ_1 and ξ_2 are auxiliary constants, that bound the magnitude of terms $L_1^\top P L_1$ and $L_2^\top P L_2$, respectively. Values ξ_1 and ξ_2 can be added into the optimization criterion, with appropriate weighting factors. The previous inequalities can be transformed into LMIs using Schur complements.

3.5 Sliding mode analysis

All derivations so far were done with the implicit assumption that sliding modes do not occur neither in the original system, nor in the designed observer. In the discussion that follows we will show that the properties of the designed observers are retained, under the presence of sliding modes, in the system and in the designed observer. Note that even in the case when the system dynamics is continuous sliding modes may exist in the designed observer. This is the special case of the following analysis.

We will consider sliding modes along the switching surface ($H^\top x = 0$ for the system and $H^\top \hat{x} + K(\hat{y} - y) = 0$ for the observer) under the assumption that we have constructed an observer that satisfies equations (3.15), and we are going to show that the estimation error remains eventually bounded. The mode of the system where $H^\top x < 0$ ($H^\top x > 0$) is referred to as the first mode (second mode), and in an analogous way for the observer.

First, consider the case where sliding occurs in the designed observer along the plane $H^\top \hat{x} = 0$. Then, the dynamics of the observer is given by a convex combination of the constituting linear dynamics (i.e. we use Filippov solutions as the formalization of the sliding dynamics (Filippov (1988))):

$$\begin{aligned} \dot{\hat{x}} &= \lambda \{A_1 \hat{x} + Bu + L_1(y - \hat{y})\} + \\ &\quad (1 - \lambda) \{A_2 \hat{x} + Bu + L_2(y - \hat{y})\}, \\ \dot{\hat{y}} &= C \hat{x}, \end{aligned} \tag{3.22}$$

where $\lambda \in [0, 1]$. Consider next the situation where the system is in the first

mode. Then the error dynamics is given by:

$$\begin{aligned}\dot{e} &= \dot{x} - \dot{\hat{x}} = \lambda\{(A_1 - L_1C)e\} + \\ &\quad (1 - \lambda)\{(A_2 - L_2C)e + \Delta Ax\},\end{aligned}\tag{3.23}$$

which is a convex combination of the first and the second mode of the error dynamics (3.5). Since $\dot{V}(e)$ is negative when (3.18) holds, for both modes, it is also negative for their convex combinations under (3.18). Hence, the error is eventually bounded, as proven in theorem 3.4.5. A similar argument holds when the system is in the second mode, and the observer is in the sliding motion.

Consider now the case when a sliding mode exists on the switching plane of the system. Then, the system dynamics is given by a convex combination of the constituting linear dynamics:

$$\begin{aligned}\dot{x} &= \mu\{A_1x + Bu\} + (1 - \mu)\{A_2x + Bu\} \\ y &= Cx\end{aligned}\tag{3.24}$$

where $\mu \in [0, 1]$. If the observer is in the first mode, the error dynamics is given by:

$$\begin{aligned}\dot{e} &= \dot{x} - \dot{\hat{x}} = \mu\{(A_1 - L_1C)e\} + \\ &\quad (1 - \mu)\{(A_1 - L_1C)e - \Delta Ax\},\end{aligned}\tag{3.25}$$

which is a convex combination of the first and the third mode of the error dynamics. Hence, $\dot{V}(e)$ is negative when (3.18) holds. A similar argument holds for the case when the system is in the sliding mode, and the observer is in the second mode.

Consider now the situation where there are sliding modes in both the system and the observer. Then the dynamics of the system is given by (3.24) and the dynamics of the observer is given by (3.22). The error dynamics follows then as:

$$\begin{aligned}\dot{e} &= (\mu - \lambda)\{(A_2 - L_2C)e + \Delta Ax\} + \\ &\quad (1 - \mu)\{(A_2 - L_2C)e\} + \lambda\{(A_1 - L_1C)e\},\end{aligned}$$

if $\mu - \lambda \geq 0$, and

$$\begin{aligned}\dot{e} &= (\lambda - \mu)\{(A_1 - L_1C)e - \Delta Ax\} + \\ &\quad (1 - \lambda)\{(A_2 - L_2C)e\} + \\ &\quad \mu\{(A_1 - L_1C)e\},\end{aligned}\tag{3.26}$$

if $\lambda - \mu \geq 0$. We see that the error dynamics is again given as a convex combination of the modes of the error dynamics (3.5), and is, by a similar argument as in the previous cases, eventually bounded.

To summarize the above analysis, we conclude that the estimation error under sliding modes is eventually bounded.

3.6 Examples

In this section the presented theory will be illustrated by an experimental example of a piecewise linear beam and an academic example.

Example 3.6.1 In this example we will present an experimental observer design for a piecewise linear beam with a one-sided spring (Fey (1992); Heertjes (1999)). Practical systems with similar dynamics are, for example, suspension bridges and building cranes.

The experimental setup is depicted in figure 3.1. The schematic representation of the setup is given in figure 3.2. The setup consists of a metal beam which is supported at both ends by leaf springs. A one-sided spring acts in the middle of the beam. One-sided spring realized with another beam, which is clamped at both ends and placed in parallel to the first one. When the middle of the beam moves downwards it is in contact with the spring, when it moves upwards the spring is not active. Therefore, two dynamic modes may be distinguished in the motion of the beam.

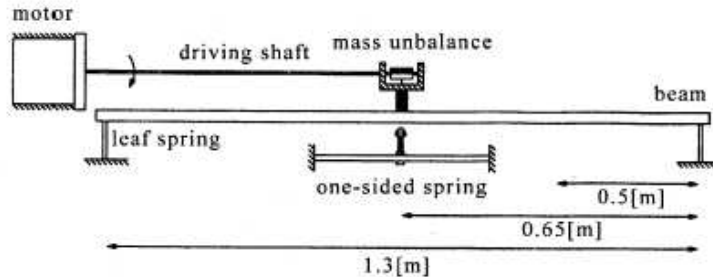


Figure 3.1: Experimental setup

The beam is excited by a periodic force u , applied in the middle of the beam. The force u is produced by a rotating mass unbalance, which is driven by a tacho-controlled motor, that enables a constant rotation speed. The force u can be measured with a piezoelectric force transducer.

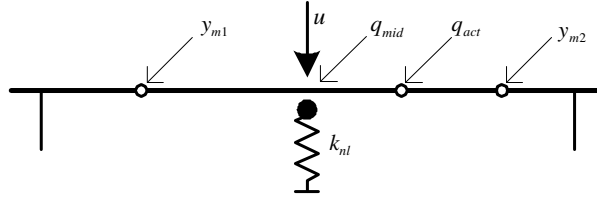


Figure 3.2: Schematic representation of the experimental setup

The beam is modelled using the finite element method (FEM), and a model with 111 degrees of freedom was obtained. Using a component mode synthesis method (for details see Fey (1992); Heertjes (1999)), a reduced model with 3 degrees of freedom (3-DOF) was obtained, and used for the observer design.

The 3-DOF model contains two interface DOFs, q_{mid} and q_{act} which represent physical displacements of the middle of the beam, and at the location of the additional actuator, respectively. Furthermore, the 3-DOF model contains one generalized DOF, q_ξ , that accounts for the first eigenmode of the beam. Note that adding more eigenmodes to the model might make the model more accurate, at the cost of increased model complexity.

The equations of motion for the 3DOF model of the piecewise linear beam can be written as:

$$M\ddot{q} + B\dot{q} + Kq + f_{nl}(q) = hu, \quad (3.27)$$

where $q = [q_{mid} \ q_{act} \ q_\xi]^\top$, and $h = [1 \ 0 \ 0]^\top$. The matrices M, B and K are mass, damping and stiffness matrices, obtained from the reduction method, and have the following numerical values:

$$M = \begin{bmatrix} 4.4935 & -2.3259 & 0.8713 \\ -2.3259 & 7.6177 & 2.2290 \\ 0.8713 & 2.2290 & 2.3738 \end{bmatrix}$$

$$B = \begin{bmatrix} 117.2507 & -29.7689 & 41.5850 \\ -29.7689 & 104.1515 & 31.4193 \\ 41.5850 & 31.4193 & 36.5486 \end{bmatrix}$$

$$K = 10^6 \begin{bmatrix} 2.5282 & -0.3453 & 1.0256 \\ -0.3453 & 1.0507 & 0.2961 \\ 1.0256 & 0.2961 & 0.6135 \end{bmatrix}.$$

The force f_{nl} represents the force of the one-sided spring:

$$f_{nl}(q) = k_{nl}h \min(0, h^\top q) = \begin{cases} k_{nl}hh^\top q & \text{if } q_{mid} < 0 \\ 0 \in \mathbb{R}^3 & \text{if } q_{mid} \geq 0, \end{cases} \quad (3.28)$$

where $k_{nl} = 1.98 \cdot 10^5 \text{Nm}^{-1}$ is the stiffness of the one-sided spring. The relation between the states of the FEM model and the states of the 3-DOF model is given by

$$p \approx T \cdot q, \quad (3.29)$$

where p denotes the states of the FEM model. The matrix $T \in \mathbb{R}^{111 \times 3}$ is obtained from the model reduction procedure and has the following structure:

$$T = [t_1 \mid t_2 \mid \cdots \mid t_{111}]^\top, \quad (3.30)$$

where $t_i \in \mathbb{R}^3$.

In a state space formulation the model (3.27) has the following form:

$$\dot{x}(t) = \begin{cases} A_1 x(t) + Bu(t), & \text{if } H^\top x(t) < 0 \\ A_2 x(t) + Bu(t), & \text{if } H^\top x(t) > 0, \end{cases} \quad (3.31a)$$

where $x = [q^\top \quad \dot{q}^\top]^\top$, $H = [h^\top \quad 0 \quad 0 \quad 0]^\top$, and

$$A_1 = \begin{bmatrix} 0 & I \\ -M^{-1}(K + k_{nl}) & -M^{-1}B \end{bmatrix}, \quad A_2 = \begin{bmatrix} 0 & I \\ -M^{-1}K & -M^{-1}B \end{bmatrix},$$

$$B = \begin{bmatrix} 0 \\ -M^{-1}h \end{bmatrix}.$$

Note that the model (3.31) has continuous dynamics over the switching plane $H^\top x = 0$.

We measured the displacement at two positions m_1 and m_2 along the beam, using linear displacement transducers as sensors. The *measured displacements* are denoted by y_{m1} and y_{m2} , respectively (cf. figure 3.2).

Note that the displacement in the middle of the beam q_{mid} is not measured. Hence, it is not possible to deduce the currently active dynamics (mode) of the system directly from the measurements. To incorporate the measurements at position m_1 and m_2 in the model (3.31) we will add two output equations:

$$y_1 = C_1 x \quad (3.31b)$$

$$y_2 = C_2 x \quad (3.31c)$$

where the matrices C_1 and C_2 have the following numerical values:

$$C_1 = \begin{bmatrix} -0.9579 & 1.2165 & -0.2642 & 0 & 0 & 0 \end{bmatrix},$$

$$C_2 = \begin{bmatrix} 0.0801 & -1.2013 & -0.8670 & 0 & 0 & 0 \end{bmatrix}.$$

For the system (3.31) we design the observer of the following form:

$$\dot{\hat{x}} = \begin{cases} A_1 \hat{x} + Bu + L_1(y_{m1} - \hat{y}_1), & \text{if } H^\top \hat{x} < 0 \\ A_2 \hat{x} + Bu + L_2(y_{m1} - \hat{y}_1), & \text{if } H^\top \hat{x} > 0 \end{cases} \quad (3.32a)$$

$$\hat{y}_1 = C_1 \hat{x} \quad (3.32b)$$

$$\hat{y}_2 = C_2 \hat{x} \quad (3.32c)$$

Note that we use only the measurement y_{m1} in the observer equation. Measurement y_{m2} will be used to verify the observer. (3.32a). Measurement position m_1 is chosen such that both pairs (A_1, C_1) and (A_2, C_2) are detectable (cf. remark 3.4.6), as otherwise it is not possible to design the observer using the presented theory. Observer design (finding gains L_1 and L_2) is performed using the methodology from theorem 3.4.3, and we obtained the following values:

$$L_1 = 10^4 \begin{bmatrix} 0.0134 & 0.0145 & -0.0353 & 0.5402 & 0.9448 & -2.6460 \end{bmatrix}^\top,$$

$$L_2 = 10^4 \begin{bmatrix} 0.0134 & 0.0145 & -0.0353 & 0.7989 & 1.0893 & -2.8705 \end{bmatrix}^\top.$$

We performed experiments at two frequencies of the periodic excitation u : 15Hz and 35Hz. The results are depicted in figures 3.3 and 3.4, respectively. In figure 3.3a) we plotted the (open-loop) prediction of y_2 obtained from the model (3.31) versus the measured value y_{m2} . In figure 3.3b) we plotted the prediction \hat{y}_2 obtained from the observer (3.32) versus the measured value y_{m2} . Finally, in figure 3.3c) we plotted the model prediction error $e_m = y_2 - y_{m2}$ and the observer prediction error $e_o = \hat{y}_2 - y_{m2}$. The same values are plotted in figures 3.4a,b,c), for the excitation frequency of 35Hz.

The error in the observer prediction of y_{m2} is, roughly, 1% relative to the peak-to-peak magnitude of y_{m2} at the frequency of 15Hz, and 6% at the frequency of 35Hz. This is probably caused by the fact that the accuracy of the model deteriorates as the frequency of the excitation u grows. The quality of the state estimation crucially depends on the quality of the model. It is of interest to investigate the ways to make the observer more robust with respect to the modelling errors, possibly by making a tradeoff with the rate of convergence.

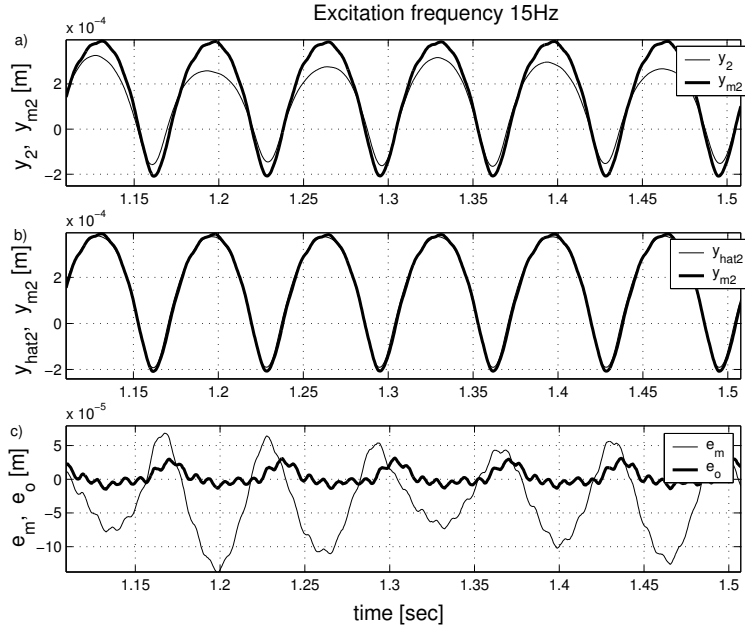


Figure 3.3: Excitation frequency of 15Hz a) Measured displacement y_{m2} versus the model prediction y_2 b) Measured displacement y_{m2} versus the observer prediction \hat{y}_2 c) Model prediction error e_m versus the observer prediction error e_o

Example 3.6.2 To demonstrate also the theory for discontinuous vector fields, we consider the bimodal system

$$\dot{x} = \begin{cases} A_1 x + Bu, & \text{if } H^\top x < 0 \\ A_2 x + Bu, & \text{if } H^\top x > 0 \end{cases} \quad (3.33)$$

$$y = Cx,$$

with:

$$A_1 = \begin{bmatrix} -1 & -0.2 \\ 0.2 & -1 \end{bmatrix}, A_2 = \begin{bmatrix} -1 & 0.2 \\ -0.2 & 0.3 \end{bmatrix}$$

$$B = \begin{bmatrix} 1 \\ 0 \end{bmatrix}, H = \begin{bmatrix} 1 \\ 0 \end{bmatrix}, C = \begin{bmatrix} 0 & 1 \end{bmatrix}.$$

We see that the switching is driven by the first state variable x_1 , while x_2 is measured. Hence, the discrete mode can not be reconstructed directly from the measurements (cf. remark 3.3.2).

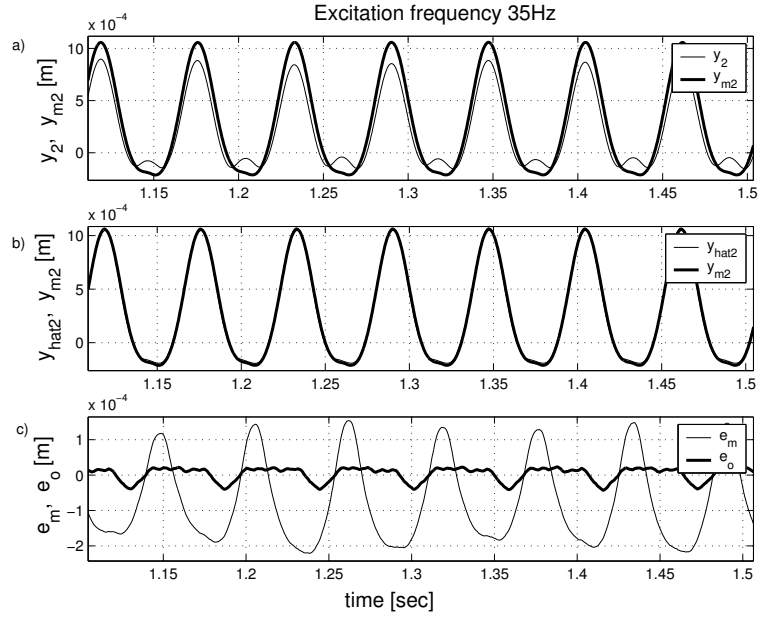


Figure 3.4: Excitation frequency of 35Hz a) Measured displacement y_{m2} versus the model prediction y_2 b) Measured displacement y_{m2} versus the observer prediction \hat{y}_2 c) Model prediction error e_m versus the observer prediction error e_o

We will design an observer for the system (3.33) of the form:

$$\begin{aligned} \dot{\hat{x}} &= \begin{cases} A_1 \hat{x} + Bu + L_1(y - \hat{y}), & \text{if } H^\top \hat{x} < 0 \\ A_2 \hat{x} + Bu + L_2(y - \hat{y}), & \text{if } H^\top \hat{x} > 0 \end{cases} \\ \hat{y} &= C\hat{x}, \end{aligned}$$

Linear matrix inequalities were solved using the LMItool (El Ghaoui and Commeau (1999)). For the value of $\varepsilon = 0.1$, the following feasible solution was obtained:

$$L_1 = \begin{bmatrix} 2.09 \\ 4.38 \end{bmatrix}, \quad L_2 = \begin{bmatrix} 2.41 \\ 5.78 \end{bmatrix}$$

with $\gamma_2 = 1.3998$, and $\eta x_{max} \approx 0.12$

An input signal that takes values in $\{-1, 0, +1\}$, with a period of 1s was applied to the system. The initial conditions for the system were chosen as $x(0) = \begin{bmatrix} -1 & -1 \end{bmatrix}^\top$, and for the observer as $\hat{x}(0) = \begin{bmatrix} 1 & 1 \end{bmatrix}^\top$. Note that

the system and the observer start in different modes. The simulation results are shown in figure 3.5 and figure 3.6. In figure 3.5 we see that a sliding patch exists in the interval $[4.5, 5.5]$. From figure 3.7 we see that the observer error remains within the determined bounds, as predicted by the analysis.

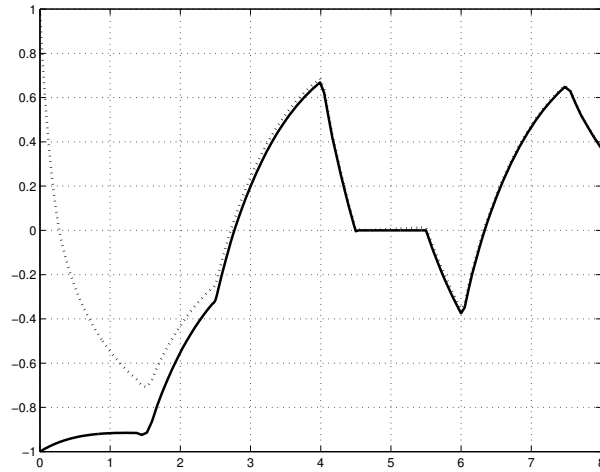


Figure 3.5: System (solid) and observer (dotted) response for the state x_1

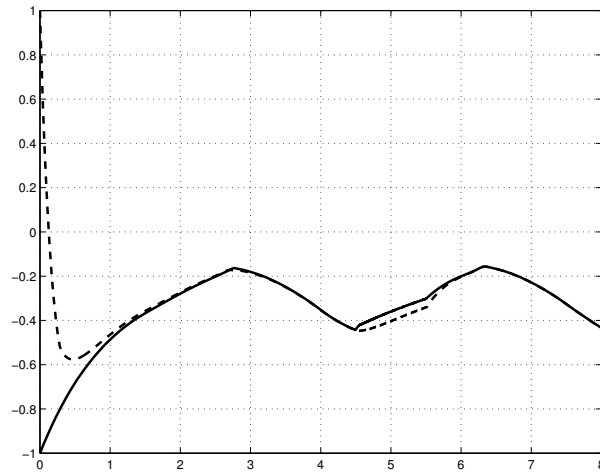


Figure 3.6: System (solid) and observer (dotted) response for the state x_2

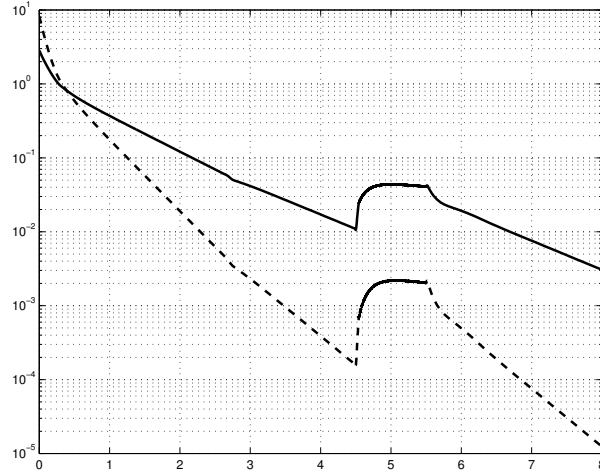


Figure 3.7: Norm of the error $\|e\|$ (solid); Lyapunov function of the error $e^\top P e$ (dotted) on log scale

3.7 Main results for the discrete time case

As an observer for the discrete time PWA system (3.2), we propose a bimodal system with the following structure:

$$\hat{x}(k+1) = \begin{cases} A_1 \hat{x}(k) + Bu(k) + L_1(y(k) - \hat{y}(k)), & \text{if } H^\top \hat{x}(k) < 0 \\ A_2 \hat{x}(k) + Bu(k) + L_2(y(k) - \hat{y}(k)), & \text{if } H^\top \hat{x}(k) > 0 \end{cases} \quad (3.34a)$$

$$\hat{y}(k) = C\hat{x}(k) \quad (3.34b)$$

where $\hat{x}(k) \in \mathbb{R}^n$ is the estimated state at time k and L_1 and $L_2 \in \mathbb{R}^{n \times p}$ are matrices.

Remark 3.7.1 We may consider the switching surface of the form:

$$H^\top \hat{x} + K(\hat{y} - y) = 0$$

for the observer (3.34). In order to simplify the exposition we chose to treat the case with $K = 0$. Derivation of results for $K \neq 0$ is straightforward.

The dynamics of the state estimation error $e = x - \hat{x}$ is then described by

$$e(k+1) = \begin{cases} (A_1 - L_1 C)e(k), & H^\top x(k) < 0, H^\top \hat{x}(k) < 0 \\ (A_2 - L_2 C)e(k) + \Delta A x(k), & H^\top x(k) < 0, H^\top \hat{x}(k) > 0 \\ (A_1 - L_1 C)e(k) - \Delta A x(k), & H^\top x(k) > 0, H^\top \hat{x}(k) < 0 \\ (A_2 - L_2 C)e(k), & H^\top x(k) > 0, H^\top \hat{x}(k) > 0, \end{cases} \quad (3.35)$$

where $x(k)$ satisfies (3.2a) and $\hat{x}(k)$ satisfies (3.34a). By substituting $\hat{x} = x - e$ in (3.35), we see that the right-hand side of the state estimation error dynamics is piece-wise linear in the variable $\text{col}(e, x)$. The problems of observer design can be formally stated as follows:

Problem 3.7.2 Determine the observer gains L_1, L_2 in (3.34) such that global asymptotic stability of the estimation error dynamics (3.35) is achieved, for all sequences $x(1), x(2), \dots$, satisfying (3.2) for some given input sequence $u(1), u(2), \dots$

Problem 3.7.3 Determine $\eta > 0$, and L_1, L_2 in (3.34) such that for all bounded sequences $x(0), x(1), \dots$ satisfying (3.2) it holds that

$$\limsup_{k \rightarrow \infty} \|e(k)\| \leq \eta \limsup_{k \rightarrow \infty} \|x(k)\|, \quad (3.36)$$

which means that if the sequence x is (eventually) bounded by x_{max} , then e should be eventually bounded by ηx_{max} .

3.7.1 Continuous dynamics

In order to obtain stable error dynamics we search for a Lyapunov function of the form

$$V(x) = x^\top P x, \quad (3.37)$$

where $P = P^\top > 0$, such that:

$$V(e(k+1)) - V(e(k)) \leq -\mu e(k)^\top e(k), \quad (3.38)$$

for $e(k) \neq 0$ and some $\mu > 0$. Considering the first and the fourth mode of error dynamics (3.35), (3.38) becomes:

$$e^\top \{(A_1 - L_1 C)^\top P (A_1 - L_1 C) - P + \mu I\} e \leq 0 \quad (3.39a)$$

$$e^\top \{(A_2 - L_2 C)^\top P (A_2 - L_2 C) - P + \mu I\} e \leq 0 \quad (3.39b)$$

for each $e \neq 0$. Considering the second and third mode of the error dynamics (3.35) we get the following inequalities:

$$\begin{bmatrix} e \\ x \end{bmatrix}^\top \begin{bmatrix} (A_2 - L_2 C)^\top P (A_2 - L_2 C) - P + \mu I & (*) \\ \Delta A^\top P (A_2 - L_2 C) & \Delta A^\top P \Delta A \end{bmatrix} \begin{bmatrix} e \\ x \end{bmatrix} \leq 0 \quad (3.39c)$$

$$\begin{bmatrix} e \\ x \end{bmatrix}^\top \begin{bmatrix} (A_1 - L_1 C)^\top P (A_1 - L_1 C) - P + \mu I & (*) \\ -\Delta A^\top P (A_1 - L_1 C) & \Delta A^\top P \Delta A \end{bmatrix} \begin{bmatrix} e \\ x \end{bmatrix} \leq 0 \quad (3.39d)$$

Note that (3.39c),(3.39d) can not be negative definite if $\Delta A \neq 0$, because the term in the lower right corner is always at least positive-semidefinite. Inequalities (3.39a)-(3.39d) do not need to hold in the whole (e, x) space, but only when the respective modes of the error dynamics are active. The second and the third mode of (3.35) are active only when:

$$x^\top H H^\top (x - e) \leq 0. \quad (3.40)$$

Combining (3.40) with (3.39c),(3.39d) via S -procedure, and taking the Schur complement of the obtained matrices leads to the following theorem.

Theorem 3.7.4 *The state estimation error dynamics (3.35) is globally asymptotically stable if there exist matrices $P > 0$, L_1, L_2 constants $\lambda_1, \lambda_2 \geq 0$ and $\mu > 0$ such that the following set of matrix inequalities is satisfied:*

$$\begin{bmatrix} P & 0 & (A_i - L_i C)^\top P & 0 \\ 0 & P & 0 & (*) \\ (*) & 0 & P - \mu I & (*) \\ 0 & \Delta A^\top P & -\frac{1}{2}\lambda_i H H^\top & \lambda_i H H^\top \end{bmatrix} \geq 0 \quad (3.41)$$

for $i = 1, 2$.

The previous result is applicable only to systems with continuous maps. Indeed, the term in the lower right corner is positive semidefinite by construction, and of rank at most 1. The following inclusion must hold (see discussion after theorem 3.4.3 for details):

$$\ker H^\top \subseteq \ker \Delta A$$

which implies:

$$A_2 = A_1 + G H^\top$$

for some G of suitable dimensions.

3.7.2 Discontinuous dynamics

In order to obtain results applicable for discontinuous maps we search for another way to relax the requirements (3.39a)-(3.39d). Condition (3.38) will be required when the appropriate dynamics is active and

$$\|e\|^2 \geq \varepsilon^2 \|x\|^2. \quad (3.42)$$

Combining (3.42) with (3.39c), (3.39d) and (3.40) we get the following theorem:

Theorem 3.7.5 *Consider the system (3.2), observer (3.34) and the estimation error dynamics (3.35). The state estimation error e is eventually bounded by e_{max} , under the assumption that x is bounded by x_{max} if there exist matrices $P > 0$, L_1, L_2 , and constants $\lambda_1, \lambda_2 \geq 0$ and $\mu, \alpha > 0$ such that the following set of matrix inequalities is satisfied:*

$$\begin{bmatrix} P & 0 & (A_i - L_i C)^\top P & 0 \\ 0 & P & 0 & (*) \\ (*) & 0 & P - (\mu + \alpha)I & (*) \\ 0 & \Delta A^\top P & -\frac{1}{2}\lambda_i H H^\top & \lambda_i H H^\top + \alpha \varepsilon I \end{bmatrix} \geq 0 \quad (3.43)$$

for $i = 1, 2$. Moreover, if

$$\gamma_1 I \leq P \leq \gamma_2 I \quad (3.44)$$

then

$$e_{max} \leq \sqrt{\frac{\gamma_2}{\gamma_1}} \varepsilon x_{max}. \quad (3.45)$$

The proof of the previous theorem is similar to the proof of continuous time case (theorem 3.4.3).

Equation (3.45) explicitly gives an eventual upper bound of the estimation error. The observer gains L_1 and L_2 can be determined so as to minimize this upper bound, which amounts to minimizing γ_2/γ_1 and ε , under (3.43). If it is possible to design Luenberger observers for both constituting linear dynamics with a common Lyapunov function of the form (3.37), equations (3.43) can always be made feasible for large enough ε (cf. remark 3.4.6).

3.8 Examples

We present some examples of observer design the using developed theory.

Example 3.8.1 Consider the system

$$\begin{aligned} x(k+1) &= \begin{cases} A_1 x(k) + Bu(k), & \text{if } H^\top x(k) < 0 \\ A_2 x(k) + Bu(k), & \text{if } H^\top x(k) > 0 \end{cases} \\ y(k) &= Cx(k), \end{aligned} \quad (3.46)$$

with the following parameter values:

$$\begin{aligned} A_1 &= \begin{bmatrix} \cos(\frac{\pi}{3}) & \sin(\frac{\pi}{3}) \\ -\sin(\frac{\pi}{3}) & \cos(\frac{\pi}{3}) \end{bmatrix} \\ A_2 &= \begin{bmatrix} \cos(\frac{2\pi}{3}) & \sin(\frac{2\pi}{3}) \\ -\sin(\frac{2\pi}{3}) & \cos(\frac{2\pi}{3}) \end{bmatrix} \\ B &= \begin{bmatrix} 1 \\ 0 \end{bmatrix}, H = \begin{bmatrix} 1 \\ 0 \end{bmatrix}, C = [0 \quad 1], \end{aligned}$$

which is discontinuous over the switching plane. Note that the first state determines the mode, while the second state is measured. Hence, the discrete mode can not be determined directly from the measurements (cf. remark 3.3.2).

We will design an observer for the system (3.46) of the form:

$$\begin{aligned} \hat{x}(k+1) &= \begin{cases} A_1 \hat{x}(k) + Bu(k) + L_1(y(k) - \hat{y}(k)), & \text{if } H^\top \hat{x}(k) < 0 \\ A_2 \hat{x}(k) + Bu(k) + L_2(y(k) - \hat{y}(k)), & \text{if } H^\top \hat{x}(k) > 0 \end{cases} \\ \hat{y}(k) &= C\hat{x}(k) \end{aligned}$$

Solving (3.43) with $\varepsilon = 0.1$ we obtain the following values for the gains of observer (3.34):

$$L_1 = \begin{bmatrix} 0.8662 \\ 0.5031 \end{bmatrix}, \quad L_2 = \begin{bmatrix} 0.8662 \\ 0.4982 \end{bmatrix}$$

with $e_{max} \leq 0.13x_{max}$ (equation (3.45)).

The simulation results are depicted in figure 3.8. The input is chosen as a sequence of normally distributed random numbers, with zero mean and variance 1. The initial state of the system (3.2) is $x(0) = [-1 \quad -1]^\top$, and the the initial state of the observer (3.34) is $\hat{x}(0) = [5 \quad 5]^\top$. Note that the system and the observer start in different modes.

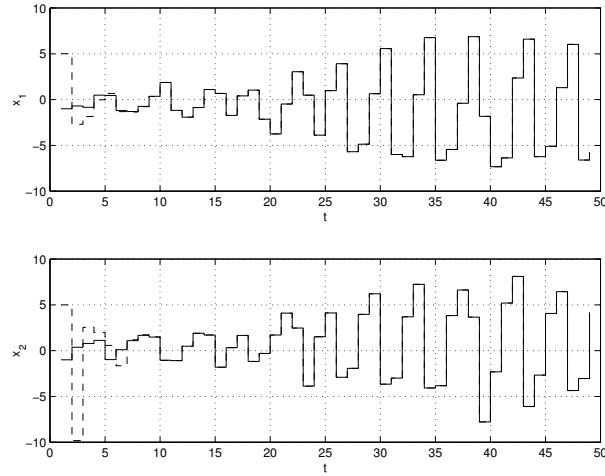


Figure 3.8: The system (solid) and observer (dashed) response (upper: state x_1 , lower: state x_2)

Example 3.8.2 Consider the system

$$\begin{aligned} x(k+1) &= \begin{cases} A_1 x(k), & \text{if } H^\top x(k) < 0 \\ A_2 x(k), & \text{if } H^\top x(k) > 0 \end{cases} \\ y(k) &= Cx(k), \end{aligned} \quad (3.47)$$

with the following parameter values:

$$\begin{aligned} A_1 &= \begin{bmatrix} 0.95 & 0.0475 \\ -0.0475 & 0.95 \end{bmatrix} \\ A_2 &= A_1^\top \\ H &= \begin{bmatrix} 1 \\ 0 \end{bmatrix}, C = \begin{bmatrix} 0 & 1 \end{bmatrix}. \end{aligned}$$

The system evolution depends only on the initial state $x(0)$. Both pairs (A_1, C) , (A_2, C) are observable. Consider two initial state vectors $x^1(0) = [a \ b]^\top$ and $x^2(0) = [-a \ b]^\top$, where $a \geq 0$. The output sequences y^1 and y^2 generated from $x^1(0)$ and $x^2(0)$, respectively, are the same for any $k > 0$, while the state trajectories are not, when $a \neq 0$. In other words, the system is unobservable (in the sense that state can not be uniquely determined from

the measured output whenever the first component of the state differs from 0).

An observer of the form

$$\begin{aligned}\hat{x}(k+1) &= \begin{cases} A_1\hat{x}(k) + L_1(y(k) - \hat{y}(k)), & \text{if } H^\top \hat{x}(k) < 0 \\ A_2\hat{x}(k) + L_2(y(k) - \hat{y}(k)), & \text{if } H^\top \hat{x}(k) > 0 \end{cases} \\ \hat{y}(k) &= C\hat{x}(k)\end{aligned}$$

is designed, using the methodology described in theorem (3.7.5). The following observer gains were obtained:

$$L_1 = \begin{bmatrix} -0.0495 \\ 0.8387 \end{bmatrix}, \quad L_2 = \begin{bmatrix} 0.0455 \\ 0.7495 \end{bmatrix}.$$

while the best found error bound that can be guaranteed is $e_{max} \leq 24x_{max}$. The simulation is depicted in figure 3.9, with initial states $x(0) = [0.2 \ 4]^\top$ and $\hat{x}(0) = [-0.3 \ 4]^\top$. We see that the state estimate \hat{x} converges towards the other possible state trajectory, starting in $[-0.2 \ 4]^\top$, yielding the same output. The observer makes the output injection error zero, and hence recovers one corresponding state trajectory (not necessarily the real one).

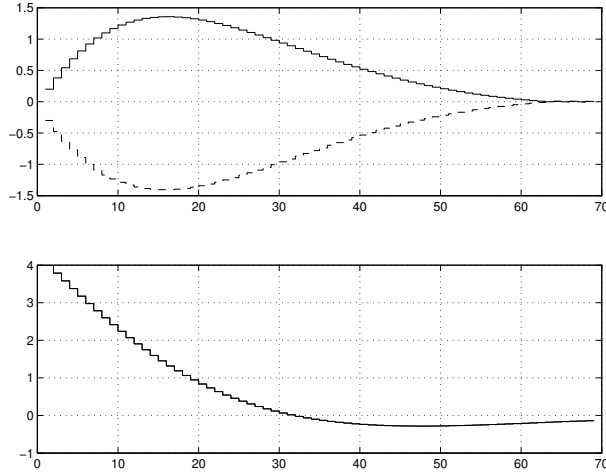


Figure 3.9: System (solid) and observer (dashed) response (upper: state x_1 , lower: state x_2)

3.9 Conclusions

We have presented observer design procedures for a class of bimodal piecewise linear systems both in continuous and discrete time. The proposed observers are of Luenberger type, but, unlike the classical Luenberger observer, the estimation error dynamics is not autonomous. Sufficient conditions for global asymptotic stability were derived. It turned out that these are only feasible in the case when the system dynamics is continuous over the switching plane. We recovered the observer design presented in Arcak and Kokotović (2001), as a special case of our observer design, for the case when the system dynamics is continuous.

For the case when the system dynamics is discontinuous over the switching plane we derive conditions that guarantee that the estimation error is asymptotically bounded relative to the system state. The achievable relative upper bound of the estimation error can be optimized. It is further shown that the desired properties are retained under the presence of sliding modes in the continuous time case. Theoretical results are illustrated by several academic examples. The developed theory is also successfully applied to the experimental case study of a piecewise linear beam. The main line of reasoning can be applied to more general classes of piece-wise affine systems, with the requirement that the input distribution matrix B is the same for all constituting affine dynamics.

In effect, for the case of discontinuous dynamics we achieved input-to-state stability of the observation error dynamics (Sontag (2000)), where the state of the observed system x is considered as the external input. It remains as an open problem whether it is possible to get global asymptotic stability of the estimation error with a Luenberger observer structure, in the case of discontinuous bimodal piecewise affine system.

Robustness of the designed observers with respect to the model uncertainty is an important issue, which remains to be investigated. The future work will also focus on utilizing the obtained observers for feedback stabilization of the considered class of bimodal piecewise linear systems, as well as on broadening the class of piecewise affine (and general hybrid) systems to which the presented techniques are applicable. It is straightforward to form the observer error dynamics for a general case of a piecewise affine system (see (1.1) in chapter 1). To relax the requirements on the derivative of the Lyapunov function an approach similar to Johansson and Rantzer (1998a) can be used. The major difficulty, however, is to understand the conditions implied by such relaxations (such as the continuity requirement implied by relaxation used in the proof of the theorem 3.4.3).

Data-Based Hybrid Modelling of the Component Placement Process in Pick-and-Place Machines

4.1 Introduction 4.2 Experimental setup 4.3 Identification algorithm 4.4 Identification with free and impact modes	4.5 Identification with saturation 4.6 Conclusion
--	---

In this paper an experimental study in the identification of the electronic component placement process in pick-and-place machines is presented. Unilateral contact and saturation phenomena characterize the hybrid dynamics of the system. Furthermore, the mode switch cannot be measured and identification algorithms for hybrid systems, that are capable to reconstruct both the modes and the switching law, must be used. Piece-Wise AutoRegressive eXogenous (PWARX) models, which consist of a number of ARX modes together with the partition of the regressor space into regions where each model is valid are identified. Reconstructed models are able to capture the relevant dynamics of the experimental setup. Practical insights on hybrid system identification and comments on possible improvements of the identification algorithm complement the quantitative results.

This chapter is based on Juloski et al. (2003b) and Juloski et al. (2004b).

4.1 Introduction

In this paper an experimental study in the identification of the electronic component placement process in pick-and-place machines is presented. Pick-and-place machines are used to automatically place electronic components on printed circuit boards (PCBs), and form a key part of an automated PCB assembly line. A pick-and-place machine works as follows: the PCB is placed in the working area of the mounting head; the mounting head,



Figure 4.1: Fast component mounter (courtesy of Assembleon)

carrying an electronic component (using, for instance, a vacuum pipette), is navigated to the position where the component should be placed on the PCB; the component is placed, released, and the process is repeated with the next component. A fast component mounter, consisting of twelve mounting heads working in parallel, is shown in figure 4.1. The throughput of such a configuration can be up to 96.000 placed components per hour (Assembleon (2002)).

Consider the subtask of the component placement on the PCB. Assuming that the mounting head, carrying the component, is in the right position above the PCB, the component is pushed down until it comes in contact with the PCB and then released. The PCB is not rigid, but, depending on the material, has certain elasticity properties. The whole operation should be as fast as possible (to achieve maximal throughput), while satisfying technological and safety constraints (e.g. the exerted forces must not damage the component).

As detailed in section 4.2, during the placement process, switching between different modes of operation occurs. This motivates the search for the model in the form of a hybrid system. Research on hybrid systems identifica-

tion has been mainly concerned with the reconstruction of Piece-Wise ARX (PWARX) models, which can be further recast into piecewise affine (Sontag (1981)), mixed logic dynamics (Bemporad and Morari (1999)) or linear complementarity (Heemels et al. (2000)) systems. A PWARX model consists of a finite number of ARX modes, together with a polyhedral partition of the regressor space into regions where each mode is active. Several techniques for identification of PWARX systems have been proposed (Ferrari-Trecate et al. (2003); Bemporad et al. (2000b, 2003); Vidal et al. (2003b)). In this work the algorithm developed by Ferrari-Trecate et al. (2003) is adopted. The algorithm is briefly summarized in Section 4.3.

The identification of the component placement process aims at providing models for analysis and control design. In particular, Model Predictive Control (MPC) and verification algorithms for PWA and MLD systems (Bemporad and Morari (1999)), (Bemporad et al. (2000c)) can be straightforwardly applied to hybrid systems in the PWARX form. Generally speaking, MPC and verification algorithms for PWA systems can be recast into mixed-integer programming problems where the process model enters the constraints. Therefore, the application of these techniques is subordinated to the availability of dynamic models of the system considered. From one side, it is of interest to obtain models with the smallest number of states and modes, as the computational complexity of control and verification methods may increase dramatically with model complexity (Bemporad and Morari (1999)), (Bemporad et al. (2000c)). On the other hand, it is important to note that such methods require the *simulation* of the process over the horizon of N steps, where $N > 1$. Therefore, models optimized for one-step-ahead predictions may not be satisfactory since an accurate simulation performance is required.

The fact that models tailored to one-step-ahead prediction may perform poorly in simulation is well-known in the context of ARX systems (Ljung (1999)), and it can become more noticeable for PWARX systems. Indeed, prediction errors due to imperfect estimates in mode parameters and regions, may lead to a wrong choice of the next mode, so triggering large-error propagation phenomena. Since all the existing identification algorithms for hybrid systems seek for one-step-ahead predictive models, it is of paramount importance to check the model quality in simulation.

In sections 4.4 and 4.5 the identification results are presented. Models of increasing complexity are considered and their simulation properties discussed. It is shown that the quality of the simpler models, capturing a subset of the system modes, is satisfactory. Moreover, despite the use of black-box algorithms that do not exploit any physical knowledge on the system, the reconstructed modes admit a physical interpretation. The more complex mo-

dels, that take into account an increasing number of system modes, are less satisfactory. Their responses, together with some physical insight on the system, allow to single out the model elements that are not correctly identified. In particular, this information may be of help in designing new identification experiments or devising new identification strategies for improving the model quality.

4.2 Experimental setup

In order to study the placement process, an experimental setup was made as depicted in figure 4.2. A scheme of the setup is presented in figure 4.3. The setup consists of the mounting head, from an actual pick-and-place machine, which is fixed above the impacting surface (the small disc in the figure 4.2). The impacting surface is in contact with the ground via the spring (the spring c_2 in figure 4.3, within the outer tube in figure 4.2). The mechanical construction under the impacting surface is such that only the movement on the vertical axis is enabled (inner tube, which can slide inside the outer tube in figure 4.2). This construction exhibits linear and dry friction phenomena, represented in figure 4.3 by the damper d_2 and the block f_2 , respectively. The chosen design of the impacting surface simulates the elasticity properties of the PCB as well as hard mechanical constraints due to saturations. It also introduces some side effects, such as dry friction.

The mounting head contains: a vacuum pipette which can move on the vertical axis (the mass M in figure 4.3) and which is connected via the spring to the casing (the spring c_1 in figure 4.3); an electrical motor which enables the movement (represented by force F in figure 4.3); and a linear optical encoder, which measures the position of the pipette, relative to the upper retracted position. The position axis is pointed downward, i.e. the value of the position increases when the pipette moves downward. The motion of the pipette is also subject to friction phenomena (the damper d_1 and the dry friction block f_1 in figure 4.3).

The dynamics of the experimental setup exhibits, in a first approximation, four different modes of operation:

upper saturation: the pipette is in the upper retracted position (i.e. can not move upward, due to the physical constraints);

free mode: the pipette is not in contact with the impacting surface, but is not in the upper saturation;



Figure 4.2: Photo of the experimental setup

impact mode: the pipette is in contact with the impacting surface, but is not in lower saturation;

lower saturation: the pipette is in the lower extended position, (i.e. can not move downward due to the physical constraints).

The control input is the voltage applied to the motor, which is converted up to a negligible time constant to the force F . The input signal for the identification experiment should be chosen in a way that all modes are sufficiently excited. However, conditions for the design of persistently exciting inputs are not available for hybrid models. To obtain the data for identification, the input signal $u(t)$ is chosen as:

$$u(t) = a_k \quad \text{when} \quad t \in [kT, (k+1)T) \quad (4.1)$$

where $T > 0$ is fixed, and the amplitude a_k is a random variable, with uniform distribution in the interval $[a, b]$. By properly choosing the boundaries of the interval $[a, b]$ only certain modes of the system are excited. For instance only free and impact modes can be excited, without reaching upper and lower saturations.

Some features of the data sets obtained for the input signal (4.1) are shown in figure 4.4. In figure 4.4a the effect of dry friction damping can be noticed. In figure 4.4b small changes in the input signal produce no

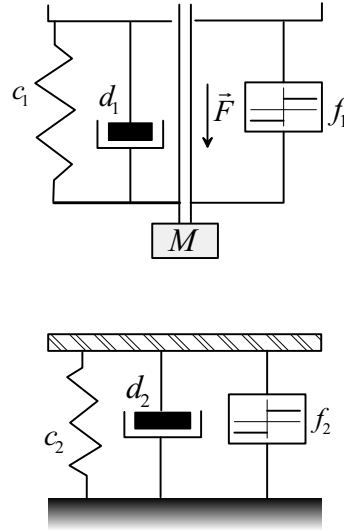


Figure 4.3: Schematic representation of the experimental setup

change in position, because of the dry friction in stick phase. In figure 4.4c the system is excited so that the lower saturation is reached. The lower saturation effectively acts as a velocity reset map, active when certain position is reached (≈ 25 in figures 4.4c and 4.4d). Figure 4.4d shows the system behavior when both upper and lower saturations are reached. The bouncing effect can be observed when reaching upper saturation, due to the elastic impact with the mechanical constraints.

Waveforms in the experimental setup were sampled at 4kHz. Control hardware in the pick-and-place machines enables sampling and control at much lower frequencies. Hence, models of the process at lower sampling frequencies are of interest. Data used for identification are obtained by re-sampling the original signals at 50Hz. All plots in the paper have samples as units on the time axis. Values of the position are given in scaled encoder units¹, and the values of input are given in volts. In all plots the original input signals are multiplied by the scaling factor -100 , in order to show them together with the system responses. However, original input signals are used in the identification experiments.

Having a physical representation of the setup, like the one depicted in figure 4.3, one would use a white-box modeling technique for identifying the

¹The exact encoder specifications were not disclosed by the manufacturer of the head.

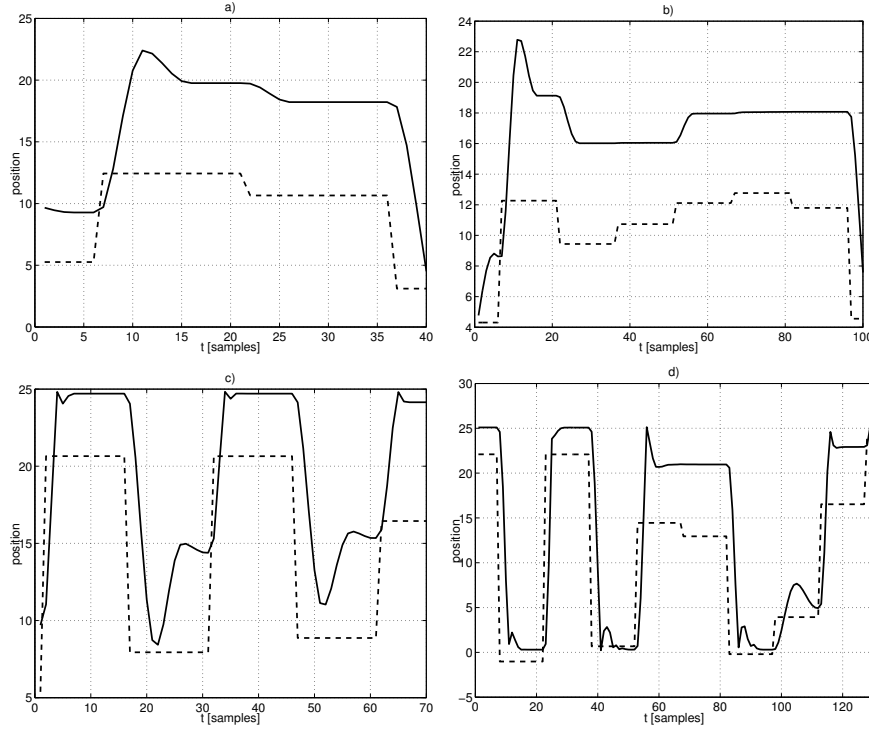


Figure 4.4: Some features of the experimental data set a),b) effects of the dry friction c)lower saturation d)upper saturation (solid: system response, dashed: scaled input)

value of the physical parameters (c_1 , c_2 , etc.). However there are major difficulties that hamper this goal. In order to illustrate them, consider a simplified representation of the system. If saturations are not reached, dry friction is absent and the springs and dampers in figure 4.3 are linear, the equations relating the force F to the position y of the head are:

$$\ddot{y} = -\frac{c_1}{M}y - \frac{d_1}{M}\dot{y} + \frac{c_1\bar{y}_1}{M} + \frac{F}{M} \quad (\text{free mode}) \quad (4.2a)$$

$$\ddot{y} = -\frac{c_1 + c_2}{M + m}y - \frac{d_1 + d_2}{M + m}\dot{y} + \frac{c_1\bar{y}_1 + c_2\bar{y}_2}{M + m} + \frac{F}{M + m} \quad (\text{impact mode}) \quad (4.2b)$$

where $y = 0$ corresponds to the head in the upper retracted position, posi-

ve forces are directed downward, the springs c_1 and c_2 are at rest for $y = \bar{y}_1$, $y = \bar{y}_2$, respectively, and m is the mass of the impacting surface. Since data are available in discrete-time, one would like to sample system (4.2) and relate the parameters of the discrete-time model to those of model (4.2) and to the sampling time. Unfortunately, a general methodology for discretizing continuous-time hybrid systems is not available (Çamlıbel et al. (2002)), the key difficulty being to account, in discrete-time, for the effects produced by mode switches happening within the sampling interval. For this reason, one resorts to black-box identification by considering an AutoRegressive eXogenous (ARX) representation for each mode

$$y(k) = \theta_{1,1}y(k-1) + \cdots + \theta_{1,n_a}y(k-n_a) + \theta_{1,n_a+1}F(k-1) + \cdots + \theta_{1,n_a+n_b}F(k-n_b) + \theta_{1,n_a+n_b+1} \quad (\text{free mode}) \quad (4.3a)$$

$$y(k) = \theta_{2,1}y(k-1) + \cdots + \theta_{2,n_a}y(k-n_a) + \theta_{2,n_a+1}F(k-1) + \cdots + \theta_{2,n_a+n_b}F(k-n_b) + \theta_{2,n_a+n_b+1} \quad (\text{impact mode}) \quad (4.3b)$$

Even if the relations between the parameters in (4.3) and in (4.2) are unclear, note that both (4.3) and (4.2) are affine models in y and F . Moreover, if $n_a = 2$ and $n_b = 1$, equations (4.3) can be obtained by sampling separately each mode of the original system.

Consider now the switching mechanism. Let $\tilde{y}(t)$ be the position of the impacting surface. In (4.2), the modes “free” and “impact” are active if $\tilde{y}(t) > y(t)$ and $\tilde{y}(t) = y(t)$, respectively. However, $\tilde{y}(t)$ is not measured, and it is not even a constant signal, because of the dynamics of the impacting surface. These facts have two major consequences on the the switching rules for (4.3). First, it is impossible to associate *a priori* a mode of operation to each data point $(y(k), F(k))$. This lack of information constitutes the key difficulty of hybrid system identification (Ferrari-Trecate et al. (2003)) and obliges one to adopt an identification algorithm that is capable to reconstruct all the modes at the same time. Second, the switching mechanism has to be reconstructed from y and F only. For these reasons, a black-box approach for the switch reconstruction is adopted, by assuming that the modes (4.3a) and (4.3b) are active if the regressors lie in \mathcal{X}_1 and \mathcal{X}_2 , respectively, where the sets \mathcal{X}_1 and \mathcal{X}_2 are disjoint polyhedra that have to be estimated. Model (4.3), endowed with this switching law, define a Piece-Wise ARX (PWARX) system, whose identification is discussed in the next section. Obviously, differences in the true and reconstructed switching mechanism may completely destroy the analogy between (4.2) and (4.3) since each one of the reconstructed modes can possibly represent a mixture of the original modes. Then, the possibility of associating the estimated modes to the true ones, has to be assessed a

posteriori.

Remark 4.2.1 An alternative way for reconstructing the system dynamics is to consider general Nonlinear ARX models of the type $y(k) = f(y(k-1), \dots, y(k-n_a), F(k-1), \dots, F(k-n_b))$ that can be estimated by resorting to nonlinear identification procedures. For control, nonlinear models can be exploited in MPC schemes (Mayne et al. (2000)) where the optimal input is computed by solving a *nonlinear* programming problem. However, it is important to note that due to nonlinearities, convergence to the optimal solution is not guaranteed. This is in sharp contrast with MPC for PWA systems, that hinges on mixed-integer linear or quadratic optimization for which the optimal solution is always achieved (Bemporad and Morari (1999)).

4.3 Identification algorithm

In this section, the skeleton of the identification algorithm proposed by Ferrari-Trecate et al. (2003) is summarized.

A PWA map $f : \mathbb{X} \mapsto \mathbb{R}$ is defined by the equations

$$f(x) = f_q(x) \quad \text{if } x \in \bar{\mathcal{X}}_q \quad (4.4)$$

$$f_q(x) = \begin{bmatrix} x^\top & 1 \end{bmatrix} \bar{\theta}_q \quad (4.5)$$

where $\mathbb{X} \subset \mathbb{R}^n$ is a bounded polyhedron, $\{\bar{\mathcal{X}}_q\}_{q=1}^s$ is a polyhedral partition of \mathbb{X} in s regions and $\bar{\theta}_q \in \mathbb{R}^{n+1}$, $q = 1, \dots, s$ are Parameter Vectors (PVs). Therefore, a PWA map is composed of s affine modes defined by the pairs $(\bar{\theta}_q, \bar{\mathcal{X}}_q)$. The data set \mathcal{N} collects the samples $(x(k), y(k))$, $k = 1, \dots, N$, generated according to the equation

$$y(k) = f(x(k)) + \eta(k) \quad (4.6)$$

where $\eta(\cdot)$ represents the measurement noise. It is assumed that the number s of modes is known. The aim of PWA regression is to estimate the PVs and the regions by using the information provided by \mathcal{N} .

When considering hybrid systems, an input/output description of a PWA system with inputs $u(k) \in \mathbb{R}^m$ and outputs $y(k) \in \mathbb{R}$ is provided by PWARX models that are defined by equation (4.6) where k is the time index and the vector of regressors $x(k)$ is given by

$$x(k) = \begin{bmatrix} y(k-1) & y(k-2) & \dots & y(k-n_a) \end{bmatrix} \quad (4.7)$$

$$u^\top(k-1) \quad u^\top(k-2) \dots u^\top(k-n_b) \quad]^\top. \quad (4.8)$$

It is apparent that, if the orders n_a and n_b are known, the identification of a PWARX model amounts to a PWA regression problem.

The essential hybrid feature of PWARX models is the ability to capture regressor-dependent mode switches. This switch mechanism is quite general. For instance ARX models with input/output PWA static nonlinearities are PWARX models. Moreover, PWARX models provide an input-output description for a fairly large class of discrete-time PWA systems without logic states (Vidal et al. (2003b)).

The regression algorithm is structured in three steps.

1. Local Regression. For $j = 1, \dots, N$ a Local Dataset (LD) \mathcal{C}_j is formed. It collects $(x(j), y(j))$ and the samples $(x, y) \in \mathcal{N}$ corresponding to the $c - 1$ nearest neighbors x to $x(j)$. The cardinality c of an LD is a parameter of the algorithm satisfying $c > n + 1$. LDs collecting only data points associated to a single mode are referred to as *pure* LDs. The remaining LDs are termed *mixed*. Linear regression is performed on each LD \mathcal{C}_j to obtain the Local Parameter Vectors (LPVs) θ_j and their empirical variance V_j . The LD centers $m_j = \frac{1}{c} \sum_{(x,y) \in \mathcal{C}_j} x$ are also computed together with the associated scatter matrix $Q_j = \sum_{(x,y) \in \mathcal{C}_j} (x - m_j)(x - m_j)^\top$. The information about the j -th local model is collected in the Feature Vector (FV) $\xi_j = [\theta_j^\top, m_j^\top]^\top$. As for the LDs, FVs are either pure or mixed. FV ξ_j are interpreted as the realization of a Gaussian random variable with variance

$$R_j = \begin{bmatrix} V_j & 0 \\ 0 & Q_j \end{bmatrix} \quad (4.9)$$

Intuitively, both V_j^{-1} and Q_j^{-1} are related to the confidence one should have on the fact that \mathcal{C}_j is pure. In fact, in the noiseless case, $\|V_j^{-1}\|$ becomes infinite for pure LDs while remaining finite for mixed LDs. Analogously, if $\|Q_j^{-1}\|$ is “small” this indicates that the regressors in \mathcal{C}_j are scattered and therefore the LD is likely to be mixed.

The key point is that pure FVs associated to the same mode are expected to be similar and then to form s distinct and dense clouds in the FV-space. Thus, as detailed below in steps 2 and 3, the problem of finding the data points associated to the same mode can be recast into the problem of finding s dense clouds of pure FVs. However, one should be warned about the presence of mixed FVs that do not carry any useful information on the true modes and form a pattern of isolated points in the FV-space.

2. Clustering. The FVs are partitioned in s groups $\{\mathcal{D}_q^*\}_{q=1}^s$ through clustering. For this purpose, a K-means algorithm (Duda and Hart (1973))

is used in order to minimize the cost functional

$$J(\{\mathcal{D}_q\}_{q=1}^s, \{\mu_q\}_{q=1}^s) = \sum_{i=1}^s \sum_{\xi_j \in \mathcal{D}_i} \|\xi_j - \mu_q\|_{R_j^{-1}}^2. \quad (4.10)$$

where $\{\mathcal{D}_q\}_{q=1}^s$ are the clusters and $\{\mu_q\}_{q=1}^s$ are the cluster centers. In principle, one would be able to collect all pure FVs characterizing the same mode in a single set \mathcal{D}_q . However, since mixed FVs are not a priori known, they will be assigned to some cluster as well. The best results are expected when they do not spoil the accuracy in clustering pure FVs. To this aim, we highlight that the confidence measures R_j^{-1} in (4.10) allow to assign less influence to mixed FVs than to pure FVs. Thus, the final clusters will mainly depend on pure FVs.

3. Estimation of the modes. By using the bijective maps $(x(j), y(j)) \leftrightarrow \mathcal{C}_j \leftrightarrow \xi_j$, sets $\{\mathcal{F}_i\}_{i=1}^s$ of data points are built according to the rule:

$$(x(j), y(j)) \in \mathcal{F}_q \Leftrightarrow \xi_j \in \mathcal{D}_q^*.$$

This means that each set \mathcal{F}_q collects data associated to similar local features. The data points in each final set \mathcal{F}_q are then used for estimating the mode PVs through weighted least squares. The regions are reconstructed on the basis of the final sets by resorting to multicategory pattern recognition algorithms (Bredensteiner and Bennett (1999)) that find the hyperplanes separating $\{x : (x, y) \in \mathcal{F}_q\}$ and $\{x : (x, y) \in \mathcal{F}_{q'}\}$ for all indexes $q \neq q'$. This allows to find the matrix H_q and the vector h_q , for $q = 1, \dots, s$, representing the polyhedra \mathcal{X}_q in terms of the linear inequalities $H_q x \leq h_q$.

For the practical use of the algorithm, some potential pitfalls are highlighted. First, the method is expected to perform poorly if the ratio between the number of mixed and pure LDs is high. Note that the number of mixed LDs increases with c . Thus, it is desirable to keep c as small as possible. On the other hand, for high noise levels large values of c may be needed in order to filter the noise corrupting pure LPVs. Another reason for choosing large values of c is to “average out” small nonlinearities affecting the modes. This point is illustrated in Section 4.4.

Second, bad identification results can be also obtained because of the inherent sub-optimality of K-means (Duda and Hart (1973)) that is a computationally cheap but approximate method for minimizing the cost J in (4.10). In (Ferrari-Trecate et al. (2003)), some strategies to alleviate this problem are given.

Finally, data points suspected to be attributed to the wrong mode can be detected a posteriori through residuals analysis or via the procedure proposed by Ferrari-Trecate and Schinkel (2003). A discussion about how to

exploit this information for improving the identification results is provided in (Ferrari-Trecate and Schinkel (2003)).

4.4 Identification with free and impact modes

In order to study the applicability of the described identification procedure to our experimental setup several data sets have been collected. They consist of 750 samples (15 s), divided in two overlapping sets of 500 points. The first set is used for identification, and the second for validation purposes. Note that 250 samples are used both for validation and identification. This allows to show, on the same picture, the fitting and the generalization properties of the reconstructed models.

In the first experiment the parameters a and b characterizing the input signal are chosen so that only the free and impact modes are excited. The identification and validation data sets are depicted in figure 4.5. The effect of the dry friction in stick phase is clearly visible in figure 4.5b on the time interval (200, 300).

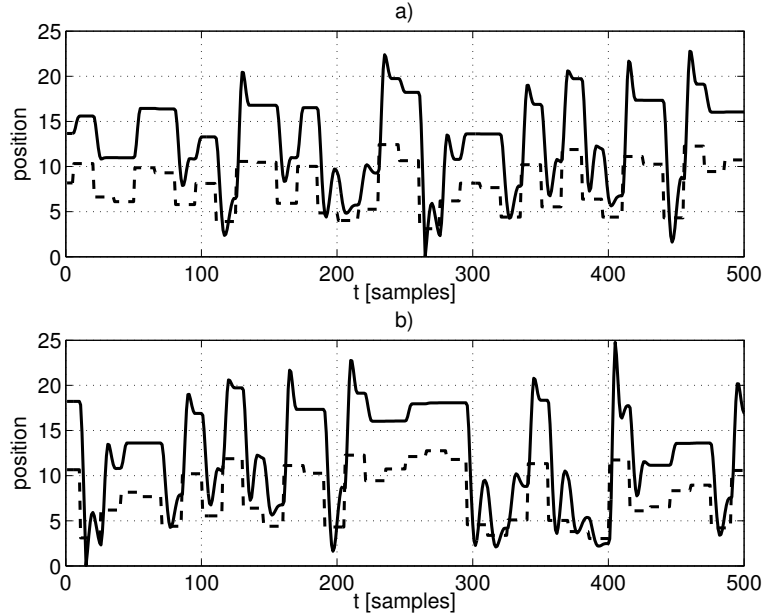


Figure 4.5: Excitation of the impact and free modes. Data set used for a) identification b) validation (solid: system response, dashed: scaled input)

PWARX models with two modes have been identified. For the first model the parameters $n_a = 2, n_b = 1$ and $c = 80$ have been used. One-step-ahead predictions on validation data are depicted in figure 4.6² together with the mode active at each time instant. The coefficients θ_q and the matrices H_q and h_q defining the regions are given in table 4.9. The difference between the predicted and the actual system response is small and visible only on certain time intervals (e.g. (200,300)). To what concerns the reconstructed modes, they capture the different physical modes of operation. In fact, from figure 4.6, one can observe that modes 1 and 2 are active when the system is likely to be in the impact and free modes, respectively.

Results of *simulation* with the identified model are shown in figure 4.7a. The response is still similar to the one of the real system, but now differences are visible.

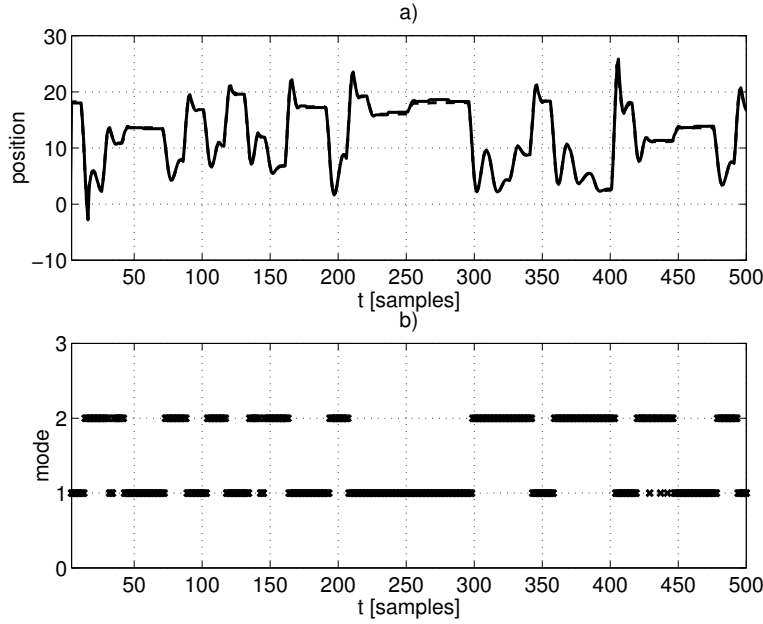


Figure 4.6: Validation of the model with $n_a = 2, n_b = 1, 2$ modes, $c = 80$.
a) One step ahead prediction for validation data (solid: model prediction, dashed: system response) b) Active mode at each time instant

²Note that in figure 4.6b, due to the thick line used to plot points it may appear that at certain time instants two modes are active. Of course, only one mode is active at any time instant.

A second model, characterized by parameters $n_a = 2, n_b = 2, c = 80$ is identified, and its simulated response is shown in figure 4.7b. Despite the increased order, the physical behavior is still not perfectly represented.

From the results shown in figure 4.7 it is clear that the differences are mainly due to the effects of the dry friction, which are not captured by the models. For instance, on the time interval (200, 300) a linear response is predicted to small step excitations, while in the physical system no movement occurs. The first model accurately simulates responses to large step excitations, while responses to small step excitations are not correct. The second model attempts to make a compromise between small and large step excitations - small step responses are better represented by the second model, but large step responses are worse.

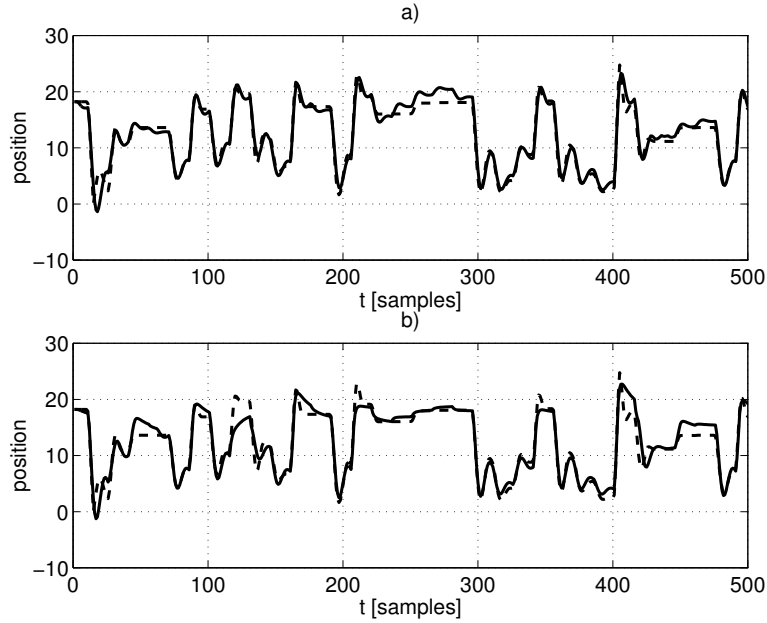


Figure 4.7: Simulation of the bimodal PWARX systems a) model with $n_a = 2, n_b = 1, c = 80$ b) model with $n_a = 2, n_b = 2, c = 80$ (solid: model output, dashed: system output)

The best bimodal PWARX model requires the use of LDs with large cardinality. For minimal theoretical values of c ($c = 4$, resp. $c = 5$) the obtained models are not usable, because the simulated output is completely dissimilar to the measured one. By increasing c , models of different quality

are obtained, and the best results correspond to $c \geq 40$. It is interesting to note that even for large values of c (i.e. $c = 90$, for a data set of 500 points) good models can be still obtained.

A possible explanation is the following. Because of the presence of dry friction (see figures 4.4a and 4.4b) responses in both modes are nonlinear. Therefore, LDs with small c produce scattered LPVs, and the clustering step is not successful in separating FVs associated to the contact and the free modes. On the other hand, LDs collecting a large number of data points produce LPVs corresponding to “averaged” linear models. Such estimates produce distinct clusters in the feature vector space, but filters out the effect of the dry friction. The effect of “averaging” is noticeable in figure 4.7b, on time interval (200, 300), where a compromise is reached between responses to large and small step signals.

The previous discussion motivates the attempt to identify a PWARX model with more modes by using the same data set. The simulated response of the model with 4 modes, $n_a = 2$, $n_b = 2$, $c = 70$ is depicted in figure 4.8a, and the active modes during the simulation are shown in figure 4.8b. From figure 4.8b, one can observe that modes 2 and 4 correspond to the free and impact modes, respectively, while modes 1 and 3 represent the behavior on the boundaries between free and impact modes. The overall model performance in simulation is better in comparison to the bimodal case, at the price of increased model complexity. Identification with higher model orders and with more modes shows no significant improvements on the response quality.

Remark 4.4.1 For assessing the quality of results, Neural Networks (NN) are used for identifying the NARX model $y(k) = f(y(k-1), y(k-2), u(k-1))$. The best results were obtained by considering a 2-layer network with 4 neurons in the hidden layer having hyperbolic tangents as activation functions. The network was trained by using an *output error* algorithm exploiting weight decay and optimal brain surgeon strategy, for avoiding over-parametrization. The experiment was performed by using the Matlab toolbox written by Nørgaard (1997). The resulting NN has 18 parameters and the simulation results are analogous to those of figure 4.7-a, i.e. the NARX model suffers from the same problems as the PWARX model with $n_a = 2$, $n_b = 1$ and $c = 80$. As discussed in (Ferrari-Trecate and Muselli (2002)) the high number of NN parameters is needed for approximating model discontinuities with a continuous NN.

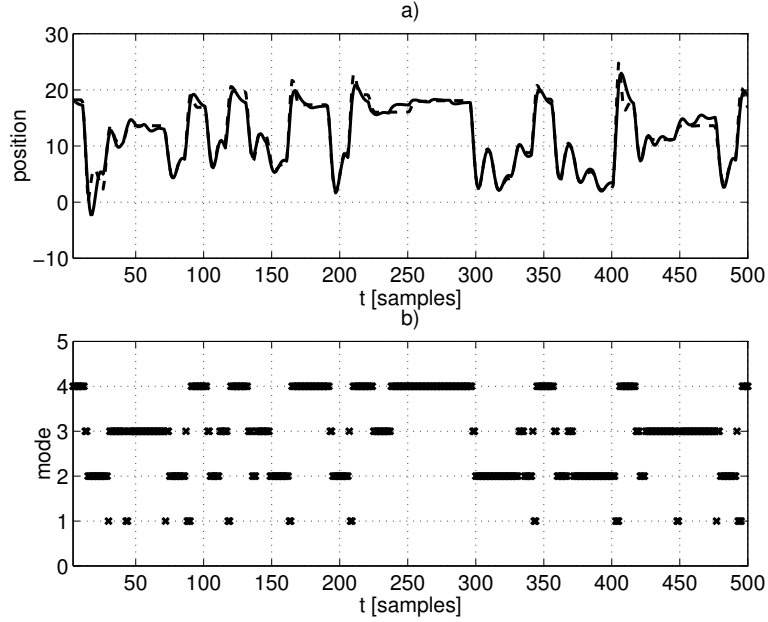


Figure 4.8: a) Simulation of the four-mode PWARX system $n_a = 2$, $n_b = 2$, $c = 70$ (solid: model output, dashed: system output) b) Active mode at each time instant

4.5 Identification with saturations

In order to get a model which is valid in wider range of operating conditions a new experiment is performed. The input was chosen so that impacts between the head and the spring occur and the lower saturation of the spring is reached. The data set was again divided in two parts (depicted in figure 4.10), where the first part is used for identification, and the other for validation.

In order to highlight the difficulties in reconstructing the lower saturation, consider again the scheme of figure 4.3. Lower saturation occurs at a fixed but unknown position y_s and resets the velocity to zero. In principle, one would enhance the models obtained in Section 4.4 with the additional dynamics $y(k) = y_s$, active when either

$$x(k-1) \in \mathcal{X}_c \text{ and } y_c(k) \geq y_s \quad (4.11)$$

or

$$y(k-1) = y_s \text{ and } F(k-1) \geq -\bar{F}(k-1) \quad (4.12)$$

Parameters	Model
$n_a = 2,$ $n_b = 1,$ $2 \text{ modes},$ $c = 80$	$\theta_1 = [1.4006 \quad -0.6299 \quad -34.4116 \quad 0.3031]^\top,$ $\theta_2 = [1.5872 \quad -0.7682 \quad -44.8641 \quad -0.7184]^\top,$
	$H_1 = \begin{bmatrix} -1.0778 & 0.26430 & 5.7984 \\ 1.0 & 0 & 0 \\ 0 & -1.0 & 0 \\ 0 & 1.0 & 0 \\ 0 & 0 & -1.0 \\ 0 & 0 & 1.0 \end{bmatrix},$
	$H_2 = \begin{bmatrix} 1.0778 & -0.26430 & -5.7984 \\ -1.0 & 0 & 0 \\ 0 & -1.0 & 0 \\ 0 & 1.0 & 0 \\ 0 & 0 & -1.0 \\ 0 & 0 & 1.0 \end{bmatrix},$
	$h_1 = [-10.282 \quad 30.0 \quad 30.0 \quad 30.0 \quad 0.2 \quad 0.2]^\top,$ $h_2 = [10.282 \quad 30.0 \quad 30.0 \quad 30.0 \quad 0.2 \quad 0.2]^\top,$

Figure 4.9: Parameters of identified model

where \mathcal{X}_c is the region associated to the contact mode, $y_c(k)$ is the predicted position in contact mode and $\bar{F}(k-1)$ is the reaction force of the impacting surface when $y = y_s$. Condition (4.11) characterizes the switching between the contact and lower saturation, whereas (4.12) captures the requirements for staying in saturation at the instants $k-1$ and k . Note that it is assumed that when the saturation is reached, the impacting surface remains in contact with the head, so neglecting bouncing phenomena of the impacting surface on the head.

Despite the fact that the above dynamics defines a PWARX model, it is not evident how to include it in the identification algorithm for several reasons. First, the region defined by (4.11) depends on the polyhedron \mathcal{X}_c that has to be estimated by itself. The identification procedure of Section 4.3 does not allow to specify constraints between different regions. Second, the reaction force $\bar{F}(k)$ is not measured and it has to be deduced from the available signals. Third, for having $y(k) = y_s$ all entries of the mode parameter, except the displacement must be constrained to zero. The introduction of a partially specified dynamics falls within the domain of *gray-box* identification, a topic that, to the authors' knowledge, has not been yet considered for hybrid systems.

Therefore, once more black-box identification approach is used and a general PWARX model with 3 modes and parameters $n_a = 2$, $n_b = 2$, $c = 40$ is identified. The response of the model in simulation is depicted in figure

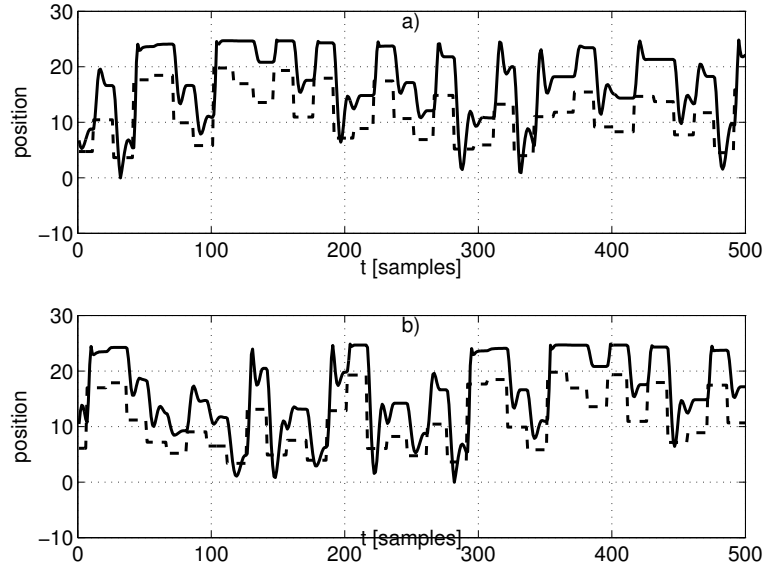


Figure 4.10: Excitation of the free, impact and lower saturation modes. Data set used for a) identification b) validation (solid: system response, dashed: scaled input)

4.11a, and the active modes are shown in figure 4.11b. The model parameters are reported in table 4.12. From figure 4.11 it is possible to observe that the third mode is triggered by the lower saturation. An analysis of the parameter vector θ_3 and the region $\mathcal{X}_3 = \{x : H_3 x \leq h_3\}$ reveals that the “lower saturation” mode can be interpreted as a mixture of the true saturation and contact (in proximity of saturation) modes. From the dynamics of the third mode is possible to compute the estimated saturation value y_s . Consider the case where the system is in saturation at time $k - 2$ and $k - 1$ and the constant force $F \sim u$ balances the reaction of the impacting surface. Then, the system will be in saturation also at time k . According to the ARX dynamics of mode 3, y_s and u must verify the linear constraints

$$y_s(1 - \theta_{3,1} - \theta_{3,2}) = (\theta_{3,3} + \theta_{3,4})u + \theta_{3,5} \text{ and } H_3[y_s \ y_s \ u \ u]^T \leq h_3 \quad (4.13)$$

The minimal and maximal predicted values of saturation can be found by solving the linear programs $\min y_s$ and $\max y_s$, respectively, in the unknowns y_s and u subject to the constraints (4.13). We found $\min y_s = 23.2$, $\max y_s = 24.2$. Note that the latter value matches quite well the saturation level visible in figure 4.11-a.

Remark 4.5.1 If the PWARX model has to be used for designing an MPC control scheme, a detailed model of the process of entering and leaving lower saturation is not necessary. In fact, by knowing only y_s , one can add to the MPC problem the constraints $y(k) \leq y_s$ and the resulting control law will take care of not driving the system in saturation. Therefore, for MPC, it is of primary importance to have a reliable description of the system in free and contact mode (as done in Section 4.4) and complement it with the estimate of y_s derived before, or better by conducting *ad hoc* experiments.

Modes 1 and 2 correspond to non-saturated modes in the experimental setup. The majority of the points associated to non-saturated behaviors is attributed to the second mode (this includes the points from both the impact and the free modes), while the points associated to the first mode mainly characterize the impact phenomena. The model output is more similar to the output of the physical system in parts of the data set that correspond to the saturated and impact behaviors.

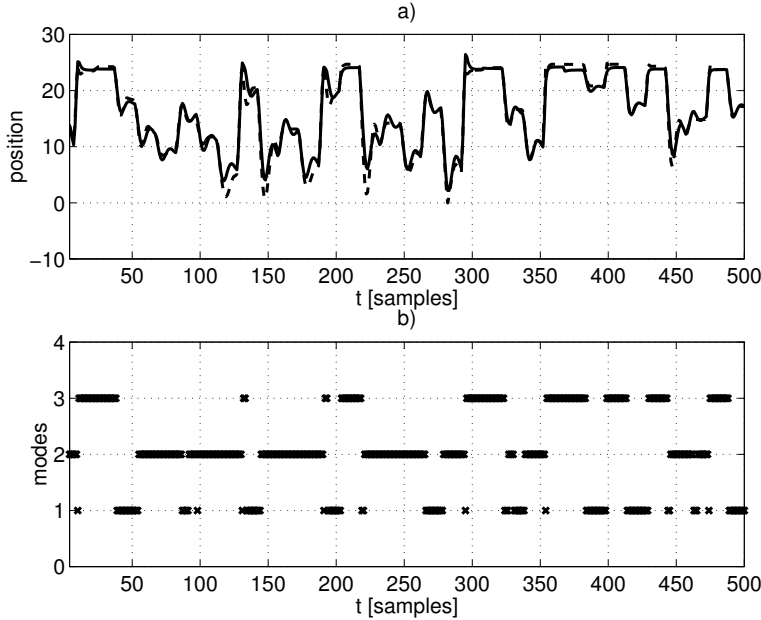


Figure 4.11: a) Simulation of the tri-modal PWARX system $n_a = 2$, $n_b = 2$, $c = 40$ (solid: model response, dashed: system response) b) Active mode at each time instant

Parameters	Model
$n_a = 2,$ $n_b = 2,$ 3 modes, $c = 40$	$\theta_1 = [1.3112 \quad -0.60069 \quad -32.820 \quad -2.1941 \quad 1.2052]^T,$ $\theta_2 = [1.4693 \quad -0.73980 \quad -36.712 \quad -8.1766 \quad 0.12148]^T,$ $\theta_3 = [0.68555 \quad -0.097315 \quad -25.474 \quad 17.555 \quad 8.3912]^T,$
	$H_1 = \begin{bmatrix} -0.38975 & -0.13906 & -5.4530 & 16.011 \\ 4.3814 & -0.72624 & -40.376 & -52.533 \\ 0 & -1.0 & 0 & 0 \\ 0 & 1.0 & 0 & 0 \\ 0 & 0 & -1.0 & 0 \\ 0 & 0 & 1.0 & 0 \\ 0 & 0 & 0 & -1.0 \\ 0 & 0 & 0 & 1.0 \end{bmatrix},$
	$H_2 = \begin{bmatrix} 0.38975 & 0.13906 & 5.4530 & -16.011 \\ 4.7711 & -0.58718 & -34.923 & -68.544 \\ 0 & -1.0 & 0 & 0 \\ 0 & 1.0 & 0 & 0 \\ 0 & 0 & -1.0 & 0 \\ 0 & 0 & 1.0 & 0 \\ 0 & 0 & 0 & -1.0 \\ 0 & 0 & 0 & 1.0 \end{bmatrix},$
	$H_3 = \begin{bmatrix} -4.3814 & 0.72624 & 40.376 & 52.533 \\ -4.7711 & 0.58718 & 34.923 & 68.544 \\ 0 & -1.0 & 0 & 0 \\ 0 & 1.0 & 0 & 0 \\ 0 & 0 & -1.0 & 0 \\ 0 & 0 & 1.0 & 0 \\ 0 & 0 & 0 & -1.0 \\ 0 & 0 & 0 & 1.0 \end{bmatrix},$
	$h_1 = [-9.2035 \quad 98.496 \quad 30.0 \quad 30.0 \quad 0.2 \quad 0.2 \quad 0.2 \quad 0.2]^T,$ $h_2 = [9.2035 \quad 107.70 \quad 30.0 \quad 30.0 \quad 0.2 \quad 0.2 \quad 0.2 \quad 0.2]^T,$ $h_3 = [-98.496 \quad -107.70 \quad 30.0 \quad 30.0 \quad 0.2 \quad 0.2 \quad 0.2 \quad 0.2]^T$

Figure 4.12: Parameters of identified model

In the last experiment parameters of the input were chosen such that both upper and lower saturations are reached. The data sets used for identification and validation are represented in figure 4.13.

A PWARX model with 4 modes and parameters $n_a = 2$, $n_b = 3$, $c = 55$ is reconstructed. The corresponding response in simulation is shown in figure 4.14a, and the active modes are depicted in figure 4.14b. From figures 4.14a and 4.14b one can conclude that modes 3 and 4 correspond to upper and lower saturations respectively. Modes 1 and 2 correspond to non-saturated behaviors. Moreover, almost all data points in non-saturated modes are

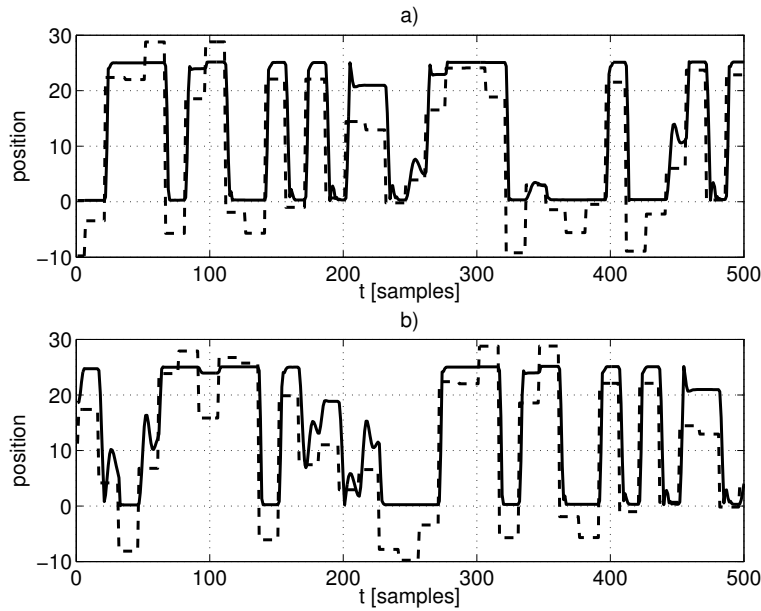


Figure 4.13: Excitation of free, impact, lower saturation and upper saturation modes. Data used for a) identification b) validation (solid: system output, dashed: scaled input)

attributed to mode 1, while mode 2 corresponds to large negative steps in the input signal, i.e. to the large transients of the output in the direction of the upper saturation.

A careful analysis of figure 4.14 reveals that:

- Responses in the portions of the data set associated to mode 1 are not satisfactory; one can conclude that the parameter vector of the mode 1 is poorly estimated.
- Responses in the portions of the data set associated with the fourth mode are satisfactory.
- By observing that the model response is good in the time instants when a switch from mode 1 to mode 3 and from 1 to 4 occurs one can conclude that the boundaries between the modes 1/3 and 1/4 are correctly identified.
- The large undershoots (negative position values, which are not physi-

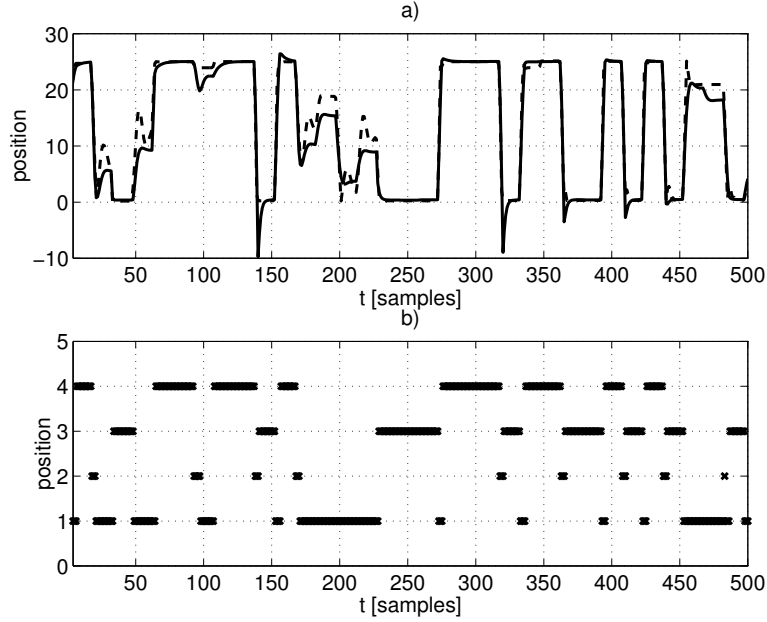


Figure 4.14: a) Simulation of the four-modal PWARX model $n_a = 2$, $n_b = 3$, $c = 55$ (solid: model response, dashed: system response) b) Active mode at each time instant

cally possible due to the mechanical constraints) in time instants after mode switch from 2 to 3 (e.g. time instants around 140 and 320) and the incorrectly predicted response around the time 100 (mode change between 2 and 4), allows to conclude that neither the parameter vector in mode 2, nor the boundaries between modes 2/3 and 2/4 are correctly identified.

- The simulated response is correct in the periods after mode switches between 1 and 3 (e.g. time interval around 230). Therefore the PV of the third mode is acceptable. Large undershoots in mode 3, after the mode changes from 2 to 3 (e.g. time instants around 140 and 320) are due to the incorrect estimation of the mode 2.

Based on physical insights one would expect that the data points are classified in the four modes, corresponding to upper saturation, lower saturation, free mode and impact mode. The previous remarks highlight that the modes corresponding to the saturations are well reconstructed, whereas

free and impact modes are not distinguished. From figure 4.13a one can see that the data set used for identification contains a small number of points corresponding to free and impact modes, compared to the number of points representing saturations. This suggests that in order to improve the results new identification experiment should be conducted to achieve a better excitation of the non-saturated modes.

4.6 Conclusion

In this paper an experimental study in the identification of the electronic component placement process in pick-and-place machines is presented. An experimental setup was made, using the component placement head from the actual pick-and-place machine and the impacting surface, designed so as to mimic the elasticity properties of the real PCB. Piecewise ARX (PWARX) models of the process have been obtained by using the methodology introduced in (Ferrari-Trecate et al. (2003)).

Despite the fact that the models are optimized for one-step-ahead prediction their performance in simulation is satisfactory, when the free and contact modes are excited. Thus, models are adequate also for model-predictive control and verification. When attempting to identify also saturations the quality of the resulting models deteriorates and limitations of the identification algorithms yielding to unsatisfactory behaviors are highlighted.

By combining physical insights on the process operation with the model responses it is possible to single out model features (i.e. mode parameters and/or regions) which are incorrectly reconstructed. This information may be used in order to design targeted identification experiments that allow to refine the results. Moreover, an accurate analysis of the physical behaviors in saturation conditions provides a relevant amount of *a priori* information, neglected by the black-box procedure adopted. Better results could be achieved by devising a *gray-box* identification procedure capable to exploit such knowledge.

The possibility of exciting an increasing number of modes with different experiments suggests also to study *incremental* identification algorithms. The basic idea would be to reconstruct first the modes visible in the simpler experiments, and then enhance the model with additional behaviors appearing in richer data sets, by keeping fixed the dynamics already identified. This idea will be developed in future research.

A Bayesian Approach to Identification of Hybrid Systems

5.1 Introduction 5.2 Preliminaries 5.3 Model class 5.4 Problem statement 5.5 Suboptimal identification algorithm	5.6 Particle filtering approximation 5.7 Partition estimation 5.8 Example 5.9 Initialization 5.10 Experimental example 5.11 Conclusions
--	--

In this paper we present a novel procedure for the identification of hybrid systems in the class of piece-wise ARX systems. The presented method facilitates the use of available a priori knowledge on the system to be identified, but can also be used as a black-box method. We treat the unknown parameters as random variables, described by their probability density functions. The identification problem is posed as the problem of maximizing the total probability that the observed data is generated by the identified model. A particle filtering method is used for a numerical implementation of the proposed procedure. A modified version of the multi-category robust linear programming (MRLP) classification procedure, which uses the information derived in the previous steps of the identification algorithm, is used for estimating the partition of the PWARX map. The proposed procedure is applied for the identification of a component placement process in pick-and-place machines.

This chapter is based on Juloski et al. (2004c) and Juloski et al. (2004d).

5.1 Introduction

In this paper we present a novel procedure for the identification of hybrid systems in the class of Piece-Wise AutoRegressive systems with eXogenous inputs (PWARX systems). PWARX models are a generalization of the classical ARX models, in that the regressor space is partitioned into a finite

number of polyhedral regions, where in each region the input-output relation is defined through an ARX-type model. PWARX models represent a broad class of hybrid systems, as they form a subclass of Piece-Wise Affine (PWA) models (Sontag (1981)), which are in turn equivalent to other hybrid modelling formalisms, such as Mixed Logic Dynamics (MLD) (Bemporad and Morari (1999)) and Linear Complementarity (LC) frameworks (van der Schaft and Schumacher (1996); Heemels et al. (2000, 2001)). A number of methods for stability analysis, optimal control design and verification have been developed for the above mentioned classes in the recent years. In this paper we will focus on the identification of hybrid systems in this class.

Based on the observed data the identification problem amounts to determining the parameters of the ARX sub-models together with the regions of the regressor space where each of the models is valid. The main problem in the identification of PWARX models is the problem of *data classification* - that is, the problem to assign each data point to one specific sub-model. When the data has been classified, the parameters of the sub-models can be determined, and the regions where each of the sub-models is valid can be estimated using techniques for data classification (Ferrari-Trecate et al. (2003)).

The problem of the identification of PWA and PWARX models has been considered before, and to date several approaches exist for identification of those models (see Roll et al. (2004) and the references therein). As pointed out in Roll et al. (2004) most of the existing approaches assume that the system dynamics is continuous, while the approaches that allow for discontinuities started appearing only recently (Ferrari-Trecate et al. (2003); Bemporad et al. (2003); Vidal et al. (2003b)). The identification procedure proposed in this paper allows for discontinuous system dynamics as well.

In the *clustering-based procedure* (Ferrari-Trecate et al. (2003)) the data classification and the parameter estimation steps are performed simultaneously by solving a suitably defined optimal clustering problem in the parameter space. In the *greedy procedure* (Bemporad et al. (2003)) the data classification and the parameter estimation steps are accomplished by partitioning a suitably defined infeasible set of linear inequalities into a minimal number of feasible subsets. In the *algebraic procedure* (Vidal et al. (2003b)) the parameter estimation is accomplished by finding the roots of a suitably defined polynomials, while the data points are classified to the sub-model that gives the smallest prediction error. For a comparison of the three above mentioned procedures see Niessen et al. (2004).

In this paper we take a Bayesian approach to the problem of identifying PWARX models. Specifically, we treat the unknown parameters as

random variables, and describe them in terms of their joint probability density function (pdf). The probability density function contains the complete stochastic information about parameters, and different parameter estimates can be easily inferred.

We assume that an *a priori* joint parameter pdf is given. If the data is classified the *a posteriori* joint parameter pdf will be computed, using Bayes' rule. Furthermore, we compute the probability that the observed data is generated by the given classification. One data classification is considered *better* than another if it has a higher probability. Following this line of reasoning, the identification problem amounts to finding *the best* data classification. This approach to model comparison is similar to the Bayesian framework which was used in MacKay (1992) for neural networks.

The classification problem is a combinatorial optimization problem, where all possible mode sequences have to be explored, in order to find an optimal solution. To reduce complexity we resort to a sequential approach, where each data point is classified to the best mode based on the information available so far. This strategy is known in the optimization literature as the *greedy strategy*, as it makes the best possible local decision in order to approach the global optimum. In order to calculate with resulting pdfs we propose a method of particle approximations.

Region estimations are based on a modification of the Multi-category Robust Linear Programming procedure (MRLP) (Bennet and Mangasarian (1994)). The modification consists in introducing a suitably defined pricing function, that assigns weights to the misclassification of data points. An advantage of using pricing functions is that more information is preserved from the classification phase. This is illustrated by the example in section 5.8.

By choosing a priori parameter probability density functions the user can supply the relevant a priori knowledge to the identification procedure. This is a major advantage of the framework presented here. Including a priori knowledge is much harder in other identification methods, such as the ones described in Ferrari-Trecate et al. (2003), Bemporad et al. (2003), and Vidal et al. (2003b).

The need for using a priori knowledge was observed in an experimental case study of a component placement process in a pick-and-place machine (Juloski et al. (2003b, 2004b)). The a priori knowledge may stem from physical insight in the system or from previous identification experiments. By choosing a priori parameter pdfs so as to correspond to the parameters of the modes of the physical system the identification procedure may be forced to identify a model that can be interpreted in physical terms. Secondly, the

approach presented here can be used to improve the previously identified models with targeted identification experiments. Also, models of increasing complexity can be built from a series of identification experiments, where in each experiment only a subset of the modes of the physical system is excited and identified. We believe that this are the important advantages in any practical identification problem. We also discuss some ways to initialize the procedure without using the a priori knowledge.

The remainder of the paper is organized as follows. Preliminaries are given in section 5.2. The class of PWARX models is introduced in section 5.3. The identification problem is formally stated in section 5.4. In sections 5.5 and 5.6 we derive the suboptimal identification algorithm, and the particle filtering approach, as a way to implement it. In section 5.7 we present modified MRLP procedure. In section 5.8 we give an example that illustrates the presented ideas. In section 5.9 we discuss several ways to obtain the a priori probability density functions of the model parameters, so as to initialize the procedure. The connection with the clustering procedure, and the improvement that our method can provide are explained in section 5.9.2. An experimental example is given in section 5.10. Conclusions are given in section 5.11.

5.2 Preliminaries

A vector of random variables $\theta_i \in \Theta_i \subseteq \mathbb{R}^n$ can be described with a probability density function (pdf) p_{θ_i} . If the pdf p_{θ_i} takes the form

$$p_{\theta_i}(\theta) = \delta(\theta - \theta_i^0), \quad (5.1)$$

where δ is the Dirac delta distribution, then $\theta_i = \theta_i^0$, with probability one, which will mean that the value of θ is known.

Different estimates of θ_i can be easily obtained from the probability density function. For instance, the *expectation* of θ_i is given as

$$\hat{\theta}_i^E = E[\theta_i] = \int_{\Theta_i} \theta p_{\theta_i}(\theta) d\theta \quad (5.2)$$

and the *maximum a posteriori probability* (MAP) estimate is given as:

$$\hat{\theta}_i^{MAP} = \arg \max_{\theta} p_{\theta_i}(\theta). \quad (5.3)$$

The covariance matrix V_i , which is a measure of the quality of the estimate $\hat{\theta}_i^E$, is defined as:

$$V_i^E = \int_{\Theta_i} (\theta - \hat{\theta}_i^E)(\theta - \hat{\theta}_i^E)^\top p_{\theta_i}(\theta) d\theta. \quad (5.4)$$

V_i^{MAP} can be defined in an analogous way for $\hat{\theta}_i^{MAP}$. We define the *dispersion* of the estimates θ_i^E and θ_i^{MAP} as the spectral radius of the covariance matrix of the estimate:

$$\rho_i^E = \rho(V_i^E) = \lambda_{\max}(V_i^E); \quad \rho_i^{MAP} = \rho(V_i^{MAP}) = \lambda_{\max}(V_i^{MAP}) \quad (5.5)$$

where $\lambda_{\max}(\cdot)$ denotes the maximal eigenvalue. Note that $\rho_i^{E,MAP} = 0$ if and only if (5.1) holds. Dispersion is useful for comparison of two different estimates of θ_i , where the smaller value of ρ indicates better estimate.

5.3 Model class

We consider piece-wise AutoRegressive eXogenous (PWARX) models of the form:

$$y(k) = f(x(k)) + e(k) \quad (5.6)$$

where $k \geq 0$, and:

$$f(x) = \begin{cases} \theta_1^\top \begin{bmatrix} x \\ 1 \end{bmatrix} & \text{if } x \in \mathcal{X}_1 \\ \vdots \\ \theta_s^\top \begin{bmatrix} x \\ 1 \end{bmatrix} & \text{if } x \in \mathcal{X}_s \end{cases} \quad (5.7)$$

is a piece-wise affine map, and $x(k)$ is a vector of regressors, defined as

$$x(k) = [y(k-1) \quad \dots \quad y(k-n_a), \quad u(k-1) \quad \dots \quad u(k-n_b)]^\top. \quad (5.8)$$

The parameters n_a and n_b in (5.8) and the number of modes s are assumed to be known. Therefore, $\theta_i \in \Theta_i \subseteq \mathbb{R}^{n+1}$, where $n = n_a + n_b$. The sets \mathcal{X}_i are assumed to be bounded polyhedrons, described by:

$$\mathcal{X}_i = \{x \mid H_i x \leq h_i\} \quad (5.9)$$

where H_i is a real valued matrix, h_i is a real valued vector, and the inequality holds element-wise. The set $\mathcal{X} = \bigcup_{i=1}^s \mathcal{X}_i$ is assumed to be a bounded polyhedron, and we assume that $\{\mathcal{X}_i\}_{i=1}^s$ is a partition of \mathcal{X} (this implies that the interiors of \mathcal{X}_i and \mathcal{X}_j do not intersect for $i \neq j$)¹. We also assume that parameter vectors θ_i and θ_j are different over different regions:

Assumption 5.3.1 For $i \neq j$, $\theta_i \neq \theta_j$.

Assumption 5.3.2 The realization of the additive noise e in the model (5.6) is a sequence of independent, identically distributed random values, with an a priori known probability density function p_e .

We define the *mode function* $\mu : \{1, \dots, T\} \rightarrow \{1, \dots, s\}$ that assigns mode $\mu(k)$ to the data pair $(x(k), y(k))$, $k = 1, \dots, T$. Ideally, given regions $\{\mathcal{X}_i\}_{i=1}^s$, μ would satisfy:

$$\mu(k) := i \text{ whenever } x(k) \in \mathcal{X}_i. \quad (5.10)$$

Hence, for a given data set $\{(x(k), y(k))\}_{k=1}^T$ the partitioning $\{\mathcal{X}_i\}_{i=1}^s$ induces the mode function μ , as given by (5.10).

The inverse problem is the *region estimation* problem, and reads as follows. Given μ find regions $\{\mathcal{X}_i\}_{i=1}^s$ such that whenever $\mu(k) = i$, we have that $x(k) \in \mathcal{X}_i$. The region estimation problem can be solved using standard techniques for data classification Ferrari-Trecate et al. (2003). The problem of region estimation therefore can, in principle, be replaced by the problem of mode estimation for each data pair. We will refer to the latter problem as the *classification problem*. These problems will be formalized in the next section.

5.4 Problem statement

The identification problem consists of estimating the values of the unknown parameter vectors θ_i , for $i = 1 \dots s$, and the regions $\{\mathcal{X}_i\}_{i=1}^s$, described by (5.9), given the data pairs $(x(k), y(k))$, for $k = 1, \dots, T$.

With $\vartheta \in \Theta \subseteq \mathbb{R}^{(n+1)s}$ we will denote a vector $\vartheta = \text{col}(\theta_1, \dots, \theta_s)$, where the operator $\text{col}(\cdot)$ stacks its operands into a column vector. Assume that the joint a priori probability density function of the parameters and the partition

¹Since regions \mathcal{X}_i are closed sets by definition (5.9) it may happen that \mathcal{X}_i and \mathcal{X}_j share a common facet. Technically, the point x , lying on the shared facet would belong to both \mathcal{X}_i and \mathcal{X}_j . We neglect this issue, as it has no consequence on the presented procedure.

$p_{\vartheta, \{\mathcal{X}_i\}_{i=1}^s}$ is given. Given the data set $\{(x(k), y(k))\}_{k=1}^T$, the a posteriori joint pdf of parameters and partition can, in principle, be computed using Bayes' rule as:

$$\begin{aligned} p_{\vartheta, \{\mathcal{X}_i\}_{i=1}^s}(\vartheta, \{\mathcal{X}_i\}_{i=1}^s \mid \{(x(k), y(k))\}_{k=1}^T) &= \\ &= \frac{p(\{(x(k), y(k))\}_{k=1}^T \mid \vartheta, \{\mathcal{X}_i\}_{i=1}^s) p_{\vartheta, \{\mathcal{X}_i\}_{i=1}^s}(\vartheta, \{\mathcal{X}_i\}_{i=1}^s)}{\int_{\Theta, \{\mathcal{X}_i\}_{i=1}^s} p(\{(x(k), y(k))\}_{k=1}^T \mid \vartheta, \{\mathcal{X}_i\}_{i=1}^s) \times \\ &\quad \times p_{\vartheta, \{\mathcal{X}_i\}_{i=1}^s}(\vartheta, \{\mathcal{X}_i\}_{i=1}^s) d\vartheta d\{\mathcal{X}_i\}_{i=1}^s} \end{aligned} \quad (5.11)$$

Given s , n_a , n_b and the data $\{(x(k), y(k))\}_{k=1}^T$, the identification problem can now be posed as the problem of finding the most likely parameter and partition values:

Problem 5.4.1 (Full identification problem)

$$\{\vartheta, \{\mathcal{X}_i\}_{i=1}^s\} = \arg \max p_{\vartheta, \{\mathcal{X}_i\}_{i=1}^s}(\vartheta, \{\mathcal{X}_i\}_{i=1}^s \mid \{(x(k), y(k))\}_{k=1}^T) \quad (5.12)$$

where the maximum is taken over all possible parameters and partitions satisfying the assumptions on the model (5.6) from section 5.3.

Problem 5.4.1 involves a joint optimization over parameters and partitions, and this is a hard non-convex optimization problem with many local minima. Therefore, we will consider a relaxation of problem 5.4.1, in that the optimization over regions and over parameters will be treated separately. This step is common in the hybrid identification literature, and gives rise to a partition/mode estimation problem on one hand, and a parameter estimation problem on the other.

Assume that the a priori joint probability density function of the parameters p_{ϑ} is given. The total probability that the observed data set $\{(x(k), y(k))\}_{k=1}^T$ was generated by the given partition $\{\mathcal{X}_i\}_{i=1}^s$ is:

$$\begin{aligned} p(\{(x(k), y(k))\}_{k=1}^T \mid \{\mathcal{X}_i\}_{i=1}^s) &= \\ &= \int_{\Theta} p(\{(x(k), y(k))\}_{k=1}^T \mid \vartheta, \{\mathcal{X}_i\}_{i=1}^s) p_{\vartheta}(\vartheta) d\vartheta. \end{aligned} \quad (5.13)$$

A partition $\{\mathcal{X}_i^1\}_{i=1}^s$ is said to be *better* than the partition $\{\mathcal{X}_i^2\}_{i=1}^s$ if it has higher probability, i.e. if:

$$p(\{(x(k), y(k))\}_{k=1}^T \mid \{\mathcal{X}_i^1\}_{i=1}^s) > p(\{(x(k), y(k))\}_{k=1}^T \mid \{\mathcal{X}_i^2\}_{i=1}^s).$$

Given s , n_a , n_b , the data $\{(x(k), y(k))\}_{k=1}^T$ and the a priori parameter pdf p_ϑ the *partition estimation problem* can now be formally stated as the problem of finding the best partition, i.e.:

Problem 5.4.2 (Partition estimation problem)

$$\{\mathcal{X}_i\}_{i=1}^s = \arg \max p(\{(x(k), y(k))\}_{k=1}^T \mid \{\mathcal{X}_i\}_{i=1}^s) \quad (5.14)$$

where the maximum is taken over all possible partitions $\{\mathcal{X}_i\}_{i=1}^s$ satisfying the assumptions on the model (5.6) from section 5.3.

Problem 5.4.2 is a non-convex problem, posed in the regressor space \mathcal{X} of dimension n . Instead of solving problem 5.4.2, one may choose to estimate the mode sequence $\{\mu(k)\}_{k=1}^T$, and to subsequently reconstruct the partition $\{\mathcal{X}_i\}_{i=1}^s$ on the basis of the estimated mode sequence as discussed in section 5.3. In an analogous way to (5.13) we compute the total probability that the observed data set was generated by a given mode function μ :

$$p(\{(x(k), y(k))\}_{k=1}^T \mid \mu) = \int_{\Theta} p(\{(x(k), y(k))\}_{k=1}^T \mid \vartheta, \mu) p_\vartheta(\vartheta) d\vartheta \quad (5.15)$$

Under the assumption 5.3.2 we have

$$p(\{(x(k), y(k))\}_{k=1}^T \mid \vartheta, \mu) = \prod_{k=1}^T p_e(y(k) - \theta_{\mu(k)} [x(k)^\top \quad 1]^\top). \quad (5.16)$$

The classification problem now takes the form:

Problem 5.4.3 (Classification problem)

$$\mu = \arg \max p(\{(x(k), y(k))\}_{k=1}^T \mid \mu) \quad (5.17)$$

where the maximum is taken over all possible mode functions μ .

Note that the optimal mode function obtained by solving problem 5.4.3 does not coincide in general with the mode sequence induced by optimal partition obtained from problem 5.4.2. This issue will be further discussed in section 5.7.

Given the a priori joint parameter pdf p_ϑ and the partition $\{\mathcal{X}_i\}_{i=1}^s$ (or the mode function μ) we can compute the a posteriori joint pdf of the parameters,

using Bayes rule:

$$p_{\vartheta}(\vartheta \mid \{(x(k), y(k))\}_{k=1}^T, \{\mathcal{X}_i\}_{i=1}^s) = \frac{p(\{(x(k), y(k))\}_{k=1}^T \mid \vartheta, \{\mathcal{X}_i\}_{i=1}^s) p_{\vartheta}(\vartheta)}{\int_{\Theta} p(\{(x(k), y(k))\}_{k=1}^T \mid \vartheta, \{\mathcal{X}_i\}_{i=1}^s) p_{\vartheta}(\vartheta) d\vartheta} \quad (5.18)$$

The parameter estimation problem then takes the form:

Problem 5.4.4 (maximum likelihood parameter estimation)

$$\{\theta_i^{MAP}\}_{i=1}^s = \arg \max_{\vartheta} p_{\vartheta}(\vartheta \mid \{(x(k), y(k))\}_{k=1}^T, \{\mathcal{X}_i\}_{i=1}^s) \quad (5.19)$$

where the maximum is taken over all possible parameter values.

or, alternatively,

Problem 5.4.5 (expected parameter value)

$$\{\theta_i^E\}_{i=1}^s = E \vartheta, \quad (5.20)$$

where ϑ has the probability density function (5.18).

Once the joint parameter pdf (5.18) is computed problems 5.4.4 and 5.4.5 can be easily solved numerically. In the sequel we will focus on problems 5.4.3 (section 5.5) and 5.4.2 (section 5.7).

5.5 Suboptimal identification algorithm

Optimization problem 5.4.3 is a combinatorial optimization problem, where all possible mode sequences have to be explored in order to obtain an optimal solution. As the number of the collected data pairs increases such a search quickly becomes computationally intractable. Hence, we have to resort to suboptimal minimization algorithms.

We will consider the data points sequentially, and try to find the best possible classification of the data pair $(x(k), y(k))$, with data points up to $k-1$ already classified. The described optimization strategy is known in the optimization literature as the *greedy* strategy - the algorithm tries to make the best possible local decision, in order to approach the global optimum. Let $p_{\theta}(\cdot, k)$ denote the pdf of the parameter θ after k steps of the algorithm. Let $p_{\theta}(\cdot, 0)$ denote the a priori parameter pdf, i.e. $p_{\theta}(\cdot, 0) = p_{\theta}(\cdot)$.

We will assume that the joint pdf of $\theta_1, \dots, \theta_s$ at step k takes the form

$$p_{\theta_1, \dots, \theta_s}(\theta_1, \dots, \theta_s; k) = \prod_{i=1}^s p_{\theta_i}(\theta_i; k), \quad (5.21)$$

That is, for all $i \neq j$ and for all k parameters θ_i and θ_j are assumed mutually independent given data up to time step k . Under this assumption we consider the following problem:

Problem 5.5.1 For $k = 1, \dots, T$ find the most likely mode $\mu(k)$ of the data pair $(x(k), y(k))$, given the a priori joint parameter pdf $p_{\theta_1, \dots, \theta_s}(\theta_1, \dots, \theta_s; k-1)$ at step $k-1$ which is of the form (5.21), i.e.

$$\mu(k) = \arg \max_i p((x(k), y(k)) \mid \mu(k) = i). \quad (5.22)$$

In (5.22)

$$p((x(k), y(k)) \mid \mu(k) = i) = \int_{\Theta_i} p((x(k), y(k)) \mid \theta) p_{\theta_i}(\theta; k-1) d\theta. \quad (5.23)$$

and

$$p((x(k), y(k)) \mid \theta) = p_e(y(k) - \theta \begin{bmatrix} x(k)^\top & 1 \end{bmatrix}^\top) \quad (5.24)$$

The problem 5.5.1 is solved in a straightforward way, by computing (5.23) for $i = 1, \dots, s$ and choosing $\mu(k)$, according to (5.22).

If $\mu(k) = i$ the a posteriori joint parameter pdf is computed using Bayes' rule as:

$$p_{\theta_1, \dots, \theta_s}(\theta_1, \dots, \theta_s; k) = p_{\theta_{\mu(k)}}(\theta_{\mu(k)}; k) \prod_{\substack{i=1 \\ i \neq \mu(k)}}^s p_{\theta_i}(\theta_i; k-1). \quad (5.25)$$

where

$$p_{\theta_{\mu(k)}}(\theta; k) = \frac{p_e(y(k) - \theta^\top \begin{bmatrix} x(k)^\top & 1 \end{bmatrix}^\top) p_{\theta_{\mu(k)}}(\theta; k-1)}{\int_{\Theta_i} p_e(y(k) - \theta^\top \begin{bmatrix} x(k)^\top & 1 \end{bmatrix}^\top) p_{\theta_{\mu(k)}}(\theta; k-1) d\theta} \quad (5.26)$$

Hence, if the parameters were independent at step $k-1$, from (5.25) it follows that after classifying the k -th data point they will remain independent. Furthermore, the a posteriori joint parameter pdf is obtained by updating the pdf of the parameter that generated the data pair, while the pdfs of the other parameters remain unchanged.

Now, we are ready to formally state the algorithm for classification and parameter estimation.

Algorithm 5.5.2 (classification and parameter estimation)

- **step 1:** Obtain the *a priori* probability density functions $p_{\theta_i}(\cdot; 0)$ for $i = 1, \dots, s$; set $k = 1$.
- **step 2:** Assign the data pair $(x(k), y(k))$ to the mode $\mu(k)$ with the highest likelihood using (5.22)
- **step 3:** Compute the *a posteriori* pdf of the parameter $\theta_{\mu(k)}$, $p_{\theta_{\mu(k)}}(\cdot; k)$ using (5.26). For all $j \neq \mu(k)$, set $p_{\theta_j}(\cdot, k) = p_{\theta_j}(\cdot; k - 1)$.
- **step 4:** $k = k + 1$; goto step 2 until $k > T$ \diamond

The schematic representation of the algorithm 5.5.2, for the case $s = 2$ is given in figure 5.1.

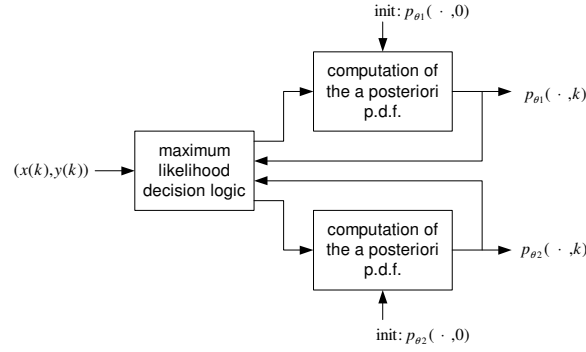


Figure 5.1: Schematic representation of algorithm operation for two modes

The algorithm 5.5.2 is derived by considering data points one at a time. It is possible, along the same lines, to derive a family of suboptimal algorithms, that would classify $m \leq T$ data points in each step. Note that, as m increases the complexity of the combinatorial optimization problem that has to be solved in each step increases exponentially, and for $m = T$ the optimization problem becomes the classification problem 5.4.3.

5.6 Particle filtering approximation

Analytical solutions to (5.22) and (5.26) are intractable for general noise and parameter probability density functions. To turn algorithm 5.5.2 into a feasible computational scheme, we opt for the particle filtering approach

(Arulamapalam et al. (2002)). Here we present only the main idea of this approach. For a detailed exposition on implementing, tuning and convergence results for particle filters see e.g. Arulamapalam et al. (2002), Doucet et al. (2001), Crisan and Doucet (2002) and references therein.

The underlying idea of particle filtering methods is to approximate the pdf $p_{\theta_i}(\cdot; k)$ defined over a dense set Θ_i with a pdf supported in a finite number of points $\theta_i^{l,k} \in \Theta_i$, $l = 1, \dots, N$ called particles. The pdf $p_{\theta_i}(\cdot; k)$ is then approximated as:

$$p_{\theta_i}(\theta; k) \approx \hat{p}_{\theta_i}(\theta; k) := \sum_{l=1}^N w_i^{l,k} \delta(\theta - \theta_i^{l,k}). \quad (5.27)$$

where $w_i^{l,k} > 0$ is a weight associated with the particle $\theta_i^{l,k}$.

Algorithms that sample particles $\theta_i^{l,k}$ according to any given probability density function can be found in the literature (i.e. Metropolis-Hastings algorithm, Gibbs sampler etc. (Fishman (1996))).

Estimates (5.2) and (5.4) can be obtained from (5.27) in a straightforward way. Combining (5.27) with (5.23) we obtain the following approximation for (5.23):

$$p((x(k), y(k)) \mid \mu(k) = i) \approx \sum_{l=1}^N w_i^{l,k-1} p_e(y(k) - \theta_i^{l,k-1} x(k)) \quad (5.28)$$

To compute the recursion (5.26) we use a modification of the Sample Importance Resampling (SIR) particle filtering algorithm (Arulamapalam et al. (2002)). This results in the following computational scheme:

Algorithm 5.6.1 (SIR particle filtering)

- FOR $l = 1$ TO N
 - diversify particles: $\theta_i^{l,k} = \theta_i^{l,k-1} + \varepsilon^l$, where $\varepsilon_l \sim \mathcal{N}(0, \Sigma_\varepsilon)$
 - compute weights $w_i^{l,k} = p((x(k), y(k)) \mid \theta_i^{l,k})$ using (5.24)

END FOR

- normalize:

$$w_i^{l,k} := \frac{w_i^{l,k}}{\sum_{l=1}^N w_i^{l,k}},$$

for $l = 1, \dots, N$

- resample N times from distribution (5.27) to obtain the new set of particles $\theta_i^{l,k}$, where $w_i^{l,k} = N^{-1}$ \diamond

Algorithms for sampling distributions of the type (5.27) are standard (see for instance (Arulamapalam et al., 2002, algorithm 2)). Since we are using the SIR algorithm for estimating the constant parameter it is necessary to diversify the particles (Berzuini and Gilks (2001)). For this purpose we add the normally distributed random term ε^l to each particle in the first step of the algorithm 5.6.1. Variance matrix Σ_ε is the tuning parameter in the algorithm. This method of particle diversification is simple, but increases the variance of the estimates. Other particle filtering algorithms with better statistical properties but higher computational load, can be found in the literature (see for instance Berzuini and Gilks (2001)).

5.7 Partition estimation

Once the entire data set has been passed through the algorithm 5.5.2, the final pdfs of the parameters $p_{\theta_i}(\cdot; T)$ are available and all data points can be attributed to the mode with the highest likelihood, using (5.22). In other words, the mode function μ is re-estimated, using $p_{\theta_1, \dots, \theta_s}(\cdot; T)$, in order to obtain the most likely μ . After this classification, standard techniques from pattern recognition can be applied to determine the regions $\{\mathcal{X}_i\}_{i=1}^s$ (see e.g. Bennet and Mangasarian (1994)).

However, the method of highest likelihood classification does not necessarily classify the data points to the correct mode. This problem is especially important when the hyperplanes defined by two parameter vectors θ_i and θ_j intersect over the region \mathcal{X}_j . Then, data points near this intersection may be wrongly attributed to the mode i . This issue will be illustrated in the example in section 5.8. Wrongly attributed data points may in turn lead to errors in determining separating hyperplanes. In this section we propose a modified version of the MRLP algorithm from Bennet and Mangasarian (1994) that aims to alleviate this problem.

Define the set \mathcal{D}_i as:

$$\mathcal{D}_i = \{x(k) \mid \mu(k) = i\} \quad (5.29)$$

where $\mu(k)$ is computed as in (5.22), with $p_{\theta_i}(\cdot, T)$. Hence, \mathcal{D}_i consists of all data points that are attributed to the mode i on the basis of the a posteriori pdf $p_{\theta_i}(\cdot; T)$.

Definition 5.7.1 (Bennet and Mangasarian (1994)) The sets $\{\mathcal{D}_i\}_{i=1}^s$ are *piecewise-linearly separable* if there exist $w_i \in \mathbb{R}^n$, $\gamma_i \in \mathbb{R}$ for $i = 1, \dots, s$ such that:

$$\left\langle \begin{bmatrix} x \\ 1 \end{bmatrix}, \begin{bmatrix} w_i \\ \gamma_i \end{bmatrix} \right\rangle > \left\langle \begin{bmatrix} x \\ 1 \end{bmatrix}, \begin{bmatrix} w_j \\ \gamma_j \end{bmatrix} \right\rangle \quad (5.30)$$

for all $x \in \mathcal{D}_i$ and $j \neq i$. Here $\langle \cdot, \cdot \rangle$ denotes the standard inner product in \mathbb{R}^{n+1} .

Given w_i, γ_i the mode of the data point x can be estimated as:

$$\tilde{\mu}(x) = \arg \max_i \left\langle \begin{bmatrix} x \\ 1 \end{bmatrix}, \begin{bmatrix} w_i \\ \gamma_i \end{bmatrix} \right\rangle. \quad (5.31)$$

and the hyperplane that separates regions \mathcal{X}_i and \mathcal{X}_j is given by:

$$\{x \in \mathbb{R}^n \mid (w_i - w_j)x = \gamma_i - \gamma_j\}. \quad (5.32)$$

If the sets \mathcal{D}_i are piecewise linearly separable then the matrices H_i , h_i defining the region \mathcal{X}_i as in (5.9) can then be formed as:

$$H_i = \text{col}_j((w_i - w_j)^\top), \quad h_i = \text{col}_j(\gamma_i - \gamma_j), \quad (5.33)$$

where $j = 1, \dots, s$, $j \neq i$, and the operator $\text{col}(\cdot)$ stacks its arguments into a column vector. Note that only regions with up to $s - 1$ vertices can be described in this way.

If the sets \mathcal{D}_i are not piecewise linearly separable some data points are going to violate (5.30). If the regressor $x \in \mathcal{D}_i$ is classified to the region \mathcal{X}_j (i.e. if $\tilde{\mu}(x) = j$) the *violation* $\zeta_{ij}(x) : \mathcal{D}_i \rightarrow \mathbb{R}$ is given as

$$\zeta_{ij}(x) = (-x(w_i - w_j) + (\gamma_i - \gamma_j) + 1)_+ \quad (5.34)$$

where $q_+ = \max\{q, 0\}$. Standard MRLP algorithm finds w_i, γ_i by minimizing the sum of averaged violations (5.34), through a single linear program (Bennet and Mangasarian (1994)).

In our case we will weight the violations (5.34) according to the following principle: if the probability that the regressor $x \in \mathcal{D}_i$ belongs to the mode i is approximately equal to the probability that it belongs to mode j , then the corresponding violation $\zeta_{ij}(x)$, if positive, should not be penalized highly. We define the *weighting function* $\xi_{ij} : \mathcal{D}_i \rightarrow \mathbb{R}$ as

$$\xi_{ij}(x(k)) = \log \frac{p((x(k), y(k)) \mid \mu(k) = i)}{p((x(k), y(k)) \mid \mu(k) = j)}. \quad (5.35)$$

Since for any $j \neq i$

$$p((x(k), y(k)) \mid \mu(k) = i) > p((x(k), y(k)) \mid \mu(k) = j)$$

the weight (5.35) is always nonnegative, and is equal to zero when the two likelihoods are exactly equal.

The weighting function (5.35) takes into account only the relative size of the mode likelihoods. If outliers are present in the data set, mode likelihoods may be negligible, but their ratio, formed as in (5.35), may still be significant. Another possible choice of the weighting function ξ_{ij} , which takes into account also the absolute sizes of mode likelihoods is:

$$\begin{aligned} \xi_{ij}(x(k)) &= p((x(k), y(k)) \mid \mu(k) = i) - \\ &\quad - p((x(k), y(k)) \mid \mu(k) = j). \end{aligned} \quad (5.36)$$

The optimization problem can be stated as:

$$\min_{w_i, \gamma_i} \sum_{i=1}^s \sum_{\substack{j=1 \\ j \neq i}}^s \sum_{x \in \mathcal{D}_i} \xi_{ij}(x) \zeta_{ij}(x). \quad (5.37)$$

Problem (5.37) can be further cast as a linear program, in a same way as in Bennet and Mangasarian (1994).

By introducing pricing functions more information is preserved from the classification phase in the region estimation phase. This is an advantage over the region estimation in procedures presented in Bemporad et al. (2003) and Vidal et al. (2003b). We will illustrate this issue with an academic example in the next section.

5.8 Example

Let the data $\{(x(k), y(k))\}_{k=1}^{100}$ be generated by the system of type (5.6) where:

$$f(x) = \begin{cases} \begin{bmatrix} 0.5 & 0.5 \end{bmatrix} \begin{bmatrix} x \\ 1 \end{bmatrix}, & \text{if } x \in [-2.5, 0) \\ \begin{bmatrix} -1 & 2 \end{bmatrix} \begin{bmatrix} x \\ 1 \end{bmatrix}, & \text{if } x \in [0, 2.5] \end{cases} \quad (5.38)$$

and $e(k)$ is a sequence of normally distributed random numbers, with zero mean and variance $\sigma_e^2 = 0.025$. The data set of $T = 100$ data points together with the true model is shown in figure 5.2.

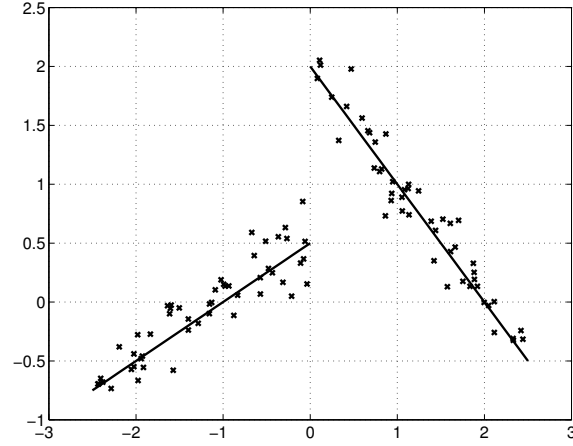


Figure 5.2: Data set used for identification together with the true model

A priori pdfs are chosen as $p_{\theta_1}(\theta_1) = p_{\theta_2}(\theta_2) = \mathcal{U}([-2.5, 2.5] \times [-2.5, 2.5])$. A particle approximation to this pdf, with $N = 200$ particles for each pdf, is given in figure 5.3, left. The particle filtering algorithm 5.6.1 is applied, with $\Sigma_\varepsilon^2 = \text{diag}\{0.001, 0.001\}$ and the final particle distribution at the step $k = 100$ is shown in figure 5.3, right. The estimates of the parameter vectors are:

$$\theta_1^E = \begin{bmatrix} 0.4143 \\ 0.5340 \end{bmatrix}, \quad \theta_2^E = \begin{bmatrix} -0.8467 \\ 1.8432 \end{bmatrix} \quad (5.39)$$

Data points are classified using (5.22), and the results are depicted in figure 5.4a. Several data points that belong to mode 1 are attributed to mode 2. These points are near the virtual intersection of the two planes defined by the parameter vectors. In figure 5.4b weighting function (5.35) for misclassification of points is shown. The weight for misclassification of wrongly attributed points is small in comparison to the weight for misclassification of the correctly attributed points. The region for mode 1 is estimated as $x \geq 0.0228$ while the region corresponding to mode 2 is estimated as $x < 0.0228$. The identified model, together with the true model and the data set is depicted in figure 5.5.

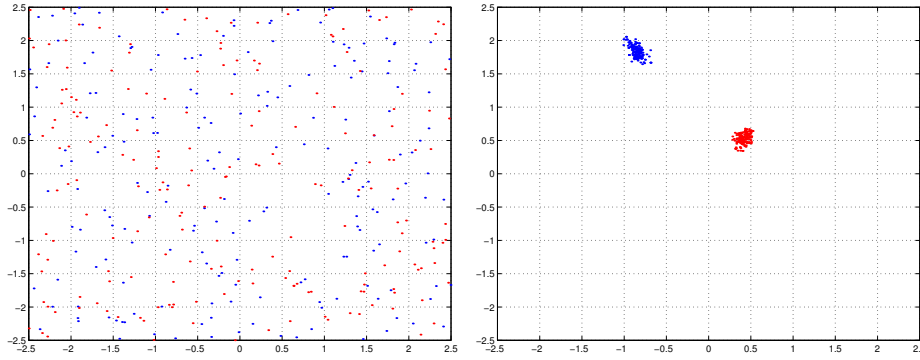


Figure 5.3: **left:** Particle approximation to the initial pdfs of the parameters θ_1, θ_2 (red dots: particles of p_{θ_1} , blue dots: particles of p_{θ_2}) **right:** Final pdf of the parameters θ_1 (red dots), θ_2 (blue dots)

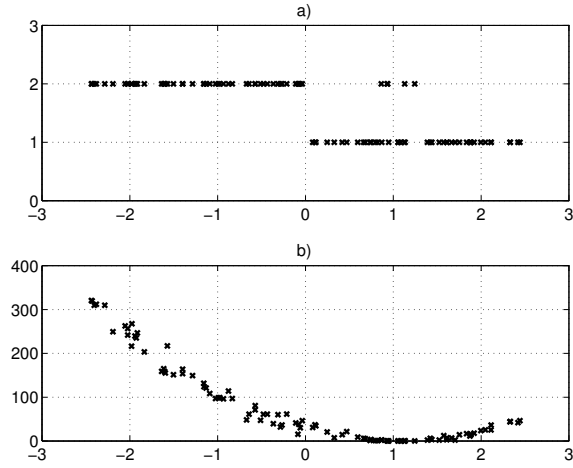


Figure 5.4: a) Data points attributed to modes b) Price function for the wrong classification

5.9 Initialization

In this section we will discuss in more detail three different ways to obtain a priori probability density functions $p_{\theta_i}(\cdot; 0)$, $i = 1, \dots, s$.

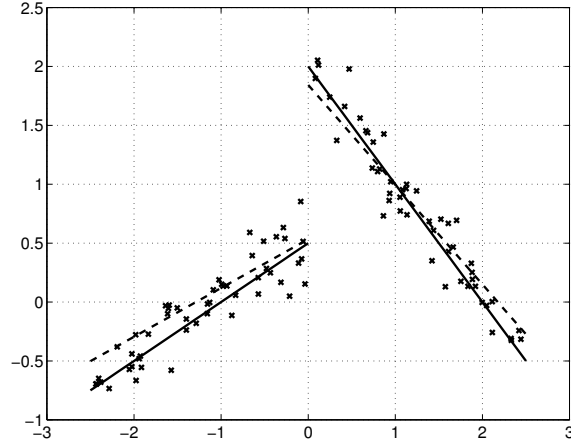


Figure 5.5: True model (solid), identified model (dashed) and the data set used for identification

5.9.1 Initialization using mode knowledge

If $m > n + 1$ data pairs $(x(k_1), y(k_1)), \dots, (x(k_m), y(k_m))$ are attributed to the mode i , the least squares estimate of the value of the parameter vector θ_i^{LS} may be obtained as:

$$\begin{aligned}\theta_i^{LS} &= (\Phi_i^\top \Phi_i)^{-1} \Phi_i^\top y_i, \\ \Phi_i &= \begin{bmatrix} x(k_1) & x(k_2) & \cdots & x(k_m) \\ 1 & 1 & \cdots & 1 \end{bmatrix}^\top \\ y_i &= [y(k_1) \quad y(k_2) \quad \cdots \quad y(k_m)]^\top.\end{aligned}\tag{5.40}$$

The empirical covariance matrix of θ_i^{LS} can be computed as (Ljung (1999)):

$$\begin{aligned}V_i &= \frac{SSR_i}{m - (n + 1)} (\Phi_i^\top \Phi_i)^{-1}, \\ SSR_i &= y_i^\top (I - \Phi_i (\Phi_i^\top \Phi_i)^{-1} \Phi_i^\top) y_i\end{aligned}\tag{5.41}$$

This information is sufficient to describe the parameter θ_i as a normally distributed random variable:

$$p_{\theta_i}(\cdot; 0) = \mathcal{N}(\theta_i^{LS}, V_i)\tag{5.42}$$

Samples from the normal distribution can be easily obtained with some of the mentioned algorithms for sampling from general multidimensional distributions (or using built-in MATLAB functions).

5.9.2 Initialization via clustering procedure

In this section we will show that our procedure can be initialized using the ideas from the clustering procedure (Ferrari-Trecate et al. (2003)). For the sake of completeness we discuss relevant steps from the clustering procedure briefly. For the detailed exposition see Ferrari-Trecate et al. (2003).

For each regressor $x(l)$ in the data set, we collect $c > n + 1$ nearest regressors, and form a *local data set* (LD) \mathcal{C}_l . The idea behind this procedure is that regressors that are close in the regressor space are likely to belong to the same partition; we distinguish two types of LDs - *pure* LDs - when all the regressors collected in one LD indeed belong to the same partition, and *mixed* LDs, when they do not. For the procedure to work properly the ratio between the number of pure and mixed LDs should be high.

From each LD we can obtain an estimate θ^l , using (5.40), and the variance V^l of the estimate θ^l , using (5.41). To each estimate the following confidence measure is assigned:

$$w^l = \frac{1}{\sqrt{(2\pi)^{n+1} \det(V^l)}}. \quad (5.43)$$

Ideally, pure LDs will produce good estimates, with high values of w^l , while for mixed LDs w^l will be low. Estimates obtained from pure LDs are expected to form groups (clusters) in the parameter space, while estimates from mixed LDs will be isolated points.

The next step is to form s clusters $\{\mathcal{D}_i\}_{i=1}^s$ in the parameter space, by solving the following optimization problem:

$$\min_{\{\mathcal{D}_i\}_{i=1}^s, \{m_i\}_{i=1}^s} J(\{\mathcal{D}_i\}_{i=1}^s, \{m_i\}_{i=1}^s), \quad (5.44)$$

where the clustering functional J is given as:

$$J(\{\mathcal{D}_i\}_{i=1}^s, \{m_i\}_{i=1}^s) = \sum_{i=1}^s \sum_{\theta^l \in \mathcal{D}_i} \|\theta^l - m_i\|_{V^l}^2 \quad (5.45)$$

where m_i is the center of the cluster \mathcal{D}_i . Optimization problem (5.44) is computationally hard, but there exist efficient algorithms able to provide sub-optimal solutions, e.g. K -means algorithm (Ferrari-Trecate et al. (2003)). Weight V^l in (5.45) is used to minimize the influence of θ^l that correspond to mixed LDs, which in turn may lead to wrong assignment of those parameter vectors.

Points attributed to i -th cluster, $\theta^l \in \mathcal{D}_i$, together with the associated weights w^l can be used to form a probability density function of type (5.27):

$$p_{\theta_i}(\theta) = q^{-1} \sum_{\theta^l \in \mathcal{D}_i} w^l \delta(\theta - \theta^l) \quad (5.46)$$

where q is a normalizing constant:

$$q = \sum_{\theta^l \in \mathcal{D}_i} w^l. \quad (5.47)$$

In the clustering procedure, after the clustering step, bijective relation

$$(x(l), y(l)) \leftrightarrow \mathcal{C}_l \leftrightarrow \theta^l \in \mathcal{D}_i$$

is used to classify data pairs to modes. Data pairs $(x(l), y(l))$ that correspond to mixed LDs may be wrongly classified. In our procedure, mixed LDs yield a point with low weight in the discrete approximation of the parameter pdf. This point will be discarded in the SIR particle filtering algorithm 5.6.1, and will have no adverse consequences on the classification of the corresponding data pair.

5.9.3 Brute force initialization

Parameters θ_i can be estimated in an optimal way as the solution of the following problem:

$$\{\theta_i\}_{i=1}^s = \arg \min_{\theta_i} \sum_{k=1}^T \|y(k) - \theta_{\mu(k)} [x^\top \ 1]^\top\|^2 \quad (5.48)$$

When the sequence $\mu(k)$, $k = 1, \dots, T$ is known problem (5.48) is an ordinary least squares problem. In our case, since modes are not known, problem (5.48) is a combinatorial optimization problem, where all possible mode sequences must be explored, and is computationally intractable for larger values of T .

In order to obtain a rough estimate of the parameter values small enough subset of the complete data set $(x(k), y(k))$, $k = 1, \dots, T$ can be chosen, and the computationally tractable problem of type (5.48) can be formulated. Solution of this problem gives the estimates of the parameter values $\hat{\theta}_i$, together with the variances of the estimates V_i . This information is sufficient to describe the parameters as $\theta_i \sim \mathcal{N}(\hat{\theta}_i, V_i)$

5.10 Experimental example

In order to demonstrate the proposed identification procedure we applied it to the data collected from the experimental setup made around the mounting head from the pick-and-place machine. The purpose of the setup is to study the component placement process on the printed circuit board (PCB) in the controlled conditions. Same experimental setup was previously successfully identified using the clustering procedure (Ferrari-Trecate et al. (2003)). The experimental setup and the identification results with the clustering procedure are described in more detail in Juloski et al. (2003b, 2004b).

A photo and the schematic representation of the experimental setup are given in figure 5.6. The setup consists of the mounting head, from an actual pick-and-place machine, which is fixed above the impacting surface (the small disc in figure 5.6a). The impacting surface is in contact with the ground via the spring (the spring c_2 in figure 5.6b), within the outer tube in figure 5.6a. The mechanical construction under the impacting surface is such that only the movement on the vertical axis is enabled (inner tube, which can slide inside the outer tube in figure 5.6a). This construction exhibits linear and dry friction phenomena, represented in figure 5.6b by the damper d_2 and the block f_2 , respectively. The chosen design of the impacting surface simulates the elasticity properties of the PCB as well as hard mechanical constraints due to saturations. It also introduces some side effects, such as dry friction.

The mounting head contains: a vacuum pipette which can move on the vertical axis (the mass M in figure 5.6b) and which is connected via the spring to the casing (the spring c_1 in figure 5.6b); an electrical motor which enables the movement (represented by force \vec{F} in figure 5.6b); and a position sensor, which measures the position of the pipette, relative to the upper retracted position. The position axis is pointed downwards, i.e. the value of the position increases when the pipette moves downwards. The motion of the pipette is also subject to friction phenomena (the damper d_1 and the dry friction block f_1 in figure 5.6b).

The dynamics of the experimental setup exhibits, in a first approximation, four different modes of operation:

- **upper saturation:** the pipette is in the upper retracted position (i.e. can not move upwards, due to the physical constraints)
- **free mode:** the pipette is not in contact with the impacting surface, but is not in the upper saturation
- **impact mode:** the pipette is in contact with the impacting surface,

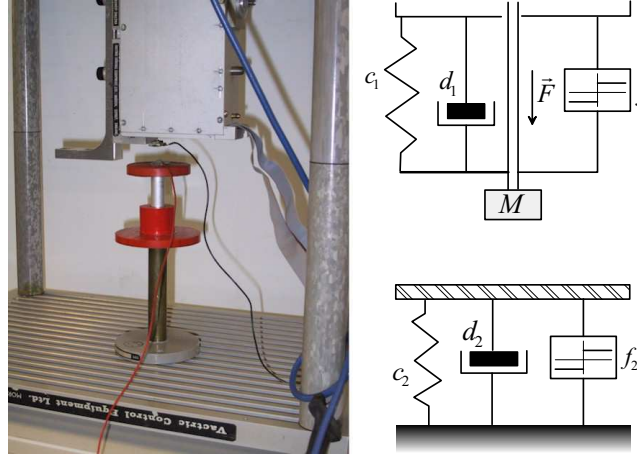


Figure 5.6: **left:** a) Photo of the experimental setup **right:** b) Schematic representation of the experimental setup

but is not in lower saturation

- **lower saturation:** the pipette is in the lower extended position, (i.e. can not move downwards due to the physical constraints)

We stress that the switch between the impact and free modes does not occur at a constant head position, because of the movement of the impacting surface. For the upper and lower saturations, although they occur at a fixed position, they introduce dynamic behaviors due to the bouncing when hitting the constraints.

The control input is the voltage applied to the motor, which is converted up to a negligible time constant to the force \vec{F} . The input signal for the identification experiment should be chosen in a way that modes of interest are sufficiently excited. To obtain the data for identification, the input signal $u(t)$ is chosen as:

$$u(t) = a_k \quad \text{when} \quad t \in [kT, (k+1)T) \quad (5.49)$$

where $T > 0$ is fixed, and the amplitude a_k is a random variable, with uniform distribution in the interval $[a, b]$. By properly choosing the boundaries of the interval $[a, b]$ only certain modes of the system are excited. For instance only free and impact modes can be excited, without reaching upper and lower saturations.

Physical insight into the operation of the setup facilitates the initialization of the procedure. For instance, although the mode switch does not occur at a fixed height of the head, with a degree of certainty data points below certain height may be attributed to the free mode, and, analogously data points above certain height may be attributed to the impact mode. Data points that belong to saturations can also be distinguished. This a priori information may be exploited in a way described in the section 5.9.1.

In the sequel we present two identification experiments: in the first experiment only free and impact modes are excited; in the second experiment free, impact and lower saturation modes are excited. Collected data sets consist of 750 points, and are divided into two overlapping sets of 500 points: one is used for identification, while the second is used for validation of the identified models.

In all examples weighting function (5.36) is used. As a probability density function of the noise we used $p_e \sim \mathcal{N}(0, 1)$.

5.10.1 Bi-modal identification

The data set used for identification is depicted in figure 5.7. Portions of the data set that are used for initialization of free and impact mode are marked with \times and \circ respectively. Models with $s = 2, n_a = 2, n_b = 1$ are identified. Particle filtering algorithm used 300 particles. The process of parameter estimation and classification took 59,3 seconds, on Pentium 4 2Ghz computer, with 512Mb of memory (no swapping to disc occurred). Region estimation took around 3 minutes, using the CPLEX software, on the same computer.

The final classification of data points is depicted in figure 5.8a. In figure 5.8b spectral radii of variance matrices $\rho_{1,2}^E$ at each step of the classification are depicted. *Simulation* of the identified model, together with the modes active during the simulation is depicted in figure 5.9.

From figure 5.8a we see that the identification procedure separated the data points into two groups, that correspond to impact and free modes. From figure 5.8b we see that the estimates of the parameters, described by the spectral radii of the covariance matrices (5.5), improve during the iterations of the algorithm.

From the comparison of the simulated response of the model and the measured response we see that the identified model is satisfactory. However, the system response in both impact and free modes is nonlinear, because of the presence of dry friction. The effects of the dry friction are especially pronounced in the impact mode, and can be observed in figure 5.7, for

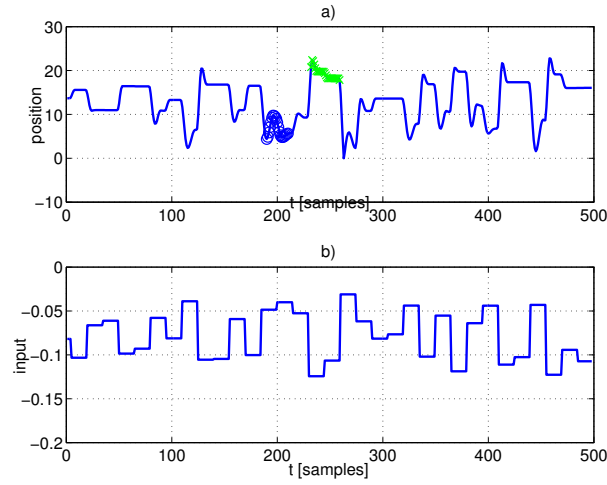


Figure 5.7: Bi-modal identification. Data set used for identification a) position (portion marked with \circ (around time 200): data points used for the initialization of the free mode; portion marked with \times (around time 250): data points used for initialization of impact mode b) input signal

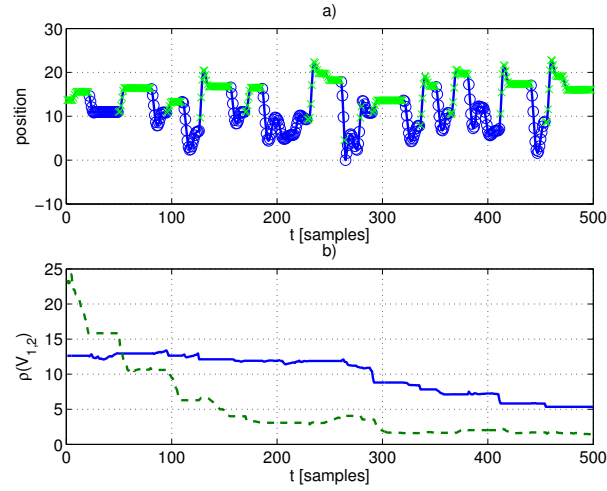


Figure 5.8: Bi-modal identification. a) Classified data points (\circ : free mode, \times : impact mode) b) $\rho_{1,2}^E$ (solid line: free mode; dashed line: impact mode)

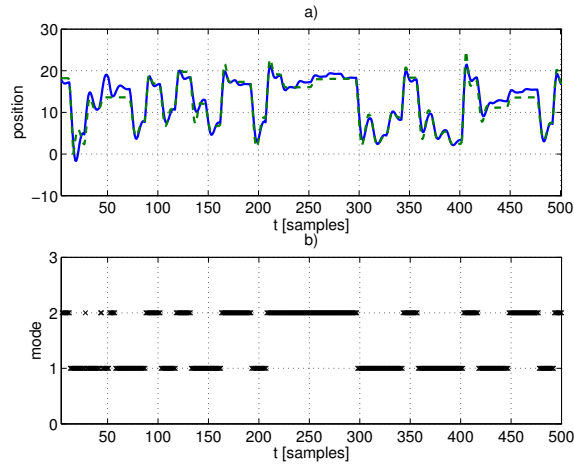


Figure 5.9: Bi-modal identification a) Simulation of the identified model (solid line: simulated response, dashed line: measured response b) modes active during the simulation

instance on a time interval around 300, where small changes in the input signal produce no change in the measured output, because the dry friction is in stick phase. Since the impact and the free modes are described by one linear model each, the effects of the dry friction can not be properly described in the identified model. For instance, the discrepancy between the simulated and measured response in figure 5.9 on the time interval around 250 is due to this effect. While the dry friction is in the stick phase in the real system, and no change in the position is visible, the identified model predicts a linear step response.

5.10.2 Identification with lower saturation

The data set used for identification is depicted in figure 5.10. Portions of the dataset that are used for initialization of free, impact and lower saturation mode are marked with \times , \circ and $+$, respectively. Particle filtering algorithm used 300 particles. Models with $s = 3, n_a = 2, n_b = 2$ are identified. The process of parameter estimation and classification took 79,6 seconds, on Pentium 4 2Ghz computer, with 512Mb of memory (no swapping to disc occurred). Region estimation took around 9 minutes, using the CPLEX software, on the same computer.

Final classification of data points is depicted in figure 5.11a. In figure

5.11b spectral radii of variance matrices $\rho_{1,2,3}^E$ at each step of the classification are depicted. Simulation of the identified model, together with the modes active during the simulation is depicted in figure 5.12. The parameters of the identified model are given in the figure 5.13.

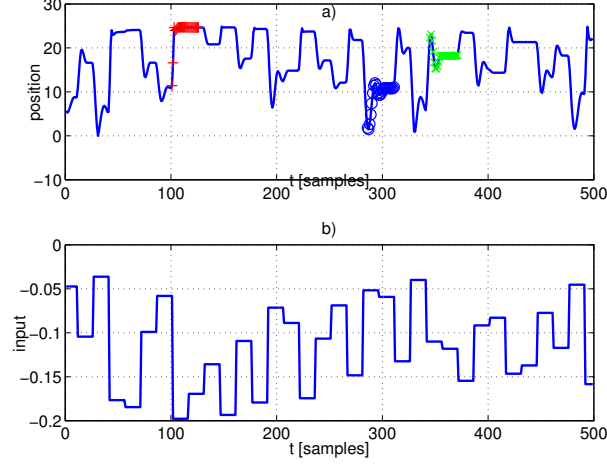


Figure 5.10: Identification with saturations. Data set used for identification a) position (portion marked with + (around time 100): data points used for the initialization of the lower saturation mode; portion marked with o (around time 300): data points used for initialization of impact mode; portion marked with x (around time 360): data points used for the initialization of free mode b) input signal

From figure 5.11a we see that data points are classified into three groups, corresponding to the impact, free and saturation modes. From 5.11b we see that the estimates of the parameters are improving during the iterations of the algorithm. From figure 5.12 we see that the simulated response is satisfactory, and that the modes active during the simulation correspond well to intuitive classification of data. Response in the free mode does not match the measured response precisely, while the responses in impact and saturation modes are predicted remarkably well.

It is interesting to consider further the saturation mode. From the physical considerations we know that the position of the mounting head stays close to the certain value saturation level y_s , as long as the system is in saturation. To gain some insight about the predicted saturation level y_s from the identified model, consider the "steady state" case where the system is in

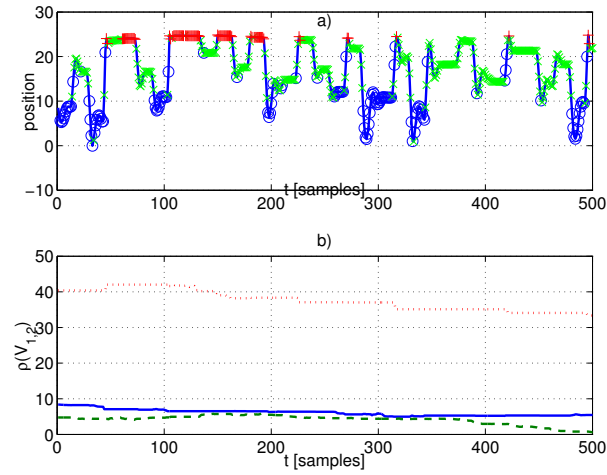


Figure 5.11: Identification with saturations. a) Classified data points (\circ : free mode, \times : impact mode; $+$ lower saturation) b) $\rho_{1,2,3}^E$ (solid line: free mode; dashed line: impact mode; dotted line: lower saturation)

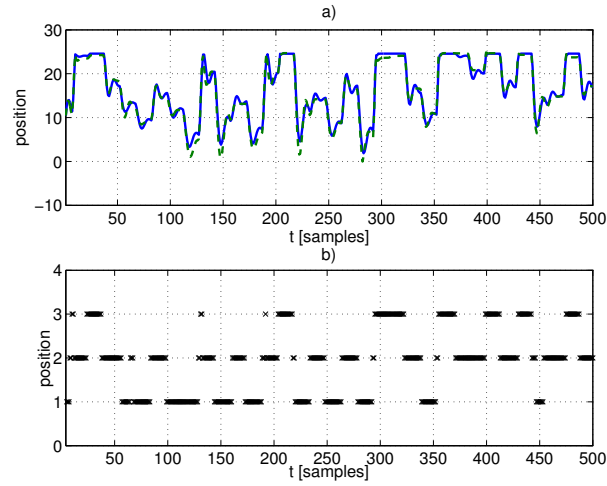


Figure 5.12: Identification with saturations. a) Simulation of the identified model (solid line: simulated response, dashed line: measured response) b) modes active during the simulation

$$\begin{aligned}
\theta_1 &= [1.5234 \quad -0.7407 \quad -35.5370 \quad -5.9786 \quad -0.2236]^\top, \\
\theta_2 &= [1.3163 \quad -0.6682 \quad -31.1894 \quad -10.5764 \quad 1.5656]^\top, \\
\theta_3 &= [-0.1161 \quad 0.0647 \quad 2.1464 \quad -1.2081 \quad 25.9239]^\top, \\
H_1 &= \begin{bmatrix} 0.039677 & 0.012028 & -14.109 & -17.308 \\ 99.531 & -57.568 & -3159.7 & -121.09 \\ -1 & 0 & 0 & 0 \\ 1 & 0 & 0 & 0 \\ 0 & -1 & 0 & 0 \\ 0 & 1 & 0 & 0 \\ 0 & 0 & -1 & 0 \\ 0 & 0 & 1 & 0 \\ 0 & 0 & 0 & -1 \\ 0 & 0 & 0 & 1 \end{bmatrix}, \\
H_2 &= \begin{bmatrix} -0.039677 & -0.012028 & 14.109 & 17.308 \\ 99.491 & -57.58 & -3145.6 & -103.79 \\ -1 & 0 & 0 & 0 \\ 1 & 0 & 0 & 0 \\ 0 & -1 & 0 & 0 \\ 0 & 1 & 0 & 0 \\ 0 & 0 & -1 & 0 \\ 0 & 0 & 1 & 0 \\ 0 & 0 & 0 & -1 \\ 0 & 0 & 0 & 1 \end{bmatrix}, \\
H_3 &= \begin{bmatrix} -99.531 & 57.568 & 3159.7 & 121.09 \\ -99.491 & 57.58 & 3145.6 & 103.79 \\ 1 & 0 & 0 & 0 \\ 0 & -1 & 0 & 0 \\ 0 & 1 & 0 & 0 \\ 0 & 0 & -1 & 0 \\ 0 & 0 & 1 & 0 \\ 0 & 0 & 0 & -1 \\ 0 & 0 & 0 & 1 \end{bmatrix}, \\
h_1 &= [2.8771 \quad 1588.4132 \quad 40 \quad 40 \quad 40 \quad 0.3 \quad 0.3 \quad 0.3 \quad 0.3]^\top, \\
h_2 &= [-2.8771 \quad 1585.5631 \quad 40 \quad 40 \quad 40 \quad 0.3 \quad 0.3 \quad 0.3 \quad 0.3]^\top, \\
h_3 &= [-1588.4132 \quad -1585.5631 \quad 40 \quad 40 \quad 40 \quad 0.3 \quad 0.3 \quad 0.3 \quad 0.3]^\top
\end{aligned}$$

Figure 5.13: Parameters of the identified model $s = 3$, $n_a = 2$, $n_b = 2$

saturation at time $k - 2$ and $k - 1$ (i.e. $y(k - 2) = y(k - 1) = y_s$) and the value of the input is constant in the time instants $k - 2$, $k - 1$ and such that system stays in saturation also at the time instant k (i.e. $y(k) = y_s$). According to the ARX dynamics of mode 3, y_s and u must verify the linear constraints:

$$y_s(1 - \theta_{3,1} - \theta_{3,2}) = (\theta_{3,3} + \theta_{3,4})u + \theta_{3,5} \text{ and } H_3[y_s \ y_s \ u \ u]^\top \leq h_3 \quad (5.50)$$

The minimal and maximal values that the output y can have under the previously stated assumptions can be found by solving the linear programs $\min y_s$ and $\max y_s$, respectively, in the unknowns y_s and u subject to the constraints (5.50). We found $\min y_s = 24.3903$, $\max y_s = 24.5047$. These values very precisely correspond to the values that the measured output takes while in saturation. In Juloski et al. (2004b) the minimal and maximal values of y_s under the same assumptions were determined from the model identified using the clustering procedure, and the following values were obtained: $\min y_s = 23.2$, $\max y_s = 24.2$. The computed minimal and maximal values of y_s identified using our procedure are much tighter than the values

identified with the clustering procedure.

5.11 Conclusions

In this paper we have presented a novel method for the identification of hybrid systems in PWARX form. The presented method facilitates to incorporate available a priori information on the system to be identified, but can also be initialized and used as a black-box method.

Unknown model parameters are treated as random variables described by their probability density functions (pdf). We define the optimality criterion for the identified model as the total probability that the observed data is generated by the model, and derive an algorithm that gives suboptimal solutions with respect to the defined criterion. A modified MRLP procedure, based on pricing functions is used for the estimation of the regions. Pricing functions preserve the valuable information from the classification phase for the region estimation. The applicability and the effectiveness of the proposed algorithm is illustrated by an academic and experimental example.

The suboptimal approach taken in the derivation of the proposed algorithm is to consider one data pair in each step of the algorithm (sequential processing), and to determine the optimal classification of the considered data pair, assuming that all previously considered data is processed optimally. In other words, the proposed algorithm aims to find the best possible local decision, with the purpose to approach the global optimum. In the optimization literature this approach to optimization is known as the greedy approach.

Another possible suboptimal approach for solving the classification problem would be to first classify all of available data on the basis of the available a priori knowledge (batch-wise processing), and after that compute the a posteriori parameter pdfs on the basis of all data points that are classified to the respective mode (or estimate the parameters in some other way, e.g. using least squares, as in section 5.9.1). Conceptually speaking, this approach would give good results if the a priori knowledge on the parameter values is precise enough to enable good classification. But, if this is the case, sequential processing is expected to perform equally well.

We use particle filtering approximations to represent and compute with the general probability density functions. However in some special cases (such as uniform or normal distributions for e and/or parameters) exact computations may be possible. In such cases the specific properties of the algorithm may be inferred from the explicit expressions of the update rule

for determining a posteriori distributions in Algorithm 5.5.2. This will be investigated in future research.

Further research will also focus on the investigation of properties of the presented method: the influence of the quality of the available a priori knowledge, the convergence properties of the proposed algorithm and the relation between obtained sub-optimal solutions and the optimal ones.

Conclusions and recommendations

6.1 Summary of contributions	6.3 Identification of hybrid systems
6.2 Observer design for hybrid systems	6.4 Outlook

In this thesis we investigated observer design and identification methods for certain classes of hybrid systems. We will now give an overview of main results and contributions and discuss open problems and possible directions and starting points for future research.

6.1 Summary of contributions

The main contributions of the thesis are:

- An observer design method for Lur'e systems with multivalued mappings, including a novel theoretical analysis.
- A new observer design procedure for a class of bimodal piecewise affine systems. The distinguishing feature of the designed observers is that they do not require the information on the currently active dynamics.
- A novel (Bayesian) approach to identification of hybrid systems, that facilitates the use of a priori knowledge.
- Two experimental case studies illustrate the observer designs, and show the applicability of the presented theory.
- An experimental case study in hybrid identification, that demonstrates the practical applicability of the clustering-based and Bayesian procedures. This case study is used as a benchmark example in hybrid identification (Niessen et al. (2004); Bemporad et al. (2004)).

6.2 Observer design for hybrid systems

6.2.1 Detailed overview of contributions

In chapter 2 we considered Lur'e systems of the form:

$$\begin{aligned}\dot{x} &= Ax - Gw + Bu \\ w &\in \varrho(Hx) \\ y &= Cx,\end{aligned}\tag{6.1}$$

where ϱ is a maximal monotone set-valued mapping. We consider an absolutely continuous function x a solution of a differential inclusion (6.1), if it satisfies (6.3) almost everywhere. As we saw, several classes of hybrid systems can be described as an interconnection of linear dynamics in a feedback configuration with a maximal monotone mapping, such as : linear relay systems, certain piecewise linear systems, linear complementarity systems and electric circuits with switching elements.

We proposed two Luenberger-type observer structures. The most general observer structure had the form:

$$\begin{aligned}\dot{\hat{x}} &= (A - LC)\hat{x} - G\hat{w} + Ly + Bu \\ \hat{w} &\in \varrho((H - KC)\hat{x} + Ky) \\ \hat{y} &= C\hat{x}.\end{aligned}\tag{6.2}$$

The considered class of systems and proposed observers can be non-smooth and non-Lipschitz, and hence, even the existence and uniqueness of solutions is not guaranteed.

The observer designs are based on rendering the linear part of the observer error dynamics strictly positive real. This can be accomplished by solving a suitably defined set of linear matrix inequalities.

Under the assumption that a solution of the system (6.1) exists (may not be unique, given the initial condition), we proved that the designed observers are well-posed (i.e. solution to the observer dynamics exists and is unique). Well-posedness is crucial in ensuring the proper behavior of the numerical implementation of the observer. We also proved that the estimated state exponentially converges to the true state of the system. The results are illustrated on an experimental case study with a drill-string setup.

In chapter 3 we considered a class of bimodal piecewise linear systems, in both continuous and discrete time. The considered class of systems in

continuous time has the form:

$$\begin{aligned}\dot{x} &= \begin{cases} A_1x + Bu, & \text{if } H^\top x < 0 \\ A_2x + Bu, & \text{if } H^\top x > 0 \end{cases} \\ y &= Cx, \end{aligned} \quad (6.3)$$

and we proposed Luenberger-type observers of the form:

$$\begin{aligned}\dot{\hat{x}} &= \begin{cases} A_1\hat{x} + Bu + L_1(y - \hat{y}), & \text{if } H^\top \hat{x} + K(y - \hat{y}) < 0 \\ A_2\hat{x} + Bu + L_2(y - \hat{y}), & \text{if } H^\top \hat{x} + K(y - \hat{y}) > 0 \end{cases} \\ \hat{y} &= C\hat{x}. \end{aligned} \quad (6.4)$$

The characteristic feature of the proposed observers is that the information on the currently active dynamics of the observed system is not needed, while several other approaches require that the mode is known (Alessandri and Coletta (2001a,b, 2003); Iulia Bara et al. (2000); Schinkel et al. (2003)).

We derived a constructive procedure for determining the observer gains L_1, L_2 and K , by solving a suitably defined system of linear matrix inequalities. The proposed design procedure yields globally asymptotically stable observers. However, it turned out that this approach is only feasible when the system dynamics is continuous over the switching plane. In this case we recovered the observer design procedure proposed by Arcak and Kokotović (2001) for Lur'e systems with slope-bounded nonlinearities, as a special case.

In the case of discontinuous vectorfield we obtained observers that have bounded relative estimation error, with respect to the state of the original system. We have successfully applied the developed theory on an experimental case study of a piecewise linear beam with a one-sided spring.

6.2.2 Discussion and recommendations

Both observer designs are based on stabilization of the observation error dynamics, by using quadratic Lyapunov functions. In certain cases the global asymptotic stability of the observation error may still be achieved in this way. However, for the considered class of bi-modal piecewise affine systems when the dynamics is discontinuous our design procedure guarantees only that the estimation error will be bounded, relative to the bound of the state (i.e. relative to the bound of the disturbance term). It remains as an open problem whether it is possible to achieve global asymptotic stability of the observation error dynamics for this class of systems.

Explicit algebraic feasibility conditions for the design of observers of type (6.2) can be obtained in the same way as the explicit feasibility conditions

for observer designs presented in Arcak and Kokotović (2001). Explicit feasibility conditions for the observer designs (6.4) are not known. As observer designs from Arcak and Kokotović (2001) are a special case of the observer (6.4) for the class (6.3) with continuous dynamics, feasibility conditions from Arcak and Kokotović (2001) are a good starting point for investigating this issue.

Our observer design procedure for a class (6.3) with discontinuous dynamics may be feasible even in the case when the underlying system is not observable. However, the designed observer is not useable because the guaranteed error bound is much larger than the bound of the state. This reflects the fact that the state can not be uniquely determined from the measured outputs. It is of interest to explore the connections between the observability conditions presented in literature (Bemporad et al. (2000a); Collins and van Schuppen (2004); Babaali and Egerstedt (2004); Vidal et al. (2003a)) and the feasibility of the presented observer designs and achievable error bounds.

The problem of using the designed observers for output-based control of the considered classes of systems is of great theoretical and practical interest. As the designed observers achieve input-to state stability (ISS) of the observer error with respect to the state of the observed system, a possible approach to output-based control design may be based on rendering the controlled system observation error-to-state stable, by choosing the suitable controller. Results from Isidori (1999), Jiang et al. (1994) and Jiang et al. (1996) that establish conditions for stability of the feedback interconnection between two input-to state stable systems may lead to stabilizing output-based controllers.

As demonstrated by experimental case studies the quality of the state estimation depends on the quality of the model of the underlying plant. In practical situations it is sometimes hard to get the accurate and simple enough model of the system (e.g. the experimental setup with the piecewise linear beam). It is desired that the observer performance deteriorates gracefully with respect to the modelling error, i.e. the observer should be *robust* w. r. t. the modelling error. To approach the robustness problem quantitatively, the modelling error can be treated as an additional external input to the observed system, with an unknown structure, but with a bounded magnitude. The modelling error then enters the observation error dynamics as an additional external input with bounded magnitude. The observer design can now be based on stabilizing the nominal observation error dynamics (i.e. without the modelling error) and rendering the gain from the disturbance to the estimation error small. Tradeoffs between this gain and convergence speed may be necessary.

6.3 Identification of hybrid systems

6.3.1 Detailed overview of contributions

In chapter 4 we presented an experimental case study in the identification of the electronic component placement process in pick-and-place machines. We used the clustering-based procedure (Ferrari-Trecate et al. (2001, 2003)), and obtained models of the system in the PWARX form.

We demonstrated that the obtained PWARX models are able to capture the relevant dynamics of the experimental setup, and have satisfactory one-step-ahead prediction and simulation performance. Hence, we conclude that the obtained models for instance, can be used for model predictive control and verification.

During this experimental work we observed the need for supplying and using available a priori knowledge in the identification procedure, in order to gain more control over the identification process and to improve the identification results. A priori knowledge may stem from physical insights into the system or from previous identification experiments. The existing procedures for the identification of PWARX systems (Ferrari-Trecate et al. (2003); Bemporad et al. (2000b, 2003); Vidal et al. (2003b)) are currently not properly equipped for handling the a priori knowledge.

In chapter 5 we presented a novel procedure for the identification of hybrid systems that facilitates the use of the available a priori knowledge on the system to be identified. The unknown parameters were treated as random variables and described with their probability density functions (pdfs) p_{θ_i} . By choosing the a priori parameter pdfs the user is now able to supply the relevant a priori knowledge to the identification procedure.

The identification problem is posed as the problem of maximizing the total probability that the observed data is generated by the identified model, given the a priori probability distributions of model parameters. This optimization problem is a combinatorial optimization problem, and as the number of the considered data points increases, finding the optimum quickly becomes computationally intractable. Hence, we developed a suboptimal optimization algorithm based on a greedy strategy, which considers one data point at a time, and tries to make the best possible local decision, in order to approach the global optimum. As analytical computation is not possible for general noise and parameter probability density functions we used particle filtering approximation to implement the proposed algorithm.

We also proposed a novel modification of the MRLP procedure, based on pricing functions, for the estimation of the regions. Pricing functions

preserve the valuable information from the classification phase for the region estimation. The operation of the proposed algorithm is illustrated by an academic example. We successfully applied the proposed procedure for the identification of the experimental example of the component placement process in pick-and-place machines.

6.3.2 Discussion and recommendations

Having the ability to handle a priori knowledge about the physical system is a major advantage of the presented identification procedure. By choosing a priori parameter pdfs so as to correspond to the parameters of the modes of the physical system the identification procedure may be forced to identify a model that can be interpreted in physical terms. Secondly, the approach presented here can be used to improve the previously identified models with targeted identification experiments. Also, models of increasing complexity can be built from a series of identification experiments, where in each experiment only a subset of the modes of the physical system is excited and identified. Further study into using the a priori knowledge in hybrid identification is of great practical importance.

Another important research topic is the theoretical investigation of the properties of the developed identification algorithm: the influence of the quality of the available a priori knowledge, the convergence properties of the proposed algorithm and the relations between the obtained sub-optimal solutions and the optimal ones. Questions of model structure selection, identifiability and persistence of excitation are also of great practical and theoretical importance. Results from statistical learning theory (see Vapnik (1998) and references therein) may provide a good starting point for this investigation.

The ideas developed in chapter 5 are not limited to the PWARX class of hybrid models. Extension to other classes of hybrid systems is possible. For example, in op den Buijs et al. (2004) the dynamics of the intercellular free calcium in the intact isolated rat heart was considered. Following the ideas of the Bayesian approach, we derived an identification algorithm and successfully identified the unknown parameters in the switched nonlinear model. Our approach is more robust with respect to the measurement noise and computationally less demanding, compared to other approaches in the physiological literature (van Riel and van der Vusse (2002); van Riel et al. (2003)). This example already shows the potential for further generalizations. This is an important future research topic.

6.4 Outlook

The theoretical results presented in this thesis were illustrated by several experimental examples. When applying the developed theory in practice, the needs for further theoretical developments became immediately obvious. For example, the experimental example of a drill string system spurred the search for numerical schemes that can reliably provide the solution of the differential inclusion, the experimental example of the piecewise linear beam makes obvious the need for robustification of the developed observers in the face of model uncertainty, and the experimental example of the component placement process prompted the investigation of ways to incorporate and handle the a priori knowledge in the hybrid identification.

Through these experimental case studies many new and interesting ideas and insights were generated. As the field of hybrid systems is extremely broad and diverse, and so far no successful unifying theory exists, the author believes that the advances in the study of hybrid systems in the near future shall and will be driven primarily by practical needs and through experimental and industrial applications.

References

- Alessandri, A., Coletta, P., 2001a. Design of Luenberger observers for a class of hybrid linear systems. In: Di Benedetto, M., Sangiovanni-Vincentelli, A. (Eds.), Proc. of Hybrid Systems: Computation and Control. Vol. 2034 of Lecture Notes in Computer Science. Springer, Rome, pp. 7–18.
- Alessandri, A., Coletta, P., 2001b. Switching observers for continuous-time and discrete-time linear systems. In: Proc. of the American Control Conference. pp. 2516–2521.
- Alessandri, A., Coletta, P., 2003. Design of observers for switched discrete-time linear systems. In: Proceedings of the American Control Conference. Denver, Colorado, USA, pp. 2785–2790.
- Angelis, G. Z., 2001. System analysis, modeling and control with polytopic linear models. Ph.D. thesis, Eindhoven University of Technology.
- Antsaklis, P. (Ed.), 2000. Proceedings of the IEEE: Special Issue on Hybrid Systems. Vol. 88.
- Antsaklis, P., Nerode, A. (Eds.), 1998. IEEE Transactions on Automatic Control: Special issue on "Hybrid Control Systems". Vol. 43.
- Arcak, M., Kokotović, P., 2001. Observer based control of systems with slope-restricted nonlinearities. IEEE Transactions on Automatic Control 46 (7), 1146–1150.
- Arulamapalam, M., Maskell, S., Gordon, N., Clapp, T., 2002. A tutorial on particle filters for online nonlinear/non-gaussian bayesian tracking. IEEE Transactions on Signal Processing 50, 174–188.
- Assembleon, 2002. web site: www.assembleon.com.
- Aubin, J., Cellina, A., 1984. Differential Inclusions. Springer-Verlag, Berlin.
- Babaali, M., Egerstedt, M., 2004. Observability of switched linear systems. In: Alur, R., Pappas, G. (Eds.), Proc. 7th International Workshop on Hybrid Systems: Computation and Control. Vol. 2993 of Lecture Notes in Computer Science. Springer-Verlag, pp. 48–63.

- Balluchi, A., Benvenuti, L., Di Benedetto, M., Sangiovanni-Vincentelli, A., 2002. Design of observers for hybrid systems. In: *Proc. of Hybrid Systems: Computation and Control: 2002*. Springer-Verlag, Berlin, pp. 76–89.
- Bemporad, A., Ferrari-Trecate, G., Morari, M., 2000a. Observability and controllability of piecewise affine and hybrid systems. *IEEE Transactions on Automatic Control*, 1864–1876.
- Bemporad, A., Garulli, A., Paoletti, S., Vicino, A., 2003. A greedy approach to identification of piecewise affine models. In: Maler, O., Pnueli, A. (Eds.), *Hybrid Systems: Computation and Control 2003*. Vol. 2623 of *Lecture Notes in Computer Science*. Prague, Czech Republic, pp. 97–112.
- Bemporad, A., Garulli, A., Paoletti, S., Vicino, A., 2004. Data classification and parameter estimation for the identification of piecewise affine models. In: *Proc. of Conference on Decision and Control*. To appear.
- Bemporad, A., Morari, M., 1999. Control of systems integrating logic, dynamics and constraints. *Automatica* 35 (3), 407–427.
- Bemporad, A., Roll, J., Ljung, L., 2000b. Identification of hybrid systems via mixed-integer programming. Tech. Rep. AUT00-28, ETH Zurich, <http://control.ethz.ch>.
- Bemporad, A., Torrisi, F., Morari, M., 2000c. Optimization-Based Verification and Stability Characterization of Piecewise Affine and Hybrid Systems. In: Lynch, N., Krogh, B. (Eds.), *Proceedings 3rd International Workshop on Hybrid Systems*, Pittsburgh, PA, USA. Vol. 1790 of *Lecture Notes in Computer Science*. pp. 45–58.
- Bennet, K., Mangasarian, O., 1994. Multicategory discrimination via linear programming. *Optimization Methods and Software* 4, 27–39.
- Berzuini, C., Gilks, W., 2001. RESAMPLE-MOVE filtering with cross-model jumps. In: Doucet, A., de Freitas, N., Gordon, N. (Eds.), *Sequential Monte-Carlo Methods in Practice*. Springer, Ch. 6, pp. 117–138.
- Boyd, S., El Ghaoui, L., Feron, E., Balakrishnan, V., 1994. *Linear Matrix Inequalities in Control Theory*. Vol. 15 of *Studies in Applied Mathematics*. SIAM.
- Branicky, M., 1998. Multiple lyapunov functions and other analysis tools for switched and hybrid systems. *IEEE Transactions on Automatic Control* 43, 475–482.

- Bredensteiner, E. J., Bennett, K. P., 1999. Multicategory classification by support vector machines. *Computational Optimizations and Applications* 12, 53–79.
- Brezis, H., 1973. *Opérateurs Maximaux Monotones*. North-Holland/American Elsevier, Amsterdam.
- Brogliato, B., 2004. Absolute stability and the Lagrange-Dirichlet theorem with monotone multivalued mappings. *System and Control Letters* 51, 343–353.
- Çamlıbel, M., Heemels, W., Schumacher, J., 2002. Consistency of a time-stepping method for a class of piecewise-linear networks. *IEEE Transactions on Circuits and Systems–I: Fundamental Theory and Applications* 49 (3), 349–357.
- Çamlıbel, M., Heemels, W., van der Schaft, A., Schumacher, J., 2003. Switched networks and complementarity. *IEEE Transactions on Circuits and Systems I: Fundamental Theory and Applications* 50, 1036 – 1046.
- Çamlıbel, M., Schumacher, J., 2002. Existence and uniqueness of solutions for a class of piecewise linear dynamical systems. *Linear Algebra and its Applications* 351, 147–184.
- Collins, P., van Schuppen, J., 2004. Observability of piecewise affine hybrid systems. In: Alur, R., Pappas, G. (Eds.), *Proc. 7th International Workshop on Hybrid Systems: Computation and Control*. Vol. 2993 of *Lecture Notes in Computer Science*. Springer-Verlag, pp. 264–279.
- Crisan, D., Doucet, A., 2002. A survey of convergence results on particle filtering methods for practitioners. *IEEE Transactions on Signal Processing* 50, 736 – 746.
- De Schutter, B., van den Boom, T., 2001. Model predictive control for max-plus-linear discrete event systems. *Automatica* 37, 1049–1056.
- Decarlo, R., Branicky, M., Pettersson, S., Lennartson, B., 2000. Perspectives and results on the stability and stabilizability of hybrid systems. *Proceedings of the IEEE* 88, 1069 – 1082.
- Del Vecchio, D., Murray, R., Perona, P., 2003. Decomposition of human motion into dynamic-based primitives with application to drawing tasks. *Automatica* 39, 2085–2098.

- Dontchev, A., Lempio, F., 1992. Difference methods for differential inclusions. *SIAM review* 34 (2), 263–294.
- Doucet, A., de Freitas, N., Gordon, N. (Eds.), 2001. *Sequential Monte Carlo Methods in Practice*. Springer.
- Duda, R., Hart, P., 1973. *Pattern classification and scene analysis*. Wiley.
- El Ghaoui, L., Commeau, J., 1999. LMITOOL: a package for LMI optimization in Scilab user's guide. Web site: <http://robotics.eecs.berkeley.edu/elghaoui/lmitool/lmitool.html>.
- Ferrari-Trecate, G., Mignone, D., Morari, M., 2002. Moving horizon estimation for hybrid systems. *IEEE Transactions on Automatic Control* 47, 1663–1676.
- Ferrari-Trecate, G., Muselli, M., 2002. A new learning method for piecewise linear regression. In: *Artificial Neural Networks - ICANN 2002: International Conference, Madrid, Spain*. Vol. 2415 of *Lecture Notes in Computer Science*. Springer Verlag, pp. 444–449.
- Ferrari-Trecate, G., Muselli, M., Liberati, D., Morari, M., 2001. A clustering technique for the identification of piecewise affine systems. In: Benedetto, M. D., Sangiovanni-Vincentelli, A. (Eds.), *Proc. 4th International Workshop on Hybrid Systems: Computation and Control*. Vol. 2034 of *Lecture Notes in Computer Science*. Springer-Verlag, pp. 218–231.
- Ferrari-Trecate, G., Muselli, M., Liberati, D., Morari, M., 2003. A clustering technique for the identification of piecewise affine systems. *Automatica* 39 (2), 205–217.
- Ferrari-Trecate, G., Schinkel, M., 2003. Conditions of optimal classification for piecewise affine regression. In: Maler, O., Pnueli, A. (Eds.), *Proc. 6th International Workshop on Hybrid Systems: Computation and Control*. Vol. 2623 of *Lecture Notes in Computer Science*. Springer-Verlag, pp. 188–202.
- Fey, R., 1992. Steady-state behaviour of reduced dynamic systems with local nonlinearities. Ph.D. thesis, Eindhoven University of Technology, The Netherlands.
- Filippov, A., 1988. *Differential Equations with Discontinuous Righthand Sides*. Mathematics and its Applications. Kluwer, Dordrecht, The Netherlands.

- Fishman, G., 1996. Monte Carlo: Concepts, Algorithms and Applications. Springer.
- Hedlund, S., Rantzer, A., 2002. Convex dynamic programming for hybrid systems. *IEEE Transactions on Automatic Control* 47, 1536–1540.
- Heemels, W., 1999. Linear complementarity systems: A study in hybrid dynamics. Ph.D. thesis, Eindhoven University of Technology.
- Heemels, W., De Schutter, B., Bemporad, A., 2001. Equivalence of hybrid dynamical models. *Automatica* 37, 1085–1091.
- Heemels, W., Schumacher, J., Weiland, S., 2000. Linear complementarity systems. *SIAM Journal on Applied Mathematics* 60.
- Heertjes, M., 1999. Controlled stabilization of long-term solutions in a piecewise linear beam system. Ph.D. thesis, Eindhoven University of Technology, The Netherlands.
- Imura, J., van der Schaft, A., 2000. Characterization of well-posedness of piecewise-linear systems. *IEEE Transactions on Automatic Control* 45, 1600 – 1619.
- Isidori, A., 1999. Nonlinear control systems II. Springer.
- Iulia Bara, G., Daafouz, J., Kratz, F., Jung, C., 2000. State estimation for a class of hybrid systems. In: *Proc. of 4th Int. Conf. on Automation of Mixed Processes: Hybrid Dynamic Systems*. Dortmund, Germany, pp. 313–316.
- Jiang, Z., Mareels, I., Wang, Y., 1996. A lyapunov formulation of the nonlinear small gain theorem for interconnected iss systems. *Automatica* 32 (8), 1211–1215.
- Jiang, Z., Teel, A., Praly, L., 1994. Small-gain theorem for iss systems and applications. *Mathematics of Control, Signals & Systems* 7, 95–120.
- Johansson, K., Rantzer, A., Astrom, K., 1999. Fast switches in relay feedback systems. *Automatica* 35, 539–552.
- Johansson, M., Rantzer, A., 1998a. Computation of piecewise quadratic lyapunov functions for hybrid systems. *IEEE Transactions on Automatic Control* 43 (4), 555–559.

- Johansson, M., Rantzer, A., 1998b. Computation of piecewise quadratic lyapunov functions for hybrid systems. *IEEE Transactions on Automatic Control* 43 (4), 555–559.
- Juloski, A., Heemels, W., Boers, Y., Verschure, F., 2003a. Two approaches to state estimation for a class of piecewise affine systems. In: *Proc. of Conference on Decision and Control 2003*. Maui, Hawaii, USA.
- Juloski, A., Heemels, W., Brogliato, B., 2004a. Observer design for Lur’e systems with multivalued mappings. Submitted for publication.
- Juloski, A., Heemels, W., Ferrari-Trecate, G., 2003b. Identification of an experimental hybrid system. In: *Proc. of IFAC Symposium on Analysis and Design of Hybrid Systems*. Saint Malo, France.
- Juloski, A., Heemels, W., Ferrari-Trecate, G., 2004b. Data-based hybrid modelling of the component placement process in pick-and-place machines. *Control Engineering Practice* 12, 1241–1252.
- Juloski, A., Heemels, W., Weiland, S., 2002. Observer design for a class of piecewise affine systems. In: *Proc. of Conference on Decision and Control 2002*. Las Vegas, USA, pp. 2606–2611.
- Juloski, A., Weiland, S., Heemels, W., 2004c. A Bayesian approach to identification of hybrid systems. In: *Proceedings of the 43rd Conference on Decision and Control*. Paradise Island, Bahamas, to appear.
- Juloski, A., Weiland, S., Heemels, W., 2004d. A Bayesian approach to identification of hybrid systems. Submitted for publication.
- Kastner-Maresch, A., 1991. Implicit Runge-Kutta methods for differential inclusions. *Numerical functional analysis and applications*, 937–958.
- Leine, R. I., van Campen, D. H., de Kraker, A., van den Steen, L., 1998. Stick-slip vibrations induced by alternate friction models. *Nonlinear dynamics* 16, 41–54.
- Liberzon, D., Hespanha, J., Morse, A., 1999. Stability of switched systems: a Lie-algebraic condition. *Systems & Control Letters* 37, 117–122.
- Ljung, L., 1999. *System Identification - Theory for the User*. Prentice Hall.
- MacKay, D., 1992. Bayesian methods for adaptive models. Ph.D. thesis, California Institute of Technology.

- Mayne, D., Rawlings, J., Rao, C., Scokaert, P., 2000. Constrained model predictive control: stability and optimality. *Automatica* 36, 789–814.
- Mihajlović, N., van Veggel, A. A., van de Wouw, N., Nijmeijer, H., 2004. Analysis of friction-induced limit sysling in an experimental drill-string system. *Transactions ASME*. To appear.
- Morse, S., Pantelides, C., Sastry, S., Schumacher, J. (Eds.), 1999. *Automatica: special issue on hybrid systems*. Vol. 35.
- Niessen, H., Juloski, A., Ferrari-Trecate, G., Heemels, W., 2004. Comparison of three procedures for the identification of hybrid systems. In: *Proceedings of the Conference on Control Applications*. Taipei, Taiwan.
- Nørgaard, M., 1997. Neural networks based system identification toolbox. Tech. Rep. 97-E-851, Technical University of Denmark, <http://www.iau.dtu.dk/research/control/nnsysid.html>.
- op den Buijs, J., Juloski, A., Ivanics, T., Ligeti, L., van der Vusse, G. J., van Riel, N. A. W., 2004. Identification of a switching model of calcium cycling in isolated rat hearts. In: *Proc. of 26th IEEE Engineering in Medicine and Biology*. IEEE, San Francisco, CA.
- Pogromsky, A., Heemels, W., Nijmeijer, H., 2003. On solution concepts and well-posedness of linear relay systems. *Automatica* 39, 2139–2147.
- Rantzer, A., Johansson, M., 2000. Piecewise linear quadratic optimal control. *IEEE Transactions on Automatic Control* 45, 629 – 637.
- Rodrigues, L., Hassibi, A., How, J., 2000. Output feedback controller synthesis for piecewise-affine systems with multiple equilibria. In: *Proc. of American Control Conference 2000*. pp. 1784–1789.
- Rodrigues, L., How, J., 2001. Observer-based control of piecewise affine systems. In: *Proc. of Conference on Decision and Control 2001*.
- Roll, J., Bemporad, A., Ljung, L., 2004. Identification of piecewise affine systems via mixed integer programming. *Automatica* 40, 37–50.
- Schinkel, M., Heemels, W., Juloski, A., 2003. State estimation for systems with varying sampling rate. In: *Proceedings of 42nd Conference on Decision and Control*. Maui, Hawaii, USA.
- Sontag, E. D., April 1981. Nonlinear regulation: The piecewise linear approach. *IEEE Trans. Autom. Control* 26 (2), 346–358.

- Sontag, E. D., 2000. The iss philosophy as a unifying framework for stability-like behavior. In: Isidori, A., Lamnabhi-Lagarrigue, F., Respondek, W. (Eds.), *Nonlinear Control in the Year 2000. Lecture Notes in Control and Information Sciences*. Springer-Verlag, pp. 443–468.
- Tyrell Rockafellar, R., 1970. *Convex Analysis*. Princeton University Press, Princeton, New Jersey.
- Tyrell Rockafellar, R., Wets, R., 1998. *Variational analysis*. Springer, Berlin.
- van Bokhoven, W., 1981. *Piecewise linear modelling and analysis*. Kluwer.
- van der Schaft, A., Schumacher, J., 1998. Complementarity modeling of hybrid systems. *IEEE Transactions on Automatic Control* 43, 483–490.
- van der Schaft, A. J., Schumacher, J. M., 1996. The complementary-slackness class of hybrid systems. *Mathematics of Control, Signals and Systems* 9, 266–301.
- van Riel, N. A. W., Ivanics, T., Ligeti, L., van der Vusse, G. J., 2003. System identification to analyse changed kinetics of serca in intact rat heart. In: *Proc. of 5th IFAC conference Modeling and control in biomedical systems*. IFAC, Melbourne, Australia, pp. 123–128.
- van Riel, N. A. W., van der Vusse, G. J., 2002. Computational analysis of calcium transients in the intact rat heart; model identification. In: *Proc. of 41st IEEE Conference on Decision and Control*. IEEE, Las Vegas, NE, pp. 2536–2537.
- Vapnik, V., 1998. *Statistical learning theory*. John Wiley.
- Vidal, R., Chiuso, A., Soatto, S., Sastry, S., 2003a. Observability of linear hybrid systems. In: Maler, O., Pnueli, A. (Eds.), *Proc. 6th International Workshop on Hybrid Systems: Computation and Control*. Vol. 2623 of *Lecture Notes in Computer Science*. Springer-Verlag, pp. 526–539.
- Vidal, R., Soatto, S., Ma, Y., Sastry, S., 2003b. An algebraic geometric approach to the identification of a class of linear hybrid systems. In: *Proceedings of 42nd IEEE Conference on Decision and Control*. Maui, HI, USA, pp. 167–172.
- Vidyasagar, M., 1993. *Nonlinear Systems Analysis*. Prentice Hall, Engelwood Cliffs, New Jersey.

-
- Wen, J., 1988. Time domain and frequency domain conditions for strict positive realness. IEEE Transactions on Automatic Control 33 (10), 988–992.
- Yakubovich, Y. A., 1964,1965. The matrix inequality method in the theory of the stability of nonlinear control systems, part I,II,III, translation from russian. Avtomatika i Telemekhanika 25,26.

Acknowledgement

This thesis presents part of the results of the four years of research on the project "Analysis and Synthesis of Embedded Systems with Discrete and Continuous Control", which was financially supported by the grant EES.5173 of the Dutch technology foundation STW/PROGRESS. Companies Philips CFT and Assembleon from Eindhoven participated in the project.

There are many people who helped me and to them I owe my gratitude.

Dr. Maurice Heemels, my co-promotor, invested a lot of time, energy and patience in my work during the past four years. Working with him was a unique and enriching experience, sometimes non-smooth, but never monotone. Had it not been for him, I am sure that my journey towards the PhD degree would have been much different, and certainly much less efficient.

I am grateful to my first promotor, Prof. Paul van den Bosch, for his continuous support and the freedom he gave me in my work. In the beginning, his trust in me and my abilities helped me to regain the trust in myself. I would also like to thank Prof. Henk Nijmeijer, who kindly agreed to be my second promotor and provided a lot of suggestions for improving the final version of the thesis.

Dr. Siep Weiland helped me many times to shape my fuzzy ideas into precise mathematical formulations. In our first discussion, his very first words were: "I do not have too much time, so please, no nonsense." In many meetings that followed I tried to keep to the same principle, and discovered that people will listen if I have something sensible to say. I would also like to thank Dr. Weiland for taking part in my promotion committee.

I spent two months, August and September 2003 at INRIA in Paris, with Dr. Giancarlo Ferrari-Trecate. Discussions we had served as an inspiration for the development of the Bayesian method for identification of hybrid systems, which is presented in chapter 5. I would also like to thank Dr. Ferrari-Trecate for being the member of the core committee for this thesis.

I would also like to thank Prof. Arjan van der Schaft for being the member of the core committee for the thesis.

Experimental results presented in chapters 2 and 3 of the thesis were obtained together with Nenad Mihajlović and Apostolos Doris. Ben Smeets, formerly from Assembleon, Eindhoven provided the experimental setup with

the mounting head, discussed in chapters 4 and 5. Will Hendrix made the “impacting surface” for the same setup, with unintentional mechanical imperfections that made the identification results so much more interesting. These experimental results add the new dimension to the work presented here.

Numerous discussions with Pieter Cuijpers, Dr. Michel Reniers and Prof. Jan Friso Groote about “bridging the gap” between the computer science and control theory helped me choose my research directions in the early stages of the project. I would like to thank Erik Gaal and Arno de Vet from Philips CFT for their participation in our project meetings, and for their sometimes critical, but always constructive remarks and comments.

I had a lot of pleasure working with Hans Niessen, my former master student. I hope that he learned from me as much as I learned from him. I had a lot of pleasure and fun working with my former officemate Jorn op den Buijs. To him, I wish good luck and success in his future studies.

Bart Stouten pointed me to the beginning of the breadcrumb trail that led to my first paper. I had many interesting and inspiring discussions with Dr. Natal van Riel and Dr. Yucai Zhu.

Barbara and Udo helped me many times to make things run smoothly.

Patricia was always there when I needed someone to talk to. I would like to thank my fellow PhD students, Leo, Mircea, Mark, Maarten, Andrej, Nelis, Michiel, Heico and John and former PhD students, Mario, Annelies, Andrei, Patrick, Mathieu and Hardy for creating a friendly atmosphere in the group.

I would like to thank Dijana who brought colors into my life.

I am eternally indebted to my mother, Ljiljana, for all her love and support during the years of my studies. This thesis is therefore dedicated to her.

Aleksandar Juloski
Eindhoven, 2004

Samenvatting

Ontwerp van waarnemers en identificatie methoden voor hybride systemen - theorie en experimenten -

Technieken voor waarnemers en identificatie van enkele klassen van hybride systemen worden geïntroduceerd. Hybride systemen zijn niet-lineaire dynamische systemen met een sterke interactie tussen discreet en tijdcontinu gedrag. Voorbeelden van dit type systemen zijn te vinden op vele gebieden, zoals embedded systemen, procesregeling, automatische verkeerssystemen, elektrische circuits, mechanische, biomechanische, biologische en biomedische systemen en in de economie.

Wij presenteren een nieuwe ontwerpprocedure voor waarnemers voor een klasse van niet-gladde dynamische systemen, namelijk systemen van het Lur'e type met een monotone meerwaardige afbeelding van het terugkoppelpad. Voorbeelden zijn relaissystemen, lineaire complementariteitsystemen, elektrische circuits met schakelende componenten en sommige stuksgewijze affine systemen. We zullen bewijzen dat de voorgestelde waarnemers kunnen worden berekend en een unieke oplossing hebben en dat de waarnemer de toestand van het waargenomen systeem asymptotisch schat.

We presenteren ook een nieuwe ontwerpprocedure voor waarnemers voor een klasse van stuksgewijze affine systemen met twee modes, zowel tijd continue als tijddiscreet. We presenteren Luenberg waarnemers en leiden voldoende voorwaarden af opdat de fout dynamica globaal, asymptotisch stabiel is voor het geval dat de systeem dynamica continu is over het schakelvlak. Wanneer de systeemdynamica discreet is leiden we condities af die garanderen dat de relatieve schattingsfout asymptotisch begrensd is ten opzichte van de toestand van het waargenomen systeem. De theorie wordt geïllustreerd met enkele academische voorbeelden en een experimentele opstelling.

We presenteren een experimentele studie van de identificatie van het plaatsingsproces in een pick-and-place machine. Eenzijdig contact en verzadiging beschrijven het hybride karakter. Een verandering van mode kan niet worden gemeten zodat identificatie algoritmen voor hybride systemen moeten worden toegepast. PWARX modellen, die bestaan uit stuksgewijs ARX modellen met een onderverdeling van de regressor ruimte, worden geïdentificeerd met behulp van een clustering techniek. De gevonden modellen zijn in staat de relevante dynamica van de experimentele opstelling te schatten.

Deze studie heeft veel inzicht opgeleverd in de eigenschappen van hybride identificatie en beklemtoint de noodzaak om a-priori kennis te gebruiken in de identificatieprocedure.

De noodzaak a-priori informatie te gebruiken heeft geleid tot een nieuwe methode voor de identificatie van de klasse van hybride PWARX modellen. De methode staat het gebruik van deze a-priori informatie toe maar kan ook zonder deze informatie als black-box methode worden toegepast. De onbekende parameters worden als random variabelen met behulp van hun kansdichtheidsfunctie beschreven. Identificatie wordt nu geformuleerd als het maximaliseren van de waarschijnlijkheid dat de gemeten data afkomstig zijn van het geïdentificeerde model. Een partikel filter is gebruikt voor de numerieke implementatie. Een aangepaste versie van de op een meer-categorieën robuust lineair programmeren (MRLP) gebaseerde classificatie methode is gebruikt voor het schatten van de PWARX gebieden. De voorgestelde methode is toegepast voor de identificatie van de component plaatser van een pick-and-place machine.

Резиме

Хибридни системи: методи за пројектовање опсервера и идентификацију - теорија и експерименти -

У овој дисертацији ћемо разматрати проблеме пројектовања опсервера и идентификације за неке класе хибридних система. Хибридни системи су велика класа нелинеарних динамичких система који имају узајамно повезану дискретну и континуалну динамику. Примери хибридних система могу се пронаћи у многим дисциплинама, као што су уграђени (енгл. *embedded*) системи управљања, управљање процесима, аутоматски системи за управљање саобраћајем, електрична кола, механички и био-механички системи, биолошки и био-медицински системи и економија.

Прво ћемо представити нову конструктивну процедуру за пројектовање опсервера за једну класу не-глатких динамичких система. Наиме, реч је о системима Лурје-типа са монотоним мапом са више вредности (енгл. *monotone multivalued mapping*) у повратној спрези. Као примери система у овој класи, могу се навести различите класе хибридних система, као што су системи са релејима, линеарни комплементарни системи (енгл. *linear complementarity systems*), електрична кола са прекидачким елементима и неки део-по-део афини (енгл. *piece-wise affine*) системи. Под претпоставком да је оригинални систем добро дефинисан, доказаћемо да су и пројектовани опсервери добро дефинисани (енгл. *well posed*), односно да постоји јединствено решење за динамику опсервера, као и да опсервери асимптотски реконструишу вектор стања оригиналног система. Резултате ћемо илустровати на експерименталном уређају који репродукује торзионе вибрације које настају у системима за бушење нафте, услед трења.

Затим ћемо представити нову процедуру за пројектовање опсервера за класу део-по-део афиних система са два мода, у континуалном и дискретном времену. Пројектовани опсервери су Луенбергеровог типа. Такође ћемо извести довољне услове да динамика грешке опсервера буде глобално асимптотски стабилна, у случајевима када је динамика оригиналног система непрекидна преко прекидне површине. За случај када динамика оригиналног система има прекиде извешћемо услове који гарантују да је релативна грешка опсервера асимптотски ограничена, у

односу на вектор стања оригиналног система. Изложена теорија је илустрована на неколико академских примера, као и на експерименталном уређају са савитљивом гредом и једностраном опругом.

У другом делу дисертације ћемо приказати експериментални пример идентификације процеса постављања електронских компоненти на штампану плочу. Једностранни контакти и засићења су карактеристични за хибридную динамику овог процеса. Промена мода се не може директно мерити, те стога морамо применити алгоритам за идентификацију који може да идентификује и модове и правила активације (енгл. *switching laws*). Применом алгоритма на бази груписања (енгл. *clustering-based algorithm*) идентификоваћемо *Piece-Wise AutoRegressive eXogenous (PWARX)* моделе овог процеса. *PWARX* модел се састоји од неколико *ARX* модела, и поделе простора регресора на регионе где је сваки од поменутих *ARX* модела активан. Добијеним моделима може се описати динамика експерименталног уређаја на задовољавајући начин. Кроз ову експерименталну студију приказаћемо неколико практичних ствари о идентификацији хибридних система, а посебно ће се истаћи потреба за укључивањем *a priori* (претходног) знања у процес идентификације.

Мотивисани потребом за укључивањем *a priori* знања, развићемо нову процедуру за идентификацију хибридних система у *PWARX* форми. Изложени метод олакшава употребу *a priori* знања, али се може користити и као метод црне кутије (енгл. *black-box*). Непозанте параметре ћемо третирати као случајне величине, и описивати их функцијама густине расподеле вероватноће. Проблем идентификације тако постаје проблем максимизације тоталне вероватноће да је идентификовани модел генерисао податке који се користе за идентификацију. Процедура се може нумерички имплементирати употребом методе честичног филтрирања (енгл. *particle filtering*). За идентификацију региона употребићемо модификовану варијанту методе робустног линеарног програмирања са више категорија (енгл. *multi-category robust linear programming (MRLP)*) за класификацију узорака. Предложена процедура ће затим бити примењена за идентификацију процеса постављања електронских компоненти на штампану плочу.

Curriculum Vitae



Aleksandar Juloski was born on Aug 7, 1976 in Belgrade, Serbia and Montenegro.

He received the Dipl.Ing. degree in electrical engineering (major: control engineering) from the Faculty of Electrical Engineering, University of Belgrade in 1999. After graduation he spent one year with the Institute Mihajlo Pupin in Belgrade, developing software for embedded controllers.

From November 2000 to November 2004 he pursued his Ph.D. degree with the Control Systems Group at the Faculty of Electrical Engineering, Eindhoven University of Technology, The Netherlands, under the supervision of Prof. Paul van den Bosch. The research conducted in this period is presented in this dissertation.